High Energy Gamma-rays from Active Galactic Nuclei

Contents

1 Topics **5**
- 1.1 ICRANet participants . . . 5
- 1.2 Students . . . 5
- 1.3 Ongoing collaborations . . . 5

2 Brief description **7**

3 Publications-2020 **13**
- 3.1 Publications-2012-2019 . . . 15

4 Multiwavelength Study of High-Redshift Blazars **21**
- 4.1 Introduction . . . 21
- 4.2 The Sample . . . 26
- 4.3 Fermi-LAT observations . . . 26
  - 4.3.1 γ-ray variability . . . 28
- 4.4 Swift observations . . . 28
- 4.5 Results of data analyses . . . 30
  - 4.5.1 X-ray variability . . . 34
  - 4.5.2 γ-ray variability . . . 36
- 4.6 The origin of multiwavelength emission . . . 41
  - 4.6.1 SED modeling results . . . 46
- 4.7 Discussion and Conclusion . . . 48
- 4.8 Summary . . . 51

5 Broadband Study of High-Synchrotron-Peaked BL Lac Object 1ES 1218+304 **55**
- 5.1 Introduction . . . 55
- 5.2 Fermi-LAT data extraction and analyses . . . 57
- 5.3 X-ray and optical/UV observations . . . 61
  - 5.3.1 Swift XRT . . . 61
  - 5.3.2 NuSTAR . . . 62
  - 5.3.3 Swift UVOT . . . 64
- 5.4 The Origin of Broadband Emission . . . 64
  - 5.4.1 Broadband SED fitting . . . 67

5.5 Time dependent formation of electron spectrum: Electron cooling 69
5.6 Discussions and Conclusions 71

1 Topics

- High energy gamma-rays from active galactic nuclei
- high energy neutrinos from blazars
- High energy emission from gamma-ray bursts

1.1 ICRANet participants

- Sahakyan Narek
- Gasparyan Sargis

1.2 Students

- Harutyunyan Gevorg
- Israyelyan Davit
- Khachatryan Mher
- Mari Harutyunyan
- Vazgen Vardanyan

1.3 Ongoing collaborations

- Razmik Mirzoyan (Max Planck Institute for Physics, Munich, Germany)
- Paolo Giommi (ASI Science Data Center)
- Damien Begue (Max Planck Institute for Extraterrestrial Physics, Munich, Germany)
- Ulisses Barres de Almeida (Centro Brasileiro de Pesquisas Fisicas - CBPF/MCT)
- Bernardo Fraga (Centro Brasileiro de Pesquisas Fisicas - CBPF)

- Karlica Mile (Nova Gorica)

2 Brief description

The main scientific activities of our group are in the field of X- and gamma-ray Astrophysics and Astroparticle physics. The results from the data analysis of Swift UVOT/XRT, NuStar, Chandra and Fermi LAT telescopes are used to investigate the particle acceleration and emission processes in the different classes of active galactic nuclei. The analysis of available data allows to investigate the emission processes and relativistic outflows in the most extreme regimes (keV-TeV).
Below we present several abstracts from the papers published in 2020, also with MAGIC collaboration.

- Multiwavelength study of high-redshift blazars

High-redshift blazars are among the most powerful objects in the Universe. The spectral and temporal properties of thirty-three distant blazars ($z > 2.5$) detected in the high energy γ-ray band are investigated by analyzing the Fermi-LAT and Swift UVOT/ XRT data. The considered sources have soft time averaged γ-ray spectra ($\Gamma_\gamma \geq 2.2$) whereas those that have been observed in the X-ray band have hard X-ray spectra ($\Gamma_X = 1.01 - 1.86$). The γ-ray flux of high-redshift blazars ranges from 4.84×10^{-10} to 1.50×10^{-7} $photon\ cm^{-2}\ s^{-1}$ and the luminosity is within $(0.10 - 5.54) \times 10^{48}\ erg\ s^{-1}$ which during the γ-ray flares increases up to $(0.1 - 1) \times 10^{50}\ erg\ s^{-1}$. In the X-ray band, only the emission of PKS 0438-43, B2 0743+25 and TXS 0222+185 is found to vary in different Swift XRT observations whereas in the γ-ray band, the emission is variable for fourteen sources: the flux of B3 1343+451 and PKS 0537-286 changes in sub-day scales, that of PKS 0347-211 and PKS 0451-28 in day scales, while the γ-ray variability of the others is in week or month scales. The properties of distant blazar jets are derived by modeling the multiwavelength spectral energy distributions within a one-zone leptonic scenario assuming that the X-ray and γ-ray emissions are produced from inverse Compton scattering of synchrotron and dusty torus photons. From the fitting, the emission region size is found to be ≤ 0.05 pc and the magnetic field and the Doppler factor are correspondingly within $0.10 - 1.74$ G and $10.0 - 27.4$. By modeling the optical-UV excess, we found that the central black hole masses and accretion disk luminosities are within $L_d \simeq (1.09 - 10.94) \times 10^{46}\ erg\ s^{-1}$ and $(1.69 - 5.35) \times 10^9\ M_\odot$, respectively.

- Investigation of the Gamma-ray Spectrum of CTA 102 During the Exceptional Flaring State in 2016-2017

The flat spectrum radio quasar CTA 102 entered an extended period of activity from 2016 to 2017 during which several strong γ-ray flares were observed. Using Fermi large area telescope data a detailed investigation of γ-ray spectra of CTA 102 during the flaring period is performed. In several periods the γ-ray spectrum is not consistent with a simple power-law, having a hard photon index with an index of $\sim (1.8 - 2.0)$ that shows a spectral cutoff around an observed photon energy of $\sim (9 - 16)$ GeV. The internal γ-ray absorption via photon-photon pair production on the broad-line-region-reflected photons cannot account for the observed cut-off/break even if the emitting region is very close to the central source. This cut-off/break is likely due to a similar intrinsic break in the energy distribution of emitting particles. The origin of the spectral break is investigated through the multiwavelength modeling of the spectral energy distribution, considering a different location for the emitting region. The observed X-ray and γ-ray data is modeled as inverse Compton scattering of synchrotron and/or external photons on the electron population that produce the radio-to-optical emission which allowed to constrain the power-law index and cut-off energy in the electron energy distribution. The obtained results are discussed in the context of a diffusive acceleration of electrons in the CTA 102 jet.

- Broad-band study of high-synchrotron-peaked BL Lac object 1ES 1218+304

The origin of the multiwavelength emission from the high-synchrotron-peaked BL Lac 1ES 1218+304 is studied using the data from Swift UVOT/XRT, NuSTAR and Fermi-LAT. A detailed temporal and spectral analysis of the data observed during 2008-2020 in the γ-ray ($>$ 100 MeV), X-ray (0.3-70 keV), and optical/UV bands is performed. The γ-ray spectrum is hard with a photon index of 1.71 ± 0.02 above 100 MeV. The Swift UVOT/XRT data show a flux increase in the UV/optical and X-ray bands; the highest $0.3 - 3$ keV X-ray flux was $(1.13 \pm 0.02) \times 10^{-10} erg\, cm^{-2}\, s^{-1}$. In the 0.3-10 keV range the averaged X-ray photon index is > 2.0 which softens to 2.56 ± 0.028 in the 3-50 keV band. However, in some periods, the X-ray photon index became extremely hard (< 1.8), indicating that the peak of the synchrotron component was above 1 keV, and so 1ES 1218+304 behaved like an extreme synchrotron BL Lac. The hardest X-ray photon index of 1ES 1218+304 was 1.60 ± 0.05 on MJD 58489. The time-averaged multiwavelength spectral energy distribution is modeled within a one-zone synchrotron self-Compton leptonic model using a broken power-law and power-law with an exponential cutoff electron energy distributions. The data are well explained when the electron energy

distribution is $E_e^{-2.1}$ extending up to $\gamma_{br/cut} \simeq (1.7 - 4.3) \times 10^5$, and the magnetic field is weak ($B \sim 1.5 \times 10^{-2}$ G). By solving the kinetic equation for electron evolution in the emitting region, the obtained electron energy distributions are discussed considering particle injection, cooling, and escape.

- Open Universe survey of Swift-XRT GRB fields: Flux-limited sample of HBL blazars

We have analysed all the X-ray images centred on Gamma Ray Bursts generated by Swift over the last 15 years using automatic tools that do not require any expertise in X-ray astronomy, producing results in excellent agreement with previous findings. This work, besides presenting the largest medium-deep survey of the X-ray sky and a complete sample of blazars, wishes to be a step in the direction of achieving the ultimate goal of the Open Universe Initiative, that is to enable non expert people to fully benefit of space science data, possibly extending the potential for scientific discovery, currently confined within a small number of highly specialised teams, to a much larger population. We have used the Swift_deepsky Docker container encapsulated pipeline to build the largest existing flux-limited and unbiased sample of serendipitous X-ray sources. Swift_deepsky runs on any laptop or desktop computer with a modern operating system. The tool automatically downloads the data and the calibration files from the archives, runs the official Swift analysis software and produces a number of results including images, the list of detected sources, X-ray fluxes, SED data, and spectral slope estimations. We used our source list to build the LogN-LogS of extragalactic sources, which perfectly matches that estimated by other satellites. Combining our survey with multi-frequency data we selected a complete radio flux-density limited sample of High Energy Peaked (HBL) blazars. The LogN-LogS built with this data-set confirms that previous samples are incomplete below $\sim$ 20 mJy.

- Multiwavelength variability and correlation studies of Mrk 421 during historically low X-ray and -ray activity in 2015-2016

We report a characterization of the multi-band flux variability and correlations of the nearby (z=0.031) blazar Markarian 421 (Mrk 421) using data from Metsähovi, Swift, Fermi-LAT, MAGIC, FACT and other collaborations and instruments from November 2014 till June 2016. Mrk 421 did not show any prominent flaring activity, but exhibited periods of historically low activity above 1 TeV ($F_{>1\mathrm{TeV}} < 1.7\times10^{-12}\,\mathrm{ph\,cm^{-2}\,s^{-1}}$) and in the 2-10 keV (X-ray) band ($F_{2-10\,\mathrm{keV}} < 3.6\times10^{-11}\,\mathrm{erg\,cm^{-2}\,s^{-1}}$), during which the Swift-BAT data suggests an additional spectral component beyond the regular synchrotron

emission.The highest flux variability occurs in X-rays and very-high-energy (E>0.1 TeV) γ-rays, which, despite the low activity, show a significant positive correlation with no time lag. The HR_{keV} and HR_{TeV} show the *harder-when-brighter* trend observed in many blazars, but the trend flattens at the highest fluxes, which suggests a change in the processes dominating the blazar variability. Enlarging our data set with data from years 2007 to 2014, we measured a positive correlation between the optical and the GeV emission over a range of about 60 days centered at time lag zero, and a positive correlation between the optical/GeV and the radio emission over a range of about 60 days centered at a time lag of 43^{+9}_{-6} days.This observation is consistent with the radio-bright zone being located about 0.2 parsec downstream from the optical/GeV emission regions of the jet. The flux distributions are better described with a LogNormal function in most of the energy bands probed, indicating that the variability in Mrk 421 is likely produced by a multiplicative process.

- Testing two-component models on very high-energy gamma-ray-emitting BL Lac objects

It has become evident that one-zone synchrotron self-Compton (SSC) models are not always adequate for very-high-energy (VHE) gamma-ray emitting blazars. While two-component models are performing better, they are difficult to constrain due to the large number of free parameters. In this work, we make a first attempt to take into account the observational constraints from Very Long Baseline Interferometry (VLBI) data, long-term light curves (radio, optical, and X-rays) and optical polarisation to limit the parameter space for a two-component model and test if it can still reproduce the observed spectral energy distribution (SED) of the blazars. We selected five TeV BL Lac objects based on the availability of VHE gamma-ray and optical polarisation data. We collected constraints for the jet parameters from VLBI observations. We evaluated the contributions of the two components to the optical flux by means of decomposition of long-term radio and optical light curves as well as modelling of the optical polarisation variability of the objects. We selected eight epochs for these five objects, based on the variability observed at VHE gamma rays, for which we constructed the SEDs that we then modelled with a two-component model. We found parameter sets which can reproduce the broadband SED of the sources in the framework of two-component models considering all available observational constraints from VLBI observations. Moreover, the constraints obtained from the long-term behaviour of the sources in the lower energy bands could be used to determine the region where the emission in each band originates. Finally, we attempted to use optical polarisation data to shed new light on the behaviour of the two components in the optical band. Our observationally constrained two zone model

allows explanation of the entire SED from radio to VHE with two co-located emission regions.

- Bounds on Lorentz Invariance Violation from MAGIC Observation of GRB 190114C

On January 14, 2019, the Major Atmospheric Gamma Imaging Cherenkov telescopes detected GRB 190114C above 0.2 TeV, recording the most energetic photons ever observed from a gamma-ray burst. We use this unique observation to probe an energy dependence of the speed of light in vacuo for photons as predicted by several quantum gravity models. Based on a set of assumptions on the possible intrinsic spectral and temporal evolution, we obtain competitive lower limits on the quadratic leading order of speed of light modification.

- An intermittent extreme BL Lac: MWL study of 1ES 2344+514 in an enhanced state

Extreme High-frequency BL Lacs (EHBL) feature their synchrotron peak of the broadband spectral energy distribution (SED) at $\nu_s \geq 10^{17}$ Hz. The BL Lac object 1ES 2344+514 was included in the EHBL family because of its impressive shift of the synchrotron peak in 1996. During the following years, the source appeared to be in a low state without showing any extreme behaviours. In August 2016, 1ES 2344+514 was detected with the ground-based γ-ray telescope FACT during a high γ-ray state, triggering multi-wavelength (MWL) observations. We studied the MWL light curves of 1ES 2344+514 during the 2016 flaring state, using data from radio to VHE γ rays taken with OVRO, KAIT, KVA, NOT, some telescopes of the GASP-WEBT collaboration at the Teide, Crimean, and St. Petersburg observatories, *Swift*-UVOT, *Swift*-XRT, *Fermi*-LAT, FACT and MAGIC. With simultaneous observations of the flare, we built the broadband SED and studied it in the framework of a leptonic and an hadronic model. The VHE γ-ray observations show a flux level of 55% of the Crab Nebula flux above 300 GeV, similar to the historical maximum of 1995. The combination of MAGIC and *Fermi*-LAT spectra provides an unprecedented characterization of the inverse-Compton peak for this object during a flaring episode. The Γ index of the intrinsic spectrum in the VHE γ-ray band is $2.04 \pm 0.12_{stat} \pm 0.15_{sys}$. We find the source in an extreme state with a shift of the position of the synchrotron peak to frequencies above or equal to 10^{18} Hz.

- Broadband characterisation of the very intense TeV flares of the blazar 1ES 1959+650 in 2016

1ES 1959+650 is a bright TeV high-frequency-peaked BL Lac object exhibiting interesting features like "orphan" TeV flares and a broad emission in the high-energy regime, that are difficult to interpret using conventional one-zone Synchrotron Self-Compton (SSC) scenarios. We report the results from the Major Atmospheric Gamma Imaging Cherenkov (MAGIC) observations in 2016 along with the multi-wavelength data from the *Fermi* Large Area Telescope (LAT) and *Swift* instruments. MAGIC observed 1ES 1959+650 with different emission levels in the very-high-energy (VHE, E $>$ 100 GeV) γ-ray band during 2016. In the long-term data, the X-ray spectrum becomes harder with increasing flux and a hint of a similar trend is also visible in the VHE band. An exceptionally high VHE flux reaching $\sim$3 times the Crab Nebula flux was measured by MAGIC on the 13th, 14th of June and 1st July 2016 (the highest flux observed since 2002). During these flares, the high-energy peak of the spectral energy distribution (SED) lies in the VHE domain and extends up to several TeV. The spectrum in the γ-ray (both *Fermi*-LAT and VHE bands) and the X-ray bands are quite hard. On 13th June and 1st July 2016, the source showed rapid variations of the VHE flux within timescales of less than an hour. A simple one-zone SSC model can describe the data during the flares requiring moderate to high values of the Doppler factors ($\delta \geq 30 - 60$). Alternatively, the high-energy peak of the SED can be explained by a purely hadronic model attributed to proton-synchrotron radiation with jet power $L_{jet} \sim 10^{46}$ erg/s and under high values of the magnetic field strength ($\sim$ 100 G) and maximum proton energy ($\sim$few EeV). Mixed lepto-hadronic models require super-Eddington values of the jet power. We conclude that it is difficult to get detectable neutrino emission from the source during the extreme VHE flaring period of 2016.

3 Publications-2020

- Sahakyan N., Israyelyan D., Harutyunyan G., Khachatryan M., Gasparyan S., Multiwavelength study of high-redshift blazars, Monthly Notices of the Royal Astronomical Society, olume 498, Issue 2, 2020, p.2594-2613.
- Sahakyan N., Broad-band study of high-synchrotron-peaked BL Lac object 1ES 1218+304, Monthly Notices of the Royal Astronomical Society, Volume 496, Issue 4, 2020, pp.5518-5527
- Sahakyan, N., Investigation of the -ray spectrum of CTA 102 during the exceptional flaring state in 2016-2017, Astronomy and Astrophysics, Volume 635, id.A25, 2020, 10 pp.
- Sahakyan N., Israyelyan D., Harutyunyan G., A Multiwavelength Study of Distant Blazar PKS 0537-286, Astrophysics, volume 63, 2020, p. 459469
- Sahakyan N., Harutyunyan G., Israelyan D., Khachatryan M., Exploring the Origin of Multiwavelength Emission from High-Redshift Blazar B3 1343 + 451, Astrophysics, Volume 63, Issue 3, 2020, p.334-348
- Giommi P., Chang Y., Turriziani S., Glauch T., Leto C., Verrecchia F., Padovani P., Penacchioni A., Arneodo F., Barres de Almeida U., Brandt C., Capalbi M., Civitarese O., D; Elia V., Di Giovanni A., De Angelis M., Del Rio Vera J., Di Pippo S., Middei R., Perri M., Pollock A., Puccetti S., Ricard N., Ruffini R., Sahakyan N., Open Universe survey of Swift-XRT GRB fields: Flux-limited sample of HBL blazars, Astronomy and Astrophysics, Volume 642, id.A141, 2020, 9 pp.
- Sahakyan N., High Energy -ray variability of NGC 1275 and 3C 120, Proceedings of the International Astronomical Union, Volume 342, 2020, pp. 172-175
- MAGIC Collaboration, VERITAS Collaboration, Abeysekara, A., Benbow, W.,.... Gasparyan, S.,...Sahakyan N.,.... Villata, M., The Great Markarian 421 Flare of 2010 February: Multiwavelength Variability and Correlation Studies, The Astrophysical Journal, Volume 890, Issue 2, id.97, 2020, 21 pp.

- MAGIC Collaboration, Acciari V., Ansoldi S.,.... Gasparyan, S.,...Sahakyan N.,.... Lien, A., Multiwavelength variability and correlation studies of Mrk 421 during historically low X-ray and -ray activity in 2015-2016, Monthly Notices of the Royal Astronomical Society, DOI: 10.1093/mnras/staa3727

- MAGIC Collaboration, Acciari V., Ansoldi S.,.... Gasparyan, S.,...Sahakyan N.,.... Zari, D., The Great Markarian 421 Flare of 2010 February: Multiwavelength Variability and Correlation Studies, Astronomy and Astrophysics, Volume 635, id.A158, 2020, 10 pp.

- MAGIC Collaboration, Acciari V., Ansoldi S.,.... Gasparyan, S.,...Sahakyan N.,.... Lohfink A., New Hard-TeV Extreme Blazars Detected with the MAGIC Telescopes, The Astrophysical Journal Supplement Series, Volume 247, Issue 1, id.16, 2020, 24 p.

- MAGIC Collaboration, Acciari V., Ansoldi S.,.... Gasparyan, S.,...Sahakyan N.,.... Walker R., Monitoring of the radio galaxy M 87 during a low-emission state from 2012 to 2015 with MAGIC, Monthly Notices of the Royal Astronomical Society, Volume 492, Issue 4, 2020, p.5354-5365

- MAGIC Collaboration, Acciari V., Ansoldi S.,.... Gasparyan, S.,...Sahakyan N.,.... Tammi J., Study of the variable broadband emission of Markarian 501 during the most extreme Swift X-ray activity, Astronomy and Astrophysics, Volume 637, id.A86, 2020, 27 pp.

- MAGIC Collaboration, Acciari V., Ansoldi S.,.... Gasparyan, S.,...Sahakyan N.,.... Zari, D., A search for dark matter in Triangulum II with the MAGIC telescopes, Physics of the Dark Universe, Volume 28, article id. 100529, 2020.

- MAGIC Collaboration, Acciari V., Ansoldi S.,.... Gasparyan, S.,...Sahakyan N.,.... Zari, D., Broadband characterisation of the very intense TeV flares of the blazar 1ES 1959+650 in 2016, Astronomy and Astrophysics, Volume 638, id.A14, 2020, 16 pp.

- MAGIC Collaboration, Acciari V., Ansoldi S.,.... Gasparyan, S.,...Sahakyan N.,.... Reinthal R., Unraveling the Complex Behavior of Mrk 421 with Simultaneous X-Ray and VHE Observations during an Extreme Flaring Activity in 2013 April, The Astrophysical Journal Supplement Series, Volume 248, Issue 2, 2020, id.29

- MAGIC Collaboration, Acciari V., Ansoldi S.,.... Gasparyan, S.,...Sahakyan N.,.... Zheng W., An intermittent extreme BL Lac: MWL study of 1ES

2344+514 in an enhanced state, Monthly Notices of the Royal Astronomical Society, Volume 496, Issue 3, 2020, pp.3912-3928

- MAGIC Collaboration, Acciari V., Ansoldi S.,.... Gasparyan, S.,...Sahakyan N.,.... Zari, D., Studying the nature of the unidentified gamma-ray source HESS J1841-055 with the MAGIC telescopes, Monthly Notices of the Royal Astronomical Society, Volume 497, Issue 3, 2020, p. 3734-3745

- MAGIC Collaboration, Acciari V., Ansoldi S.,.... Gasparyan, S.,...Sahakyan N.,.... Zari, D., Bounds on Lorentz Invariance Violation from MAGIC Observation of GRB 190114C, Physical Review Letters, Volume 125, Issue 2, 2020, article id.021301

- MAGIC Collaboration, Acciari V., Ansoldi S.,.... Gasparyan, S.,...Sahakyan N.,.... Kehusmaa P., Testing two-component models on very high-energy gamma-ray-emitting BL Lac objects, Astronomy and Astrophysics, Volume 640, id.A132, 2020, 29 pp.

- MAGIC Collaboration, Acciari V., Ansoldi S.,.... Gasparyan, S.,...Sahakyan N.,.... Zari, D., MAGIC observations of the diffuse -ray emission in the vicinity of the Galactic center, Astronomy and Astrophysics, Volume 642, id.A190, 2020, 9 pp.

- MAGIC Collaboration, Acciari V., Ansoldi S.,.... Gasparyan, S.,...Sahakyan N.,.... Parkinson P., Detection of the Geminga pulsar with MAGIC hints at a power-law tail emission beyond 15 GeV, Astronomy and Astrophysics, Volume 643, id.L14, 2020, 6 p.

3.1 Publications-2012-2019

- V. Acciari,.....S. Gasparyan...N. Sahakyan, ... D. Zaric, "Testing emission models on the extreme blazar 2WHSP J073326.7+515354 detected at very high energies with the MAGIC telescopes", Monthly Notices of the Royal Astronomical Society, Volume 490, Issue 2, p.2284-2299, 2019.

- R. Ruffini, R. Moradi, J. Rueda, L. Becerra, C. Bianco, C. Cherubini, S. Filippi, Y. Chen, M. Karlica, N. Sahakyan, Y. Wang, S. Xue, "On the GeV Emission of the Type I BdHN GRB 130427A", The Astrophysical Journal, Volume 886, Issue 2, article id. 82, 13 pp., 2019.

- V. Acciari,.....S. Gasparyan...N. Sahakyan, ... D. Zaric, "Observation of inverse Compton emission from a long γ-ray burst", Nature, Volume 575, Issue 7783, p.459-463, 2019.

- V. Acciari,.....S. Gasparyan...N. Sahakyan, ... D. Zaric, "Teraelectronvolt emission from the -ray burst GRB 190114C", Nature, Volume 575, Issue 7783, p.455-458, 2019.

- N. Sahakyan, "Origin of the multiwavelength emission of PKS 0502+049", accepted for publication in Astronomy and Astrophysics, doi.org/10.1051/0004-6361/201936715, arXiv:1911.12087, 2019.

- V. Acciari,.....S. Gasparyan...N. Sahakyan, ... D. Zaric, "New hard-TeV extreme blazars detected with the MAGIC telescopes", accepted for publication in Astrophysical Journal Supplement, arXiv:1911.06680, 2019.

- P. Giommi, C. Brandt, U. Barres de Almeida, A. Pollock, F. Arneodo, Y. Chang, O. Civitarese, M. Angelis, V. DElia, J. Del Rio Vera, S. Di Pippo, R. Middei, A. Penacchioni, M. Perri, R. Ruffini, N. Sahakyan, S. Turriziani, "Open Universe for Blazars: a new generation of astronomical products based on 14 years of Swift-XRT data", Astronomy and Astrophysics, Volume 631, id.A116, 11 pp., 2019.

- T. Glauch, P. Padovani, P. Giommi, E. Resconi, B. Arsioli, N. Sahakyan, M. Huber, "Dissecting the region around IceCube-170922A: the blazar TXS 0506+056 as the first cosmic neutrino source", EPJ Web of Conferences, Volume 207, id.02003, 2019.

- V. Acciari,.....S. Gasparyan...N. Sahakyan, ... D. Zaric, "Constraints on Gamma-Ray and Neutrino Emission from NGC 1068 with the MAGIC Telescopes", The Astrophysical Journal, Volume 883, Issue 2, article id. 135, 9 pp., 2019.

- V. Acciari,.....S. Gasparyan...N. Sahakyan, ... D. Zaric, "Measurement of the extragalactic background light using MAGIC and Fermi-LAT gamma-ray observations of blazars up to z = 1", Monthly Notices of the Royal Astronomical Society, Volume 486, Issue 3, p.4233-4251, 2019.

- V. Acciari,.....S. Gasparyan...N. Sahakyan, ... D. Zaric, "Deep observations of the globular cluster M15 with the MAGIC telescopes", Monthly Notices of the Royal Astronomical Society, Volume 484, Issue 2, p.2876-2885, 2019.

- J. Rueda, R. Ruffini, Y. Wang, C. Bianco, J. Blanco-Iglesias, M. Karlica, P. Loren-Aguilar, R. Moradi, N. Sahakyan, "Electromagnetic emission of white dwarf binary mergers", Journal of Cosmology and Astroparticle Physics, Issue 03, article id. 044, 2019.

- N. Sahakyan, "Origin of the multiwavelength emission of PKS 0502+049", Astronomy and Astrophysics, Volume 622, id.A144, 10 pp. 2019.
- R. Ruffini, M. Karlica, N. Sahakyan, J. Rueda, Y. Wang, G. Mathews, C. Bianco, M. Muccino, "A GRB Afterglow Model Consistent with Hypernova Observations", The Astrophysical Journal, Volume 869, Issue 2, article id. 101, 9 pp. 2018.
- A. Abeysekara, ... N. Sahakyan, ... D. Zaric, "Periastron Observations of TeV Gamma-Ray Emission from a Binary System with a 50-year Period", The Astrophysical Journal Letters, Volume 867, Issue 1, article id. L19, 8 pp., 2018.
- P. Padovani, P. Giommi, E. Resconi, T. Glauch, B. Arsioli, N. Sahakyan, M. Huber, "Dissecting the region around IceCube-170922A: the blazar TXS 0506+056 as the first cosmic neutrino source", Monthly Notices of the Royal Astronomical Society, Volume 480, Issue 1, p.192-203, 2018.
- N. Sahakyan, "Lepto-hadronic γ-Ray and Neutrino Emission from the Jet of TXS 0506+056", The Astrophysical Journal, Volume 866, Issue 2, article id. 109, 6 pp. 2018.
- S. Gasparyan, N. Sahakyan, V. Baghmanyan, D. Zargaryan, "On the Multiwavelength Emission from CTA 102", The Astrophysical Journal, Volume 863, Issue 2, article id. 114, 11 pp., 2018.
- M. Aartsen, ... N. Sahakyan, ... T. Yuan, "Neutrino emission from the direction of the blazar TXS 0506+056 prior to the IceCube-170922A alert", Science, Volume 361, Issue 6398, pp. 147-151, 2018.
- V. Baghmanyan, M. Tumanyan, N. Sahakyan, Y. Vardanyan, "High-Energy γ -Ray Emission from PKS 0625-35", Astrophysics, Volume 61, Issue 2, pp.160-170, 2018.
- N. Sahakyan, V. Baghmanyan, D. Zargaryan, "Fermi-LAT observation of nonblazar AGNs", Astronomy & Astrophysics, Volume 614, id.A6, 11 pp., 2018.
- B. Fraga, U. Barres de Almeida, S. Gasparyan, P. Giommi, N. Sahakyan, "Time-Evolving SED of MKN421: a multi-band view and polarimetric signatures", Frontiers in Astronomy and Space Sciences, Volume 5, id.1, 2018.
- S. Gasparyan, N. Sahakyan, P. Chardonnet, "The origin of HE and VHE gamma-ray flares from FSRQs", International Journal of Modern Physics D, Volume 27, Issue 10, id. 1844007, 2018.

- D. Zargaryan, N. Sahakyan, H. Harutyunian, "Chandra observations of gamma-ray emitting radio galaxies", International Journal of Modern Physics D, Volume 27, Issue 10, id. 1844022, 2018.

- V. Baghmanyan, N. Sahakyan, "X-ray and γ-ray emissions from NLSy1 galaxies", International Journal of Modern Physics D, Volume 27, Issue 10, id. 1844001, 2018.

- D. Zargaryan, S. Gasparyan, V. Baghmanyan and N. Sahakyan, "Comparing 3C 120 jet emission at small and large scales", Astronomy & Astrophysics, Volume 608, id. A37, 10, 2017.

- U. Barres de Almeida, F. Bernardo, P. Giommi, N. Sahakyan, S. Gasparyann and C. Brandt, "Long-Term Multi-Band and Polarimetric View of Mkn 421: Motivations for an Integrated Open-Data Platform for Blazar Optical Polarimetry", Galaxies, vol. 5, issue 4, p. 90, 2017.

- V. Baghmanyan, S. Gasparyan and N. Sahakyan, "Rapid Gamma-Ray Variability of NGC 1275", The Astrophysical Journal, Volume 848, Issue 2, article id. 111, 8, 2017.

- N. Sahakyan and S. Gasparyan "High energy gamma-ray emission from PKS 1441+25", Monthly Notices of the Royal Astronomical Society, 470, 3, p.2861-2869, 2017.

- N. Sahakyan, V. Baghmanyan, and D. Zargaryan, "Gamma-ray Emission from Non-Blazar AGNs", AIP Conference Proceedings, Volume 1792, Issue 1, id.050002, 2017.

- N. Sahakyan and S. Gasparyan, "High Energy Gamma-Rays From PKS 1441+25", AIP Conference Proceedings, Volume 1792, Issue 1, id.050005, 2017.

- V. Baghmanyan, "Gamma-Ray Variability of NGC 1275", AIP Conference Proceedings, Volume 1792, Issue 1, id.050007, 2017.

- D. Zargaryan, "The Gamma-Ray Emission from Broad-Line Radio Galaxy 3C 120",AIP Conference Proceedings, Volume 1792, Issue 1, id.050008, 2017.

- N. Sahakyan, "Galactic sources of high energy neutrinos: Expectation from gamma-ray data", EPJ Web of Conferences, Volume 121, id.05005, 2016.

- Sahakyan, N., Zargaryan, D. and Baghmanyan, V. "On the gamma-ray emission from 3C 120", Astronomy & Astrophysics, Volume 574, id.A88, 5 pp., 2015.
- Sahakyan, N., Yang, R., Rieger, F., Aharonian, F. and de Ona-Wilhelmi, E. "High Energy Gamma Rays from Centaurus a" Proceedings of the MG13 Meeting on General Relativity ISBN 9789814623995, pp. 1028-1030, 2015.
- Sahakyan, N., Piano, G. and Tavani, M. "Hadronic Gamma-Ray and Neutrino Emission from Cygnus X-3", The Astrophysical Journal, Volume 780, Issue 1, article id. 29, 2014.
- Sahakyan, N., Rieger, F., Aharonian, F., Yang, R., and de Ona-Wilhelmi, E. "On the gamma-ray emission from the core and radio lobes of the radio galaxy Centaurus A", International Journal of Modern Physics: Conference Series, Volume 28, id. 1460182, 2014.
- Sahakyan, N., Yang, R. Aharonian, F. and Rieger, F., " Evidence for a Second Component in the High-energy Core Emission from Centaurus A?", The Astrophysical Journal Letters, Volume 770, Issue 1, L6, 2013.
- Yang, R.-Z., Sahakyan, N., de Ona Wilhelmi, E., Aharonian, F. and Rieger, F., "Deep observation of the giant radio lobes of Centaurus A with the Fermi Large Area Telescope", Astronomy & Astrophysics, 542, A19, 2012.
- Sahakyan, N., "High energy gamma-radiation from the core of radio galaxy Centaurus A", Astrophysics, 55, 14, 2012.
- Sahakyan, N., "On the Origin of High Energy Gamma-Rays from Giant Radio Lobes Centarus A", International Journal of Modern Physics Conference Series, 12, 224, 2012.

4 Multiwavelength Study of High-Redshift Blazars

4.1 Introduction

Blazars are one of the most luminous objects in the Universe. In the unification scheme of radio-loud active galactic nuclei (AGNs) blazars are a subclass with a relativistic jet making a small angle (a few degrees) with the observer's line of sight [162]. The jets are sources of non-thermal emission which cover the entire electromagnetic spectrum, from radio to high energy (HE; $>$ 100 MeV) or very high energy (VHE; $>$ 100 GeV) γ-ray bands [118]. This non-thermal emission is varying in short time scales [e.g., in minute scales in the γ-ray band 11, 59, 58, 115, 34, 131, 146, 82] with a substantial increase in luminosity. The flux variation as well as the observed superluminal motion, the high degree of polarization and other observed features can be explained by the relativistic beaming effects.

Blazars are usually grouped into two large classes based on the absence or presence of emission lines in their optical spectra, i.e., BL Lacertae objects (BL Lacs) have weak or no emission lines; the equivalent width (EW) of the emission line $<$ 5 Å in the rest frame, while the flat-spectrum radio quasars (FSRQs) have stronger emission lines (EW $>$ 5 Å) [162]. Based on the position of the synchrotron peak in the rest frame (ν_p^{syn}), blazars are further classified as low-synchrotron-peaked (LSP for $\nu_p^{syn} < 10^{14}$ Hz), intermediate-synchrotron-peaked (ISP for $10^{14} < \nu_p^{syn} < 10^{15}$ Hz), and high-synchrotron-peaked (HSP for $\nu_p^{syn} > 10^{15}$ Hz) objects [121, 1].

The broadband spectral energy distribution (SED) of blazars shows a typical double-peaked structure. The low-energy peak (extending from radio to UV/soft X-rays) is produced by synchrotron emission from the relativistic electrons in the jet. The HE component (above X-ray band) is often attributed to Inverse Compton (IC) scattering of photons produced either inside [synchrotron-self Compton, (SSC); 66, 29, 104] or outside of the jet [external inverse Compton, (EIC); 26, 151, 69]. The external photons can be from the accretion disk, broad-line region and dusty torus surrounding the disc. In alternative models, the HE component is due to the interaction of protons accelerated along with electrons in the jet [e.g., 33]. In this case, the blazars

Table 4.1 List of γ-ray emitting blazars at $z > 2.5$. The results of observation of distant blazars from August 4, 2008, to August 4, 2018 by *Fermi* are presented in the right part of the table.

Object	4FGL name	Class	RA	Dec	F_γ [1]	Photon index	TS	E_{max} [2]	Probability	z
GB 1508+5714	J1510.1+5702	FSRQ	227.54	57.04	0.76 ± 0.15	2.95 ± 0.15	63.50	8.76	0.8268	4.31
PKS 1351-018	J1354.3-0206	FSRQ	208.50	-2.11	1.11 ± 0.15	2.69 ± 0.09	98.49	1.30	0.7010	3.72
MG3 J163554+3629	J1635.6+3628	BCU	248.92	36.48	1.46 ± 0.27	2.84 ± 0.12	123.95	3.74	0.8413	3.65
NVSS J121915 +365718	J1219.0+3653	BCU	184.77	36.89	0.22 ± 0.08	2.20 ± 0.14	40.56	2.67	0.8273	3.53
PKS 0335-122	J0337.8-1157	FSRQ	54.47	-11.96	0.72 ± 0.16	2.69 ± 0.13	49.47	10.19	0.9245	3.44
PKS 0537-286	J0539.9-2839	FSRQ	84.99	-28.66	4.38 ± 0.18	2.72 ± 0.03	1694.80	7.60	0.9619	3.10
TXS 0800+618	J0805.4+6147	FSRQ	121.36	61.80	2.23 ± 0.14	2.82 ± 0.05	475.17	4.83	0.8441	3.03
S4 1427+543	J1428.9+5406	FSRQ	217.23	54.11	0.59 ± 0.15	2.62 ± 0.14	67.10	10.26	0.7831	3.01
GB6 J0733+0456	J0733.8+0455	FSRQ	113.47	4.93	1.14 ± 0.15	2.39 ± 0.07	197.26	17.65	0.9854	3.01
B2 0743+25	J0746.4+2546	FSRQ	116.60	25.77	2.06 ± 0.19	2.87 ± 0.07	280.99	1.52	0.7449	2.99
PKS 0347-211	J0349.8-2103	FSRQ	57.47	-21.06	3.25 ± 0.15	2.47 ± 0.03	1372.81	5.83	0.9690	2.94
S4 1124+57	J1127.4+5648	FSRQ	171.87	56.80	0.96 ± 0.13	2.75 ± 0.09	147.30	7.09	0.8495	2.89
MRSS 291-081526	J2313.9-4501	BCU	348.49	-45.02	0.89 ± 0.20	2.80 ± 0.13	81.12	2.25	0.7550	2.88
PKS 0438-43	J0440.3-4333	FSRQ	70.09	-43.55	2.24 ± 0.20	2.60 ± 0.05	574.84	2.00	0.9225	2.85
S4 2015+65	J2015.4+6556	FSRQ	303.86	65.95	0.39 ± 0.15	2.37 ± 0.15	23.77	4.34	0.7257	2.84
87GB 214302.1+095227	J2145.5+1006	BL Lac	326.38	10.12	0.048 ± 0.014	1.71 ± 0.19	40.46	67.15	0.9874	2.83
MG2 J174803+3403	J1748.0+3403	FSRQ	267.01	34.06	0.97 ± 0.13	2.31 ± 0.07	284.21	31.63	0.9934	2.76
PKS 0834-20	J0836.5-2026	FSRQ	129.13	-20.45	1.93 ± 0.19	2.94 ± 0.08	171.15	1.15	0.5796	2.75
TXS 0222+185	J0224.9+1843	FSRQ	36.24	18.72	1.72 ± 0.22	3.05 ± 0.12	101.08	2.59	0.5327	2.69
OD 166	J0242.3+1102	FSRQ	40.59	11.05	1.94 ± 0.20	2.59 ± 0.06	252.83	6.91	0.8651	2.68
CRATES J233930 +024420	J2339.6+0242	BCU	354.90	2.71	1.00 ± 0.21	2.58 ± 0.11	94.50	6.17	0.8537	2.66
TXS 0907+230	J0910.6+2247	FSRQ	137.67	22.80	1.17 ± 0.14	2.37 ± 0.06	262.58	5.38	0.9578	2.66
PMN J1441-1523	J1441.6-1522	FSRQ	220.41	-15.38	0.65 ± 0.23	2.32 ± 0.13	72.02	11.77	0.9535	2.64
CRATES J105433 +392803	J1054.2+3926	BCU	163.56	39.44	0.27 ± 0.09	2.30 ± 0.16	34.05	4.79	0.9000	2.63
MG1 J154930+1708	J1549.6+1710	BL Lac	237.41	17.18	0.17 ± 0.08	2.01 ± 0.16	44.75	17.03	0.9759	2.62
TXS 1448+093	J1450.4+0910	FSRQ	222.62	9.18	0.76 ± 0.13	2.35 ± 0.08	130.24	10.58	0.9599	2.61
PMN J0226+0937	J0226.5+0938	FSRQ	36.63	9.63	0.48 ± 0.12	2.18 ± 0.10	96.49	56.42	0.9523	2.61
PKS 0451-28	J0453.1-2806	FSRQ	73.29	-28.11	5.83 ± 0.17	2.66 ± 0.02	3118.20	10.77	0.9815	2.56
B3 0908+416B	J0912.2+4127	FSRQ	138.06	41.46	1.51 ± 0.14	2.42 ± 0.05	539.57	12.10	0.9903	2.56
TXS 1616+517	J1618.0+5139	FSRQ	244.52	51.67	0.69 ± 0.13	2.68 ± 0.12	72.65	12.38	0.8408	2.56
B3 1624+414	J1625.7+4134	FSRQ	246.45	41.57	1.38 ± 0.14	2.49 ± 0.06	395.12	9.69	0.9787	2.55
B3 1343+451	J1345.5+4453c	FSRQ	206.39	44.88	15.01 ± 0.16	2.25 ± 0.008	34652.79	24.25	0.9994	2.53
PKS 2107-105	J2110.2-1021c	FSRQ	317.56	-10.36	0.88 ± 0.18	2.66 ± 0.13	53.29	5.46	0.6500	2.50

[1] Integrated γ-ray flux in units of $\times 10^{-8} photon\ cm^{-2}\ s^{-1}$.
[2] Photon energy in GeV.

Table 4.2 Spectral parameters of the sources modeled with logparabola.

Object	F_γ [1]	α	β
PKS 1351-018	$(6.86 \pm 1.66) \times 10^{-9}$	2.20 ± 0.23	0.63 ± 0.23
PKS 0537-286	$(4.15 \pm 0.20) \times 10^{-8}$	2.66 ± 0.04	0.10 ± 0.03
TXS 0800+618	$(2.04 \pm 0.16) \times 10^{-8}$	2.67 ± 0.08	0.17 ± 0.06
B2 0743+25	$(1.72 \pm 0.23) \times 10^{-8}$	2.53 ± 0.14	0.40 ± 0.13
PKS 0347-211	$(2.69 \pm 0.17) \times 10^{-8}$	2.32 ± 0.05	0.19 ± 0.03
PKS 0438-43	$(1.15 \pm 0.23) \times 10^{-8}$	2.35 ± 0.12	0.48 ± 0.11
S4 2015+65	$(1.66 \pm 1.00) \times 10^{-9}$	2.42 ± 0.35	0.42 ± 0.31
PKS 0834-20	$(1.76 \pm 0.20) \times 10^{-8}$	2.62 ± 0.16	0.29 ± 0.13
OD 166	$(1.45 \pm 0.24) \times 10^{-8}$	2.43 ± 0.11	0.24 ± 0.08
TXS 0907+230	$(8.68 \pm 1.77) \times 10^{-8}$	2.28 ± 0.09	0.12 ± 0.06
PKS 0451-28	$(5.56 \pm 0.18) \times 10^{-8}$	2.56 ± 0.04	0.09 ± 0.02
B3 1343+451	$(1.41 \pm 0.02) \times 10^{-7}$	2.18 ± 0.01	0.07 ± 0.006

[1] Integrated γ-ray flux in units of *photon* $cm^{-2}\, s^{-1}$.

also can emit VHE neutrinos [e.g., 17, 61, 41, 90, 94, 141, 142, 166, 136].

Blazars are the dominant sources in the extragalactic γ-ray sky. Among the total 5000 sources in the Fermi Large Area Telescope (*Fermi*) fourth source catalog of γ-ray sources [4FGL; 5], $\sim$ 2800 are blazars, 45 are radio galaxies, and 19 are other AGNs. Low to high redshift blazars are observed showing different redshift distributions for FSRQs and BL Lacs; the distribution of FSRQs has a peak around $z = 1$ with a median of 1.14 ± 0.62 and there is a high number of FSRQs at the redshift of $\simeq 0.5 - 2.0$, while the peak of BL Lacs is at $z = 0.3$ with a mean of 0.34 ± 0.42. There are only 105 sources detected with $z > 2$ (3.75 % of total sources) and only 33 with $z > 2.5$ (1.18 %).

Blazars harboring supermassive black holes are valuable sources for studying the relativistic outflows and formation and propagation of relativistic jets. In this context, the high redshift blazars ($z > 2.5$) are of particular interest; they are the most powerful non-explosive astrophysical sources having ever been detected in the γ-ray band. Their study can shed light on the further understanding of the cosmological evolution of blazars and supermassive black holes and also on the evolution of relativistic jets across different cosmic epochs [165]. Moreover, the γ-ray observations of distant blazars are important since a limit on the density of the Extragalactic Background Light (EBL) can be derived. The γ-rays , as they propagate from their sources to the Earth, are subject to absorption through two-photon pair production when interacting with EBL photons [e.g., 155, 52]. This absorption feature is visible in the spectrum of the nearby sources only at VHEs while for distant sources

Table 4.3 Swift XRT data analyses results. For the sources, when several observations were available, they were merged to estimate the averaged X-ray spectra. The sources for which the number of counts was enough to constrain the flux and the photon index in a single observation are marked with an asterisk (*).

Object	$n_H \times 10^{20}\, cm^{-2}$	Γ_X	$Log(F_{(0.3-10)keV})/erg\, cm^{-2}\, s^{-1}$	C-stat./dof
GB 1508+5714	1.56	1.38 ± 0.52	-12.21 ± 0.21	0.58(20)
PKS 0537-286*	2.20	1.17 ± 0.04	-11.42 ± 0.02	1.28(679)
TXS 0800+618*	4.67	1.13 ± 0.10	-11.53 ± 0.04	1.08(355)
S4 1427+543	1.17	1.41 ± 0.23	-12.24 ± 0.09	1.1(102)
GB6 J0733+0456	7.72	1.65 ± 0.65	-12.80 ± 0.23	1.33(20)
B2 0743+25*	4.50	1.15 ± 0.03	-11.30 ± 0.01	1.39(773)
PKS 0347-211	4.23	1.32 ± 0.27	-12.26 ± 0.12	1.24(75)
PKS 0438-43*	1.41	1.25 ± 0.09	-11.52 ± 0.04	1.4(345)
S4 2015+65	10.6	1.79 ± 0.69	-12.28 ± 0.23	0.91(17)
MG2 J174803+3403	3.22	1.36 ± 0.47	-12.35 ± 0.18	0.61(33)
PKS 0834-20*	6.07	1.07 ± 0.09	-11.67 ± 0.04	1.12(399)
TXS 0222+185*	9.40	1.11 ± 0.04	-10.93 ± 0.02	1.89(684)
OD 166	8.97	1.86 ± 0.40	-12.37 ± 0.15	0.65(40)
TXS 0907+230	4.68	1.14 ± 0.40	-12.49 ± 0.18	1.26(40)
PMN J1441-1523	7.71	1.86 ± 0.63	-13.10 ± 0.22	0.51(25)
TXS 1448+093	2.11	2.33 ± 0.62	-13.30 ± 0.16	1.04(26)
PMN J0226+0937	6.57	1.49 ± 0.37	-12.83 ± 0.15	0.93(49)
PKS 0451-28*	2.07	1.55 ± 0.10	-11.42 ± 0.04	0.99(297)
B3 0908+416B	1.42	1.01 ± 0.46	-12.47 ± 0.19	1.11(30)
TXS 1616+517	1.98	1.25 ± 0.33	-12.77 ± 0.14	1.17(59)
B3 1343+451*	1.78	1.21 ± 0.17	-12.22 ± 0.07	0.85(160)
PKS 2107-105	6.23	1.24 ± 0.29	-12.49 ± 0.12	1.67(72)

($z > 2.0$), it can be significant already at tens of GeV. Thus, the EBL density in a redshift-dependence way can be constrained or measured by analyzing the γ-ray data [e.g., 2, 9, 57, 51]. However, if the γ-ray spectrum does not extend above 10 GeV to constrain the EBL density, by the theoretical interpretation of the data, the intrinsic source processes can be investigated and separated from the propagation effects which can be a help in the observations of distant blazars by future telescopes (e.g., CTA).

The vast majority of high redshift blazars are LSPs so the HE peak in their SEDs is at MeV below the *Fermi* band. They are sometimes also called 'MeV' blazars [28], being bright and strong X-ray emitters. In the X-ray band, these sources usually have a hard spectrum which corresponds to the rising part of the HE component, so these data are crucial for investigation of the origin of nonthermal emission [64]. Yet, due to the shift of SED peaks, for some blazars the direct thermal emission from the accretion disc is visible in the optical-UV band (the big blue bump) which can be modeled to derive the accretion disc luminosity [148] and the black hole mass and so to understand the properties

of the central source. So, the Neil Gehrels Swift Observatory ([63], hereafter Swift), taking the data in Optical/UV and X-ray bands, is an ideal instrument (within its sensitivity limit) for observing distant blazars.
Even though in the γ-ray band the distant blazars are relatively faint as compared with the X-ray band, *Fermi* observations are still crucial. The γ-ray band corresponds to the falling part of the HE component which combined with the X-ray data will fully constrain the second peak in the SED. This is fundamental allowing to derive the physical parameters of the jets. The multiwavelength observations and theoretical interpretations are a regular approach and a unique way of probing the physical condition of the plasma in the jet. From the theoretical modeling point of view, distant blazars are excellent sources for studying accretion disc-jet connection in the early epoch of quasar formation as well as for probing the environments around supermassive black holes.
Identification of distant blazars and their investigation has always been one of the actively discussed topics in the blazar research [e.g., 127, 123, 68, 93, 14, 89, 10, 88, 106, 124]. In contrast to nearby blazars, good quality multiwavelength data are missing for the high redshift blazars, which significantly complicates their detailed study. However, due to improved sensitivity of the instruments (e.g., X-ray and γ-ray observatories) and wide-field surveys in the low energy bands (e.g., Sloan Digital Sky Survey [171] or WISE **(author?)** [169]), the number of high redshift blazars with sufficient multiwavelength data has been significantly increased. Along with continuous γ-ray observations of some distant blazars since 2008 this opens new perspectives for exploring the physics of distant blazars.
Motivated by the large number of detected high redshift γ-ray emitting blazars, with the aim to characterize their multiwavelength emission properties, we perform an intense broadband study of all the thirty-three known γ-ray blazars beyond redshift 2.5. Using the improved Pass 8 dataset which is more suitable for studying weak sources, we perform a detailed spectral and temporal analysis of *Fermi* γ-ray data accumulated during 2008-2018. The γ-ray flux variation, not well explored for distant blazars, is investigated for the considered ten years, using an improved adaptive binning method. To characterize the physical properties of the considered sources in the X-ray and optical/UV bands, the data from their observation with both Swift X-ray Telescope (XRT) and Ultraviolet and Optical Telescope (UVOT) in the previous fifteen years are analyzed. This allows to collect unprecedented data in the optical/UV, X-ray and γ-ray bands, which is used to constrain the multiwavelength SEDs. Then, through theoretical modeling of these SEDs, the physical parameters characterizing the sources (disc luminosity, black hole mass, etc.) and their jets (e.g., the distribution of underlying electrons, magnetic field, power, etc.) are derived, allowing a quantitative discussion and investigation of the state

of plasma in these powerful jets. Taking into account the large number of the considered sources (thirty-three) and the amount of analyzed data, this is one of the most comprehensive studies of most distant and powerful blazars.
The paper is organized as follows. In Section 5.2, the list of high redshift blazars is presented. The *Fermi* and Swift data extraction and analyses are described in Sections 5.3 and 5.4, respectively. The data analysis results are presented in Section 5.5 and the origin of the multiwavelength emission is discussed in Section 5.6. The discussion and conclusion are given in Section 4.7 and a summary in Section 4.8.

4.2 The Sample

The fourth catalog of AGNs detected by *Fermi* contains more than 2863 AGNs detected above the 5σ limit [5]. A small fraction of them (1.18%) are distant blazars $z > 2.5$ ($\sim$ 20.7 Gpc), including twenty-six FSRQs, two BL Lacs and five blazars of uncertain type (BCU). The coordinates, redshift and synchrotron peak classification of these sources are given in Table 4.1. The most distant source at $z = 4.31$ is the FSRQ GB 1508+5714, whereas the BL Lacs 87 GB 214302.1+095227 and MG1 J154930+1708 are at $z = 2.83$ and $z = 2.62$, respectively, which is interesting, since due to low γ-ray luminosity BL Lacs are rarely observed at these distances. In this paper, the data collected by *Fermi* and Swift are analyzed to study the multiwavelength emission from high redshift blazars ($z > 2.5$) selected from the fourth catalog of AGNs detected by *Fermi* which are presented in Table 4.1. Throughout this paper, we assume the following standard cosmological parameters of $H_0 = 71\ km\, s^{-1}\, Mpc^{-1}$ and $\Omega_\Lambda = 0.730$ [60].

4.3 Fermi-LAT observations

The *Fermi* data used in the current study had been accumulated during the first ten years of operation, from 4 August 2008 to 4 August 2018. The PASS 8 events from a circular region with a radius of 12° around each source in the energy range from 100 MeV to 500 GeV were downloaded and analyzed with the Fermi Tools (1.2.1) using P8R3 instrument response functions. Good data and time intervals were selected using gtselect and gtmktime tools (with selection cuts "Event class=128" and "evtype=3") using maximum zenith angle value of 90° to avoid the γ-ray detection from the earth's limb. Using gtbin tool, the events are binned into $16.9° \times 16.9°$ a square region of interest (ROI) with pixels of $0.1° \times 0.1°$ and into 37 equal logarithmically spaced energy bins. The model file of each source (point-like sources in-

Table 4.4 Summary of Swift-UVOT observations of the considered sources. For the sources, when several observations were available, the fluxes in each band are computed from the summed images. Averaged flux in each band is in units of erg cm^{-2} s^{-1}.

Object	V	B	U	$W1$	$M2$	$W2$
PKS 1351-108 –	–	–	$(4.54 \pm 2.53) \times 10^{-14}$	–	–	
MG3 J163554+3629	–	–	$(6.93 \pm 2.72) \times 10^{-14}$	–	–	$(7.50 \pm 4.11) \times 10^{-14}$
PKS 0537-286	$(3.78 \pm 5.86) \times 10^{-15}$	$(4.53 \pm 1.56) \times 10^{-14}$	$(3.54 \pm 0.42) \times 10^{-13}$	$(4.54 \pm 2.54) \times 10^{-14}$	$(6.84 \pm 0.75) \times 10^{-14}$	$(4.61 \pm 0.55) \times 10^{-13}$
TXS 0800+618	$(7.69 \pm 0.12) \times 10^{-15}$	–	$(2.39 \pm 0.6) \times 10^{-13}$	$(5.68 \pm 0.18) \times 10^{-15}$	–	$(6.58 \pm 0.13) \times 10^{-14}$
S4 1427+543	–	$(2.52 \pm 2.03) \times 10^{-14}$	$(2.53 \pm 0.92) \times 10^{-13}$	–	$(3.88 \pm 1.4) \times 10^{-14}$	$(1.50 \pm 0.02) \times 10^{-15}$
GB6 J0733+0456	–	$(2.97 \pm 2.55) \times 10^{-14}$	–	$(9.40 \pm 0.25) \times 10^{-15}$	–	–
B2 0743+25	–	$(4.92 \pm 0.82) \times 10^{-14}$	$(3.39 \pm 0.59) \times 10^{-13}$	–	$(1.12 \pm 0.22) \times 10^{-13}$	$(4.76 \pm 0.76) \times 10^{-13}$
PKS 0347-211	–	–	$(2.80 \pm 0.52) \times 10^{-13}$	–	$(1.69 \pm 0.5) \times 10^{-13}$	$(2.03 \pm 1.09) \times 10^{-13}$
S4 1124+57	$(1.16 \pm 0.85) \times 10^{-14}$	–	–	–	–	–
PKS 0438-43	$(7.90 \pm 0.1) \times 10^{-15}$	–	$(3.45 \pm 0.38) \times 10^{-13}$	–	–	$(8.02 \pm 0.69) \times 10^{-13}$
S4 2015+65	$(1.63 \pm 0.02) \times 10^{-15}$	–	–	$(6.91 \pm 0.33) \times 10^{-14}$	–	–
87 GB 214302.1+095227	$(1.01 \pm 0.48) \times 10^{-13}$	$(2.49 \pm 0.36) \times 10^{-13}$	–	$(2.78 \pm 0.72) \times 10^{-13}$	$(3.49 \pm 0.63) \times 10^{-13}$	–
MG2 J174803+3403	$(1.92 \pm 0.32) \times 10^{-13}$	$(2.53 \pm 0.25) \times 10^{-13}$	$(4.68 \pm 0.87) \times 10^{-13}$	$(2.40 \pm 0.33) \times 10^{-13}$	$(3.73 \pm 0.61) \times 10^{-13}$	$(3.20 \pm 1.52) \times 10^{-13}$
PKS 0834-20	–	–	$(7.82 \pm 0.54) \times 10^{-13}$	$(3.84 \pm 1.72) \times 10^{-14}$	$(2.39 \pm 0.36) \times 10^{-13}$	$(7.29 \pm 0.91) \times 10^{-13}$
TXS 0222+185	–	–	$(9.36 \pm 0.89) \times 10^{-13}$	–	$(8.18 \pm 1.11) \times 10^{-13}$	$(1.12 \pm 0.21) \times 10^{-12}$
OD 166	–	–	–	–	–	$(9.19 \pm 0.36) \times 10^{-14}$
TXS 0907+230	$(9.53 \pm 4.27) \times 10^{-14}$	$(9.66 \pm 3.17) \times 10^{-14}$	$(5.28 \pm 2.66) \times 10^{-13}$	$(8.77 \pm 3.31) \times 10^{-14}$	$(2.09 \pm 1.55) \times 10^{-13}$	–
PMN J1441-1523	–	–	$(6.33 \pm 4.81) \times 10^{-14}$	–	–	–
CRATES J05433+392803	–	–	–	$(1.90 \pm 0.88) \times 10^{-16}$	–	–
TXS 1448+093	–	–	$(6.53 \pm 2.36) \times 10^{-14}$	–	–	$(1.35 \pm 0.35) \times 10^{-13}$
PMN J0226+0937	$(9.95 \pm 4.17) \times 10^{-14}$	$(5.13 \pm 0.9) \times 10^{-13}$	$(1.22 \pm 0.06) \times 10^{-12}$	$(4.39 \pm 1.53) \times 10^{-13}$	$(1.30 \pm 0.06) \times 10^{-12}$	$(1.26 \pm 0.08) \times 10^{-12}$
PKS 0451-28	–	$(9.52 \pm 1.21) \times 10^{-14}$	–	–	–	–
B3 0908+416B	$(3.45 \pm 0.11) \times 10^{-15}$	$(3.46 \pm 2.22) \times 10^{-14}$	$(2.08 \pm 0.66) \times 10^{-13}$	$(4.94 \pm 1.95) \times 10^{-14}$	$(6.87 \pm 1.91) \times 10^{-14}$	$(2.67 \pm 1.2) \times 10^{-13}$
TXS 1616+517	–	–	$(1.96 \pm 0.27) \times 10^{-13}$	–	–	$(1.25 \pm 0.34) \times 10^{-13}$
B3 1343+451	–	$(3.12 \pm 2.77) \times 10^{-14}$	$(4.54 \pm 0.55) \times 10^{-13}$	$(7.41 \pm 0.23) \times 10^{-15}$	$(2.52 \pm 0.29) \times 10^{-13}$	$(4.47 \pm 0.65) \times 10^{-13}$
PKS 2107-105	–	–	$(1.74 \pm 0.1) \times 10^{-12}$	–	–	$(1.44 \pm 0.13) \times 10^{-12}$

cluded in the ROI and background) is generated using the 4FGL-DR2 version of the 4FGL which is based on 10 years of survey. The model file includes all 4FGL sources falling within the ROI $+5^{\circ}$ region. The gll_iem_v07 and iso_P8R3_SOURCE_V2_v1 models are used to parameterize the Galactic and extragalactic diffuse emission components. The spectral parameters set for the sources located within the ROI are allowed to be free in the analysis. The normalization parameters for the two diffuse components were also kept free.

The spectral analysis was performed using the binned maximum-likelihood method implemented in the gtlike tool. The source detection significance is estimated using the test statistic (TS) [109] defined as $TS = 2 \times (logL_1 - logL_0)$ where L_1 is the likelihood of the data with a point source at the given position and L_0 without the source. The γ-ray spectral models of each considered source were assumed to be the same as in the 4FGL, and for those with a log-parabola an additional fit with the power-law model was performed. The spectra were calculated by separately running gtlike for smaller energy intervals equal in logarithmic space. Then, using the gtsrcprob tool and the model file obtained from the likelihood fitting, the energy of the highest-energy photon detected from the direction of each source is computed.

4.3.1 γ-ray variability

The γ-ray light curves are calculated using the unbinned likelihood analysis method implemented in the gtlike tool. The spectra of the considered sources were modeled by a power-law which can provide a good representation of the data over the small bins of time. The normalization and photon index of the sample sources are allowed to vary while the photon indexes of all background sources within the ROI are fixed to their best values obtained from the fit of the entire 10-year data set. As the diffuse background emission should not be variable, the parameters of the background models are fixed as well. During the fitting, the events within 0.1-300 GeV with the appropriate quality cuts mentioned above are considered.
Initially, in order to study the variability, the γ-ray light curves with 30-day binning are calculated for all sources, considering the 0.1-300 GeV range. Additional light curves with short periods (days or a week) were computed for the statistically significant ($\geq 5\sigma$) γ-ray emitting periods identified in the monthly light curves. Next, using the adaptively binned method of **(author?)** [96], the γ-ray variability is studied further. At fixed time binning, when long time intervals are used, a possible fast flux variation will be smoothed out, while using short bins might result in many upper limits during the low-activity periods. In the adaptive binning approach, the time bin widths are adjusted to produce bins with constant flux uncertainty above the optimal energy (E_0) and this appraoch is proved to be a powerful method to search for γ-ray flux variation [e.g., 132, 145, 144, 21, 62, 54, 172]. E_0 depends on the flux and photon index of each source and can be computed following **(author?)** [96]. For the considered sources, adaptive binning light curves with 15% uncertainty are generated.

4.4 Swift observations

Swift is a multi-frequency space observatory, designed as a rapid response mission for follow-up observation of gamma-ray bursts (GRBs) [63]. Although its primary scientific goal is the observation of GRBs, due to wide frequency coverage, it is suitable for blazar studies. The data from two of the instruments onboard Swift UVOT [170-600 nm; 138] and XRT [0.3-10.0 keV; 35] have been analyzed in the current paper. Twenty-nine sources from Table 4.1 (except MRSS 291-081526, CRATES J233930+024420, MG1 J154930+1708 and B3 1624+414) were at least once observed by Swift. There are available data from multiple observations of some sources; e.g., B2 0743+25, PKS 0438-43, TXS 0222+185, TXS 1448+093, PMN J0226+0937, TXS 1616+517 and PKS 2107-105 had been observed more than ten times. The Swift XRT data anal-

ysis was possible to apply only for twenty two sources (see Table 4.3) and twenty six were detected in at least one of the optical-UV Swift-UVOT filters (see Table 4.4).
Swift UVOT data from all six bands are considered when available: UVW2 (188 nm), UVM2 (217 nm), UVW1 (251 nm), U (345 nm), B (439 nm) and V (544 nm). The photometry analysis of all our sources was performed using the standard UVOT software distributed within the HEAsoft package (v6.25) and the calibration included in the CALDB (v.20170922). The source counts for each filter are extracted from a circular region with a 5″ radius around the sources, while the background ones from a region with 20″ radius not being contaminated with any signal from the nearby sources. uvotsource tool was used to convert the source counts using the conversion factors provided by [129]. The fluxes were corrected for extinction using the reddening coefficient $E(B-V)$ from the Infrared Science Archive [1]. In the case of several observations for the same source, the analysis is performed using the same background region but validated that it is not contaminated by nearby objects in any filter. Also, light curves have been generated for investigation of the flux variation in each band. Then, if no significant variation is found, the spectral points are computed from the summed images, resulting in the flux estimation with reduced uncertainties.
The XRT data, taken both in photon counting and window timing modes were analyzed with standard XRTDAS tool distributed within the HEAsoft package (v6.25), applying standard procedures, filtering and screening criteria. The source counts were selected from a 20-pixel (47″) circle centered on the coordinates of each source, while those for the background- from an annulus with the same center and inner and outer radii of 51 (120″) and 85 pixels (200″), respectively. The Cash statistics [37] on ungrouped data was used, as for many observations the number of counts was low and did not contain the minimum number of counts required for Gaussian statistics. The 0.3-10 keV X-ray spectrum of each source is fitted with XSPEC12.10.1 adopting an absorbed power-law model with a neutral hydrogen column density fixed to its Galactic value in each direction.
Initially, for the considered sources, the X-ray spectral analysis was performed for each observation. However, for most of the sources, the count rate was below 20, preventing spectral fitting, and the photon index and flux could be estimated only for a few bright sources. Then, when several observations of the same source were available, they were merged to increase the photon statistics, and the averaged X-ray spectra were obtained. The merging was done using the tool available from the UK Swift Science Data Centre [2]

[1] http://irsa.ipac.caltech.edu/applications/DUST/
[2] https://www.swift.ac.uk/user_objects/

[56]. Again XSPEC was used to fit the 0.3-10 keV spectrum, testing both the absorbed power-law and log-parabola models. We note that the spectra of many sources could be constrained only by merging the observations.

4.5 Results of data analyses

The γ-ray data analysis results obtained from the power-law fit in the range from 100 MeV to 500 GeV are presented in Table 4.1 for each source, providing the γ-ray flux (F_γ), photon index, the detection significance (TS), the energy of the highest-energy events (E_{max}) detected from each object with the probability of its association with the target. The sources are detected with $TS > 34.05$ significance, except for S4 2015+65, which appeared with $TS = 23.77$. B3 1343+451 is detected with the highest significance of $TS = 34652.79$ (186.15σ), allowing to perform a detailed spectral and variability analysis. In addition, for the sources with the spectra modeled by a log-parabola in 4FGL, an additional fit with a log-parabola model was performed, the results of which are presented in Table 4.2. The curvature of the spectra of PKS 1351-018, B2 0743+25, PKS 0438-43, S4 2015+65, PKS 0834-20, and OD 166 is substantial ($\beta = 0.24 - 0.63$), so their γ-ray spectrum quickly declines. The flux estimated from the power-law fitting which yielded soft γ-ray spectra as well does not substantially differ from that obtained with a log-parabola. The only noticeable difference is found for PKS 1351-018; the flux estimated from the log-parabola fitting is $(6.86 \pm 1.66) \times 10^{-9}$ *photon* $cm^{-2}\,s^{-1}$ as compared with $(1.11 \pm 0.15) \times 10^{-8}$ *photon* $cm^{-2}\,s^{-1}$ when the spectrum was modeled by a power-law. However, for this source $\beta = 0.63 \pm 0.23$ was estimated implying its spectrum is curved significantly. Interestingly, the log-parabola fitting of S4 2015+65 spectrum resulted in detection of the source with $TS = 27.96$.

The results presented in Table 4.1 are shown in Fig. 4.1. The γ-ray photon index versus flux (estimated from power-law fitting) is shown in the upper left panel, where the FSRQs are circles, BL LACs triangles and BCUs squares. Even though the number of sources is not enough for population studies, some difference in various blazar types can be seen. The photon index ($\sim E^{-\Gamma_\gamma}$) estimated in the 0.1-500 GeV range ranges from 1.71 to 3.05 with a mean of 2.54. The soft γ-ray spectra of the considered sources (except 87 GB 214302.1+095227 and MG1 J154930+1708) indicate that the peak of the HE component in their SED is in the MeV range. The flux of considered sources ranges from 4.84×10^{-10} to 1.50×10^{-7} *photon* $cm^{-2}\,s^{-1}$. The two BL Lacs detected beyond $z = 2.5$, 87 GB 214302.1+095227 and MG1 J154930+1708, have the lowest flux, $(4.84 \pm 1.37) \times 10^{-10}$ *photon* $cm^{-2}\,s^{-1}$ and $(1.66 \pm 0.79) \times 10^{-9}$ *photon* $cm^{-2}\,s^{-1}$, respectively, but they have a harder γ-

ray spectrum. The γ-ray photon index of 87GB 214302.1+095227, which is the only ISP object among the selected sources, is 1.71 ± 0.19 and that of MG1 J154930+1708 is $\Gamma_\gamma = 2.01 \pm 0.16$. The γ-ray flux of BCUs included in the sample ranges from 2.19×10^{-9} *photon* $cm^{-2}\, s^{-1}$ to 1.46×10^{-8} *photon* $cm^{-2}\, s^{-1}$ with Γ_γ within $2.20 - 2.84$. The FSRQs occupy the region of high flux $\geq 3.89 \times 10^{-9}$ *photon* $cm^{-2}\, s^{-1}$ and $\Gamma_\gamma \geq 2.2$ with a mean $F_\gamma \simeq 2.11 \times 10^{-8}$ *photon* $cm^{-2}\, s^{-1}$. The highest γ-ray flux of $(1.50 \pm 0.02) \times 10^{-7}$ *photon* $cm^{-2}\, s^{-1}$ was observed from the bright FSRQ B3 1343+451.
The highest energy events (E_{max}) along with the probability of being associated with the sources are given in Table 4.1. As the sources mostly have a soft γ-ray spectrum or the γ-ray data are better modeled by a log-parabola, their γ-ray spectra do not extend to HEs and the photon energies are below 20 GeV; except for 87GB 214302.1+095227, MG2 J174803+3403, PMN J0226+0937 and B3 1343+451 from which photons with 67.15, 31.63, 56.42 and 24.25 GeV have been detected.

The flux, which is a function of the distance, is compared for each source in Fig. 4.1 (upper left panel). Even though it is informative, the total energy released from each source cannot be investigated. Next, using the observed flux (F_γ) and photon index (Γ_γ), the luminosity of each source is computed as:

$$L_\gamma = 4\,\pi\, d_L^2\, \frac{\Gamma_\gamma - 1}{\Gamma_\gamma - 2}\, \frac{E_{max}^{2-\Gamma_\gamma} - E_{min}^{2-\Gamma_\gamma}}{E_{max}^{1-\Gamma_\gamma} - E_{min}^{1-\Gamma_\gamma}}\, F_\gamma \tag{4.5.1}$$

where $E_{min} = 100$ MeV and $E_{max} = 500$ GeV. Fig. 4.1 (upper right panel) shows the distribution of the considered sources in the $\Gamma_\gamma - L_\gamma$ plane. The γ-ray luminosity of considered sources ranges from 1.01×10^{47} *erg* s^{-1} to 5.54×10^{48} *erg* s^{-1}. The lowest luminosity of $(1.01 \pm 0.38) \times 10^{47}$ *erg* s^{-1} has been estimated for CRATES J105433+392803 which is of the same order with that of the two BL Lacs included in the sample; $(1.42 \pm 0.98) \times 10^{47}$ *erg* s^{-1} for 87GB 214302.1+095227 and $(1.24 \pm 0.59) \times 10^{47}$ *erg* s^{-1} for MG1 J154930+1708. The luminosity of these BL Lacs corresponds to the highest end of the luminosity distribution of BL Lacs included in the fourth catalog of AGNs detected by *Fermi* [Fig. 10 in 13]. The γ-ray luminosity of only PKS 0347-211, PKS 0451-28, PKS 0537-286 and B3 1343+451 exceeds 10^{48} *erg* s^{-1} with the highest γ-ray luminosity of $(5.54 \pm 0.06) \times 10^{48}$ *erg* s^{-1}, estimated for B3 1343+451. Naturally, as compared to the distribution of all γ-ray emitting BL Lacs and FSRQs in the $\Gamma_\gamma - L_\gamma$ plane [13], the blazars considered here occupy the highest luminosity range. We note that the luminosities shown in Fig. 4.1 (upper right panel) have been computed based on the time-averaged γ-ray flux, and even higher luminosities are expected during γ-ray flares.
Table 4.3 shows the X-ray data analysis results, for each source presenting the neutral hydrogen column density, X-ray photon index (Γ_X), flux, and C-

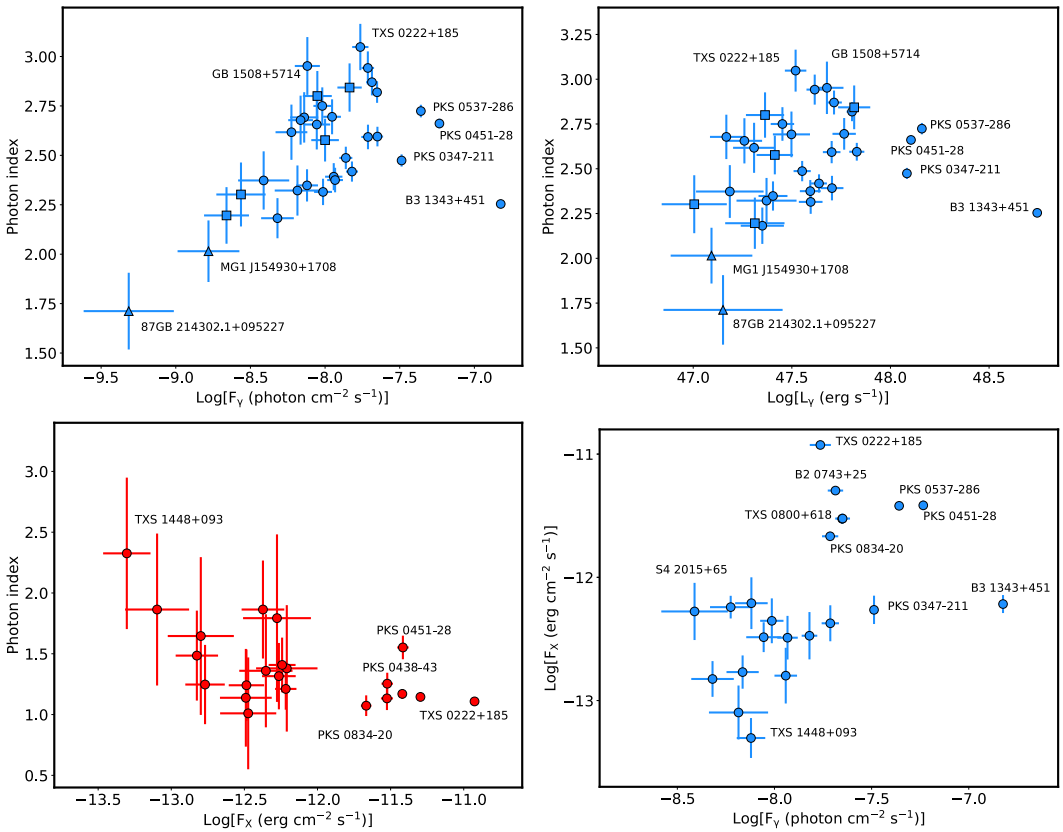

Figure 4.1 The γ-ray flux (> 100 MeV) and luminosity of considered sources versus the photon index are shown in the upper panels. BL lacs, FSRQs and BCUs are shown with triangles, circles, and squares, respectively. Lower left panel: The X-ray flux ($0.3 - 10$ keV) versus the photon index. Lower right panel: Comparison of γ-ray and X-ray (if available) fluxes.

stat/dof. The flux ranges from $\simeq 5 \times 10^{-14}\, erg\, cm^{-2}\, s^{-1}$ to $\simeq 10^{-11}\, erg\, cm^{-2}\, s^{-1}$, the highest flux of $(1.19 \pm 0.04) \times 10^{-11}\, erg\, cm^{-2}\, s^{-1}$ being observed for TXS 0222+185 ($z = 2.69$). Interestingly, from the sources considered here, only FSRQs are detected in the X-ray band; among BL Lacs, there are no observations for MG1 J154930+1708, while for 87GB 214302.1+095227, even after merging six observations, only 10 counts are detected. Also, BCUs included in Table 4.1 have not been detected in the X-ray band.
The X-ray flux is plotted versus the photon index in the lower left panel of Fig. 4.1. For several sources, the number of detected counts was not high enough, so the flux and photon index were estimated with large uncertainties. The X-ray photon index of considered sources is < 2.0, implying the X-ray spectra have a rising shape in the $\nu F\nu \sim \nu^{2-\Gamma_X}$ representation, which is natural as LSP blazars are considered. The only exception is TXS 1448+093 with $\Gamma_X = 2.33 \pm 0.62$, but even when merging its all 26 observations, the observed counts were only 25. This source is relatively faint in the X-ray band with a flux of $(5.01 \pm 1.85) \times 10^{-14}\, erg\, cm^{-2}\, s^{-1}$, so even an exposure of 2.39×10^4 sec is not enough to detect a reasonable number of counts. B3 0908+416B has the hardest X-ray spectrum with $\Gamma_X = 1.01 \pm 0.46$. In the $F_X - \Gamma_X$ plane, PKS 0451-28, TXS 0222+185, PKS 0834-20, PKS 0537-286, TXS 0800+618, B2 0743+25 and PKS 0438-43 are detached from the other sources because they have a comparably high X-ray flux, $F_{X-ray} \geq 2.13 \times 10^{-12}\, erg\, cm^{-2}\, s^{-1}$. In the lower right panel of Fig. 4.1, the γ-ray and X-ray (if available) fluxes of the considered sources are compared. Interestingly, the bright γ-ray sources PKS 0537-286 and PKS 0451-28 appear to be also bright X-ray emitters. The other bright γ-ray blazars (e.g., B3 1343+451, PKS 0451-28) do not have any distinguishable feature in the X-ray band, having a flux and photon index similar to those of the other considered sources. The bright X-ray sources TXS 0222+185, B2 0743+25, TXS 0800+618, and PKS 0834-20 appear with a similar flux in the γ-ray band, $F_\gamma = (1.72 - 2.23) \times 10^{-8}\, photon\, cm^{-2}\, s^{-1}$. In Fig. 4.6 the X-ray spectra of all sources included in Table 4.3 are shown in red.
The Swift UVOT data analysis was performed in all available filters. The results are consistent when different background regions are selected. Initially, all the single observations of the sources were analyzed to search for variability. However, the sources are relatively faint in the optical/UV bands and the large uncertainties in the flux estimation do not allow to investigate flux variation in time. Table 4.4 summarizes the results of the UVOT data analysis after merging the observations for each source, presenting the fluxes in the six UVOT filters (if available) with errors. In Fig. 4.6 these data are shown in light blue. In the SED of GB 1508+5714, PKS 1351-108, PKS 0537-286, TXS 0800+618, S4 1427+543, GB6 J0733+0456, B2 0743+25, PKS 0347-211, S41124+57, PKS 0438-43, S4 2015+65, PKS 0834-20, TXS 0222+185, TXS

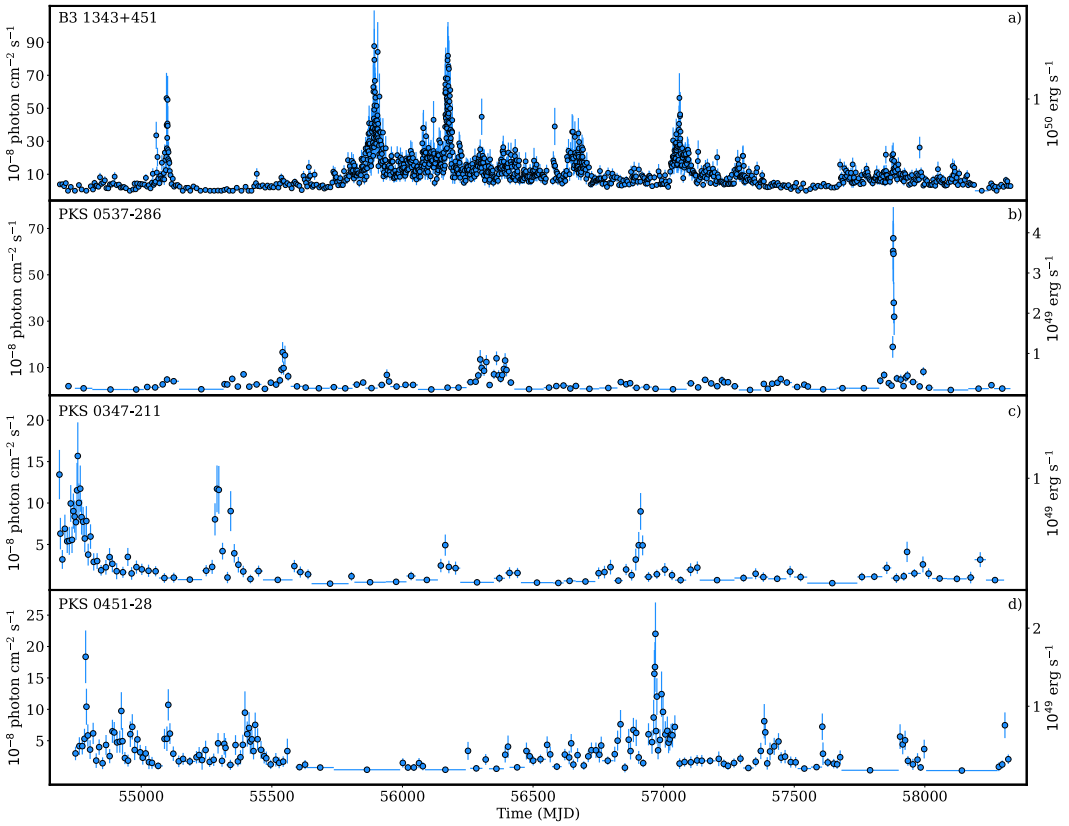

Figure 4.2 γ-ray light curve of B3 1343+451, PKS 0537-286, PKS 0347-211, and PKS 0451-28 for the period from August 2008 to August 2018 calculated using adaptively-binned timescales.

0907+230, PMN J0226+0937, PKS 0451-28 and PKS 2107-105, a thermal blue-bump component can be seen, which may represent the emission directly from the disc [73].

4.5.1 X-ray variability

The X-ray flux variability of some sources observed by Swift multiple times have been investigated. The data from each observation were processed and analyzed, but only for eight objects (marked with asterisks in Table 4.3) the number of counts was enough to constrain the flux and the photon index in a single observation. Except for PKS 0438-43, B2 0743+25 and TXS 0222+185, the X-ray emission appeared to be relatively constant, though the sources were observed in different years. For example, the X-ray flux of PKS 0537-286 was $(4.18 \pm 0.74) \times 10^{-12}\, erg\, cm^{-2}\, s^{-1}$ and $(4.53 \pm 0.89) \times 10^{-12}\, erg\, cm^{-2}\, s^{-1}$ on 26 October, 2006 and 12 May 2017, respectively. Fitting the flux observed

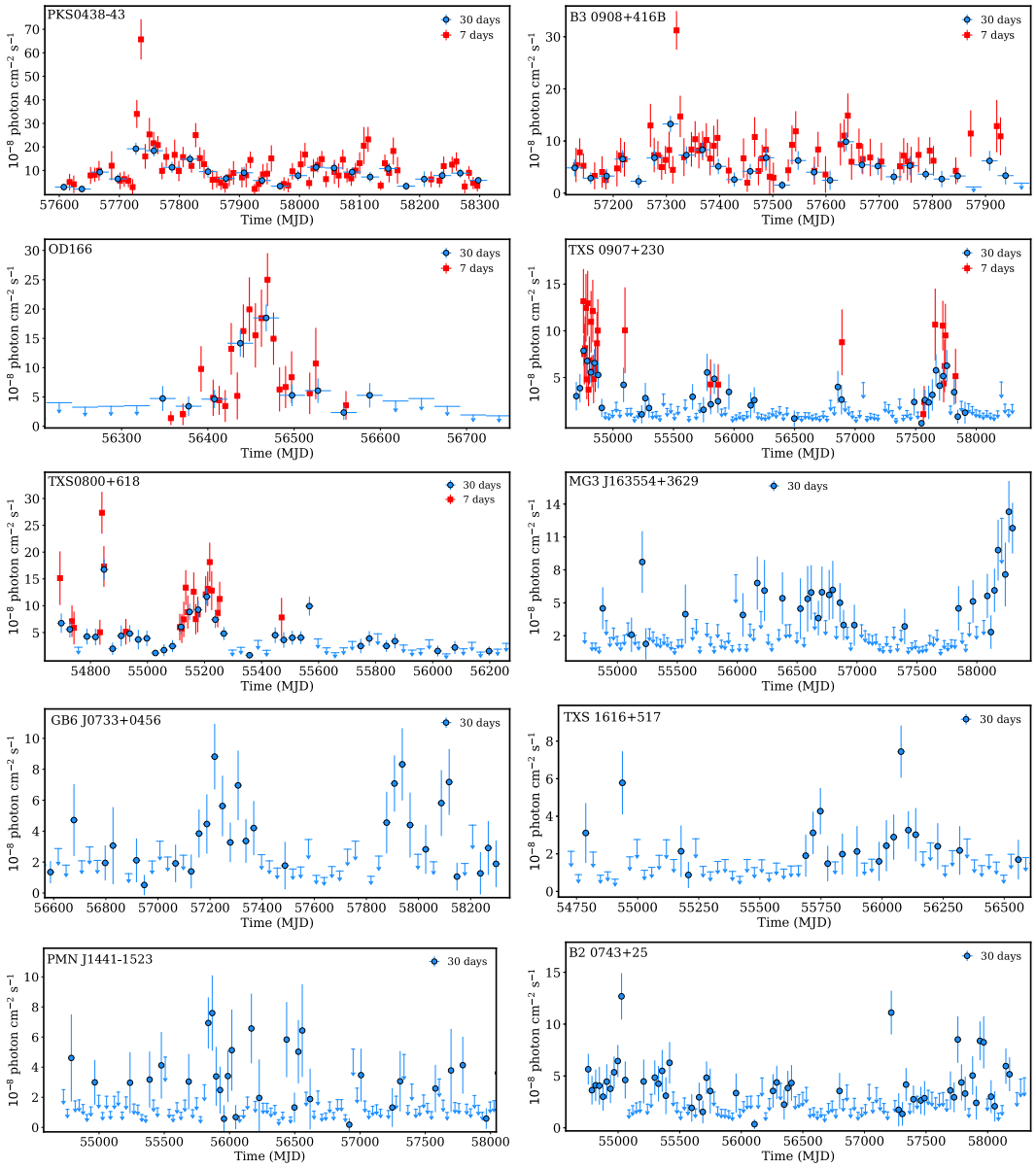

Figure 4.3 7-day (red) and 30-day (blue) binned light light curves of PKS 0438-43, B3 0908+416B, OD 166, TXS 0907+230, TXS 0800+618, MG3 J163554+3629, GB6 J0733+0456, TXS 1616+517, PMNJ 1441-1523 and B2 0743+25.

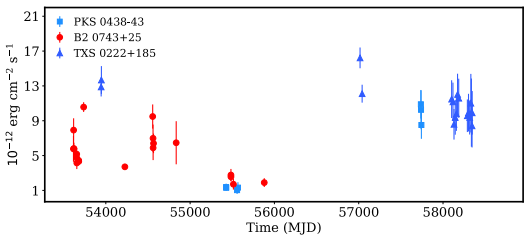

Figure 4.4 The 0.3-10 keV X-ray fluxes of PKS 0438-43, B2 0743+25 and TXS 0222+185 measured by Swift-XRT.

in different years with a constant flux, the $\chi 2$ test results in $P(\chi 2) = 0.38$ and $\chi 2/dof = 1.07$ which are consistent with no variability. Similarly, the $\chi 2$ test shows that the X-ray flux of TXS 0800+618, PKS 0834-20, PKS 0451-28 and B3 1343+451 is constant over different years. There is a marginal evidence ($P(\chi 2) = 0.038$ and $\chi 2/dof = 1.68$) that the X-ray flux of TXS 0222+185 is variable; it is mostly around $(0.96 - 1.1) \times 10^{-11}\, erg\, cm^{-2}\, s^{-1}$ which increased to $(1.62 \pm 0.13) \times 10^{-11}\, erg\, cm^{-2}\, s^{-1}$ and $(1.37 \pm 0.16) \times 10^{-11}\, erg\, cm^{-2}\, s^{-1}$ on 24 December 2014 and 31 July 2006, respectively. Instead, the $\chi 2$ test shows that the X-ray emission of PKS 0438-43 and B2 0743+25 is variable with $P(\chi 2) < 5.1 \times 10^{-6}$. PKS 0438-43 was in a bright X-ray state on 15 December 2016 with a flux of $(1.09 \pm 0.16) \times 10^{-11}\, erg\, cm^{-2}\, s^{-1}$ as compared with the flux of $(1.30 \pm 0.31) \times 10^{-11}\, erg\, cm^{-2}\, s^{-1}$ in the quiescent state. Similarly, the X-ray flux of B2 0743+25 in the high state on 01 January 2006 was $(1.06 \pm 0.56) \times 10^{-11}\, erg\, cm^{-2}\, s^{-1}$. The variation of the 0.3-10 keV X-ray flux of PKS 0438-43, B2 0743+25 and TXS 0222+185 is shown in Fig. 4.4. No variation of X-ray photon index was found, due to the large uncertainties in its estimation.

4.5.2 γ-ray variability

The continuous observation of the considered sources by *Fermi* allows a detailed investigation of their γ-ray flux variation during the considered ten years. When the source detection significance is $< 10\,\sigma$, the data are not enough for variability searches in month scales. Their emission could be variable in longer scales (6 or 12 months) more common for non-blazar AGNs [144], which is not investigated here. Initially, the light curves of all sources were calculated with the help of an adaptive binning method. However, the adaptively binned intervals were possible to compute only for the source with a detection significance of $> 37\,\sigma$. The adaptively binned light curves of B3 1343+451, PKS 0451-28, PKS 0347-211 and PKS 0537-286 computed above $E_0 = 163.9$, 163.2, 187.4 and 151.0 MeV, respectively, are shown in Fig. 4.2.

B3 1343+451 is the brightest and most variable source in the sample, and in its adaptively binned light curve (Fig. 4.2 a) several bright γ-ray emission periods can be identified: around MJD 55100, MJD 55890, MJD 56170, MJD 56640 and MJD 57060. During the bright γ-ray flaring periods, the flux changes in sub-day scales; there are 200 adaptive bins with a high flux and a width shorter than a day; the minimum adaptively binned time width is 6.33 hours observed on MJD 56176.34 when the source flux was $(7.52 \pm 1.85) \times 10^{-7}$ *photon* $cm^{-2}\, s^{-1}$ (above 163.9 MeV). Moreover, the width of 83 bins from these 200 is even shorter than 12 hours, which were mostly observed during the flares around MJD 55890 (24 bins) and MJD 56170 (35 bins). In the quiescent state (e.g., before MJD 55800, expect for the flare on MJD 55100) the γ-ray flux of the source is $\simeq (1-5) \times 10^{-8}$ *photon* $cm^{-2}\, s^{-1}$ which is lower than that averaged over 10 years (including the bright flaring states), reported in Table 4.1. The highest γ-ray flux of $(8.77 \pm 2.16) \times 10^{-7}$ *photon* $cm^{-2}\, s^{-1}$ above $E_0 = 163.9$ MeV with $\Gamma_\gamma = 2.48 \pm 0.29$ was observed on MJD 55891.7 with a detection significance of 9.1σ within a time bin having a width of 8.2 hours. It corresponds to a flux of $(1.82 \pm 0.45) \times 10^{-6}$ *photon* $cm^{-2}\, s^{-1}$ above 100 MeV which is 36.4 times higher than the γ-ray flux of the source in the quiescent state (before MJD 55800) but the Γ_γ is within the uncertainties of the value given in Table 4.1. During the hardest γ-ray emission period, $\Gamma_\gamma = 1.45 \pm 0.21$ was detected on MJD 56432 with a significance of 7.2σ, which is unusual for this source. Interestingly, there are twelve periods, mostly during the γ-ray flares, when its γ-ray spectrum was hard (≤ 1.70); one such period had been observed on MJD 55900.53 when, within a time bin having a width of 12.90 hours, Γ_γ was 1.64 ± 0.16 with a detection significance of 10.79σ. In the quiescent state, its γ-ray luminosity is $(2-4) \times 10^{48}$ *erg* s^{-1} which increased up to $\sim 1.5 \times 10^{50}$ *erg* s^{-1} during the bright γ-ray flares (Fig. 4.2 (a)).

The most distant source showing a substantial γ-ray flux increase in short periods is PKS 0537-286 at $z = 3.10$ (Fig. 4.2 b). The flaring activity of this source was first reported in [43] and the rapid (6 and 12 hours) γ-ray flux variations in **(author?)** [93]. During the extreme γ-ray flaring period from MJD 57878.05 to MJD 57881.55, the adaptively binned light curve confirms the intra-day γ-ray flux increase of PKS 0537-286 ; the adaptive time bin widths are 20.45, 15.96 and 18.90 hours. For comparison, during the flux increase around MJD 55540 and MJD 56390 the minimum time widths are 2.38 and 3.79 days, respectively. The average γ-ray flux of PKS 0537-286 is $(4.38 \pm 0.18) \times 10^{-8}$ *photon* $cm^{-2}\, s^{-1}$ (Table 4.1), but it significantly increased in MJD 55528-55553, MJD 56264-56400 and MJD 57878.0-57883.4. In the last period, during five consecutive time intervals, the γ-ray flux above 151.0 MeV was higher than 3×10^{-7} *photon* $cm^{-2}\, s^{-1}$, with a maximum of $(6.58 \pm 1.35) \times 10^{-7}$ *photon* $cm^{-2}\, s^{-1}$ observed on MJD 57879.2 with a detection significance of 10.57σ. This corresponds to a flux of $(1.29 \pm 0.26) \times$

10^{-6} *photon* $cm^{-2}\,s^{-1}$ above 100 MeV. During these periods, Γ_γ is 2.45 ± 0.23, 2.64 ± 0.27, 2.56 ± 0.28, 2.79 ± 0.34 and 2.91 ± 0.35, not significantly different from the value reported in Table 4.1 with no spectral hardening, which shows the emission is dominated by the MeV photons. However, during the flares, the luminosity of the source can be as high as $\simeq 4 \times 10^{49}\, erg\, s^{-1}$, putting PKS 0537-286 in the list of the brightest γ-ray blazars.
The adaptively binned light curves of PKS 0347-211 and PKS 0451-28 (Fig. 4.2 c and d) show several periods of γ-ray brightening, when a γ-ray flux increase within day scales is observed. For example, the shortest time interval when the flux increases is 2.65 days for PKS 0347-211, and it is 1.56 days for PKS 0451-28. The light curves of both sources reveal several γ-ray flaring periods when the flux substantially increased. For example, on MJD 54757.04 ± 2.71 the γ-ray flux of PKS 0347-211 above 187.4 MeV was $(1.57 \pm 0.41) \times 10^{-7}$ *photon* $cm^{-2}\,s^{-1}$, which corresponds to a flux of $(3.57 \pm 0.93) \times 10^{-7}$ *photon* $cm^{-2}\,s^{-1}$ above 100 MeV. In the case of PKS 0451-28, the peak γ-ray flux of $(2.20 \pm 0.50) \times 10^{-7}$ *photon* $cm^{-2}\,s^{-1}$ (above 163.2 MeV) was observed on MJD 56968.60 ± 0.79 with 9.64σ. This corresponds to a flux of $(3.70 \pm 0.84) \times 10^{-7}$ *photon* $cm^{-2}\,s^{-1}$ above 100 MeV. During this period, Γ_γ was 2.06 ± 0.19.
The light curves generated with the help of the adaptive binning method allowed to identify periods when the flux of some of the sources considered here (Fig. 4.2) increased in sub-day or days scales. It should be mentioned that expect for B3 1343+451, the short time scale variability of the other sources cannot be investigated using the regular time binning method, because in a large number of periods only upper limits are derived. Also, because of low statistics, the adaptively binned light curves were possible to compute only for the source presented in Fig. 4.2. For the other sources included in Table 4.1 the variability on week and month scales are investigated. In order to identify whether the γ-ray emission is variable or not, a simple $\chi 2$ test was performed [3]; the flux measured in each interval was fitted by a constant flux and the reduced $\chi 2$ and the probability of the flux being constant are computed.
The $\chi 2$ fitting indicated that the γ-ray emission of B3 0908+416B, TXS 0800+618, PKS 0438-43, OD 166 and TXS 0907+230 is variability in week scales while that of MG3 J163554+3629, GB6 J0733+0456, B2 0743+25, PMN J1441-1523 and TXS 1616+517 in month scales. For all these sources, $P(\chi 2) < 2.16 \times 10^{-4}$ was estimated. The γ-ray light curves of these sources with an evident increase in the flux are shown in Fig. 4.3. For example, during MJD 57729.16 ± 3.5 and MJD 57736.16 ± 3.5, the γ-ray flux of PKS 0438-43 above 100 MeV increased $15.2 - 29.3$ times as compared to its average flux and was $(3.40 \pm 0.59) \times 10^{-7}$ *photon* $cm^{-2}\,s^{-1}$ and $(6.57 \pm 0.86) \times 10^{-7}$ *photon* $cm^{-2}\,s^{-1}$, respectively. Likewise, the 7-day averaged peak values of the γ-ray flux of B3

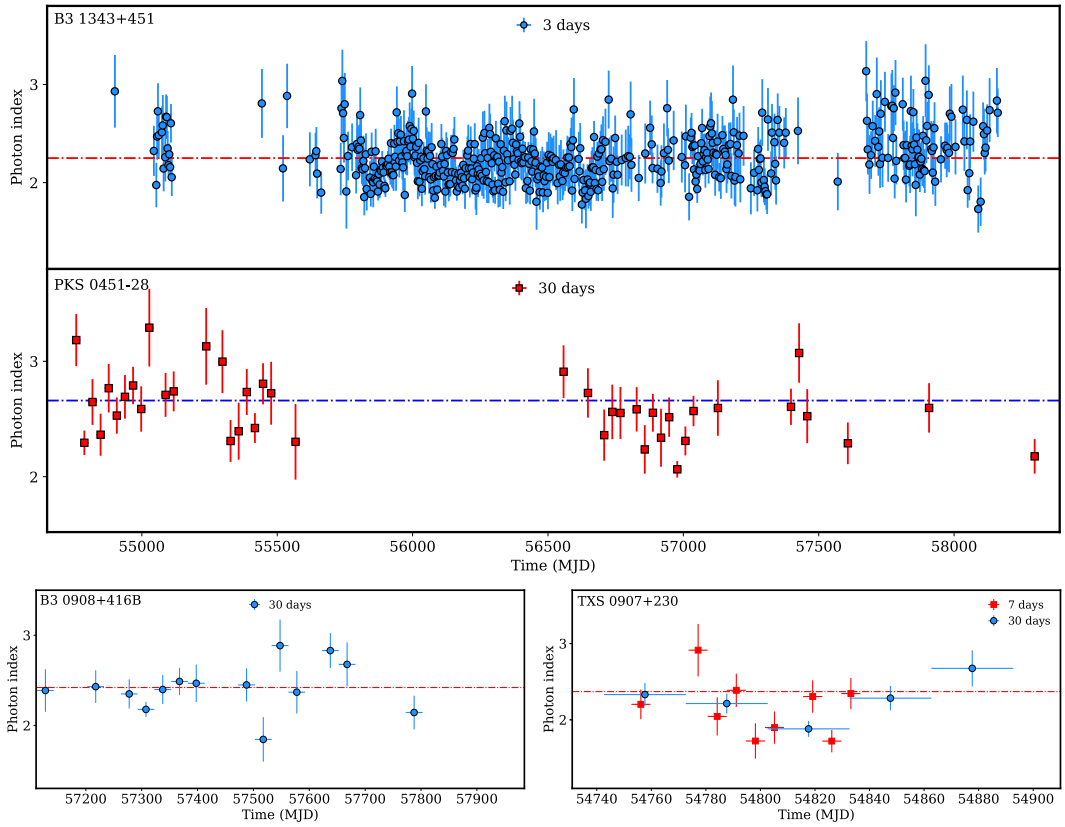

Figure 4.5 The evolution of the γ-ray photon indexes of B3 1343+451, PKS 0451-28, B3 0908+416B and TXS 0907+230 in time.

0908+416B, OD 166, TXS 0800+618 and TXS 0907+230 were $(3.12 \pm 0.37) \times 10^{-7}$ *photon* $cm^{-2}\, s^{-1}$, $(2.50 \pm 0.45) \times 10^{-7}$ *photon* $cm^{-2}\, s^{-1}$, $(2.73 \pm 0.39) \times 10^{-7}$ *photon* $cm^{-2}\, s^{-1}$ and $(1.32 \pm 0.34) \times 10^{-7}$ *photon* $cm^{-2}\, s^{-1}$, respectively, which exceed the corresponding values given in Table 4.1. The most distant γ-ray flaring blazar observed so far is MG3 J163554+3629 at $z = 3.65$; this source was reported to be in an active state on July 7 2018, when its daily averaged peak value of γ-ray flux was $(6.4 \pm 1.15) \times 10^{-7}$ *photon* $cm^{-2}\, s^{-1}$ [125]. The monthly averaged maximum γ-ray flux of $(1.33 \pm 0.28) \times 10^{-7}$ *photon* $cm^{-2}\, s^{-1}$ was observed on MJD 58267.66 ± 15 (May- June 2018). The source was also bright in γ-rays with a flux of $(1.18 \pm 0.23) \times 10^{-7}$ *photon* $cm^{-2}\, s^{-1}$ during June-July 2018 when the maximum daily averaged flux was observed [125].

For the considered sources, the γ-ray photon index evolution in time has also been investigated.The photon index is defined by the processes responsible for particle acceleration and cooling, and its significant changes are directly linked with the processes inside the jet. As the adaptively binned light curves have narrow time bins, the photon indexes are estimated with large

uncertainties which introduces difficulties for investigation of their variability. Therefore, the γ-ray light curves produced in 30 and 7 days (when available) are used to search for photon index variation, except for B3 1343+451 for which a 3-day binned light curve has been used. Moreover, in the light curves only the periods when the source detection was $TS > 25$ were considered, otherwise the large uncertainties on the photon index estimation would not allow to make definite conclusions. The simple $\chi 2$ test shows that among the considered sources only the photon index of B3 1343+451, PKS 0451-28, B3 0908+416B and TXS 0907+230 varies in time: the variation is highly significant for B3 1343+451 and PKS 0451-28 with $P(\chi 2) = 6.9 \times 10^{-4}$ and $P(\chi 2) \leq 10^{-5}$, respectively, and $P(\chi 2) \simeq 0.015$ for B3 0908+416B and TXS 0907+230. The evolution of the photon index of these sources in time is shown in Fig. 4.5 were the horizontal line corresponds to the averaged photon index estimated in ten years (Table 4.1). The photon index of B3 1343+451 clearly varies, the hardest spectrum being observed on MJD 58089.16 ± 1.5 with $\Gamma_\gamma = 1.73 \pm 0.24$; in total there are 60 periods when $\Gamma_\gamma < 2.0$. Interestingly, the γ-ray spectrum of the source was hard with 1.95 ± 0.07 when it was in a bright γ-ray flaring state on MJD 56172.16 ± 1.5. The γ-ray spectrum of PKS 0451-28 is usually soft but in the 30-day binned light curve the periods when $\Gamma_\gamma = 2.06 \pm 0.07$ and $\Gamma_\gamma = 2.17 \pm 0.15$ are observed on MJD 56977.66 ± 15 and 58297.66 ± 15, respectively. The first period overlaps with the large γ-ray flare evident in the adaptively binned light curve (see Fig. 4.2 a). The hardening of the γ-ray spectrum of B3 0908+416B on MJD 57517.66 ± 15 is remarkable when the Γ_γ changed to 1.84 ± 0.25 compared to 2.42 ± 0.05 averaged over 10 years. TXS 0907+230 is the most distant object in our sample ($z = 2.66$) with occasional hardening of its γ-ray spectrum. The 7-day binned light curve of TXS 0907+230 shows that there are three periods (on MJD 54798.16 ± 3.5, 54805.16 ± 3.5 and 54826.16 ± 3.5) when its γ-ray emission appears with an unusually hard γ-ray spectrum with $\Gamma_\gamma = 1.72 \pm 0.23$, 1.90 ± 0.21 and 1.72 ± 0.15. Yet, in the monthly binned light curve, in the bin covering these periods, Γ_γ is 1.88 ± 0.10 with a detection significance of 12.5σ. Even if the γ-ray photon index of MG3 J163554+3629 and PMN J0226+0937 appeared to be constant, hardening of their γ-ray spectra was occasionally observed. For example, for MG3 J163554+3629 $\Gamma_\gamma = 2.29 \pm 0.13$ (with 11.1σ) was observed from MJD 58282 to 58312, likewise for PMN J0226+0937 Γ_γ was 1.80 ± 0.16 (with 9.7σ) on MJD 54892-54922. The hard γ-ray spectra of the sources discussed above are shown in Fig. 4.6 in magenta; substantial changes in the γ-ray spectrum are evident. Such a hard γ-ray spectrum is more typical for BL Lacs, but it has also been occasionally observed for the FSRQs during the flares [e.g., see 117, 145, 62, 143, 124, 16].

In addition, γ-ray light curves with 30-day binning above 1 GeV are produced to investigate the flux and photon index variation in the GeV band.

Table 4.5 Parameters obtained from the modeling of multiwavelength SEDs. [1]: object name. [2]: Doppler factor. [3]: Slope of electron energy distribution. [4] and [5]: the Lorentz factors corresponding to the minimum and cutoff energy of the electron distribution. [6]: Magnetic field in units of G. [7] Radius of the emitting region in units of 10^{16} cm. [8] and [9]: Electron and magnetic field energy densities. [10]: accretion disk luminosity in units of $10^{46}\ erg\ s^{-1}$. [11] and [12]: The power of the jet in the form of the relativistic electrons (L_e) and magnetic field (L_B) in units of $10^{45}\ erg\ s^{-1}$ and $10^{43}\ erg\ s^{-1}$, respectively.

Sources	δ	α	γ_{min}	γ_{cut}	B	R	U_e	U_B	L_d	L_e	L_B
[1]	[2]	[3]	[4]	[5]	[6]	[7]	[8]	[9]	[10]	[11]	[12]
GB 1508+5714	15.72 ± 1.29	1.17 ± 0.07	26.90 ± 2.88	1.30 ± 0.10	0.19 ± 0.02	2.28	0.50	1.49	3.02	2.43	0.73
PKS 1351-018	20.47 ± 2.49	2.16 ± 0.11	2.68 ± 0.36	4.99 ± 0.71	0.20 ± 0.02	2.29	0.54	1.66	4.04	2.68	0.82
PKS 0537-286	11.50 ± 0.57	1.33 ± 0.07	15.70 ± 1.49	2.45 ± 0.16	0.28 ± 0.02	1.14	5.93	3.21	3.44	7.31	0.40
TXS 0800+618	14.04 ± 0.56	2.75 ± 0.04	13.98 ± 0.86	2.20 ± 0.02	0.26 ± 0.01	15.5	0.06	2.73	1.65	13.49	61.84
S4 1427+543	10.00 ± 0.37	2.04 ± 0.10	29.00 ± 2.55	2.79 ± 0.27	0.53 ± 0.04	1.90	0.63	10.02	1.83	2.14	3.75
GB6 J0733+0456	16.28 ± 1.36	2.80 ± 0.04	47.90 ± 3.42	15.73 ± 1.60	0.16 ± 0.03	2.98	0.12	6.22	3.40	0.98	5.20
PKS 0347-211	26.00 ± 1.02	2.79 ± 0.02	23.09 ± 1.12	2.62 ± 0.16	0.20 ± 0.01	8.15	0.03	1.61	1.99	1.72	10.08
B2 0743+25	10.02 ± 0.45	1.13 ± 0.19	7.66 ± 0.22	2.03 ± 0.08	0.36 ± 0.01	0.70	16.90	0.003	3.58	7.80	0.24
S4 1124+57	22.17 ± 1.37	2.78 ± 0.04	22.92 ± 1.45	1.28 ± 0.10	0.22 ± 0.01	5.15	0.14	1.95	1.69	3.39	4.87
PKS 0438-43	18.17 ± 1.29	2.78 ± 0.04	23.13 ± 1.54	7.19 ± 0.58	0.34 ± 0.02	5.42	0.12	4.52	3.91	3.33	12.52
S4 2015+65	17.85 ± 1.32	2.73 ± 0.05	20.63 ± 1.64	2.75 ± 0.29	0.46 ± 0.03	13.50	0.07	8.41	4.55	1.26	14.44
MG2 J174803+3403	24.50 ± 2.06	2.87 ± 0.06	14.67 ± 1.58	1.40 ± 0.49	1.45 ± 0.09	7.41	0.004	83.98	8.87	0.23	434.69
PKS 0834-20	27.42 ± 0.97	2.70 ± 0.06	20.57 ± 1.51	2.13 ± 0.18	0.37 ± 0.02	6.83	0.02	5.44	5.51	0.70	23.92
TXS 0222+185	10.03 ± 0.28	1.62 ± 0.05	19.56 ± 0.98	2.38 ± 0.10	0.35 ± 0.02	1.07	10.28	5.04	2.71	11.10	0.54
OD 166	19.02 ± 0.84	1.96 ± 0.04	2.58 ± 0.15	1.01 ± 0.03	1.15 ± 0.05	4.32	0.01	0.52	0.53	0.25	92.38
TXS 0907+230	21.66 ± 1.66	2.23 ± 0.11	20.26 ± 1.84	1.44 ± 0.10	0.31 ± 0.02	5.23	0.03	3.72	1.09	0.70	5.96
PMN J1441-1523	17.01 ± 1.50	2.19 ± 0.07	2.86 ± 0.29	3.31 ± 0.46	1.68 ± 0.14	1.47	0.07	112.38	0.17	0.14	22.85
TXS 1448+093	17.90 ± 1.13	1.52 ± 0.15	49.64 ± 5.82	0.84 ± 0.06	0.70 ± 0.05	7.96	0.003	19.44	0.56	0.17	115.93
PMN J0226+0937	25.02 ± 1.98	2.41 ± 0.04	5.37 ± 0.59	8.32 ± 0.62	1.74 ± 0.12	3.09	0.03	119.86	10.94	0.03	107.98
PKS 0451-28	26.14 ± 1.27	2.90 ± 0.28	$21.93 \pm 1.3'$	2.19 ± 0.01	0.45 ± 0.03	5.90	0.11	8.01	7.20	3.59	26.32
B3 0908+416B	23.22 ± 1.72	1.31 ± 0.25	6.41 ± 0.72	1.11 ± 0.10	0.39 ± 0.03	1.76	0.09	6.10	0.43	0.26	1.78
TXS 1616+517	10.11 ± 0.31	2.09 ± 0.09	93.28 ± 4.15	4.34 ± 0.36	0.52 ± 0.02	3.59	0.06	10.79	0.35	0.70	13.11
B3 1343+451	26.55 ± 1.04	2.48 ± 0.04	16.49 ± 1.31	8.67 ± 0.48	0.10 ± 0.01	4.16	0.11	0.42	0.48	1.76	0.68
PKS 2107-105	27.32 ± 1.34	2.30 ± 0.06	7.45 ± 0.90	3.63 ± 0.39	0.67 ± 0.05	9.48	0.0006	17.73	8.30	0.05	150.16

The periods when the source emission is significant above 1 GeV are also relevant for studying absorption through interaction with EBL photons. There are only a few periods when the considered sources have been detected above 1 GeV with a sufficient significance ($> 5\,\sigma$). The emission, in these periods, is mostly characterized by a soft γ-ray spectrum, implying these are the same components as those at lower energies. However, the periods when the sources were detected by *Fermi* correspond to only a small fraction of the total bins (30-day binning), so the poor statistics did not allow us to investigate the possible flux variation or photon index hardening above 1 GeV.

4.6 The origin of multiwavelength emission

The multiwavelength emission from blazars produced when the accelerated electrons [66, 29, 104, 26, 151, 69] or protons [48, 23, 25, 101, 102, 100, 111, 113] interact with the magnetic and photon fields, contain valuable information

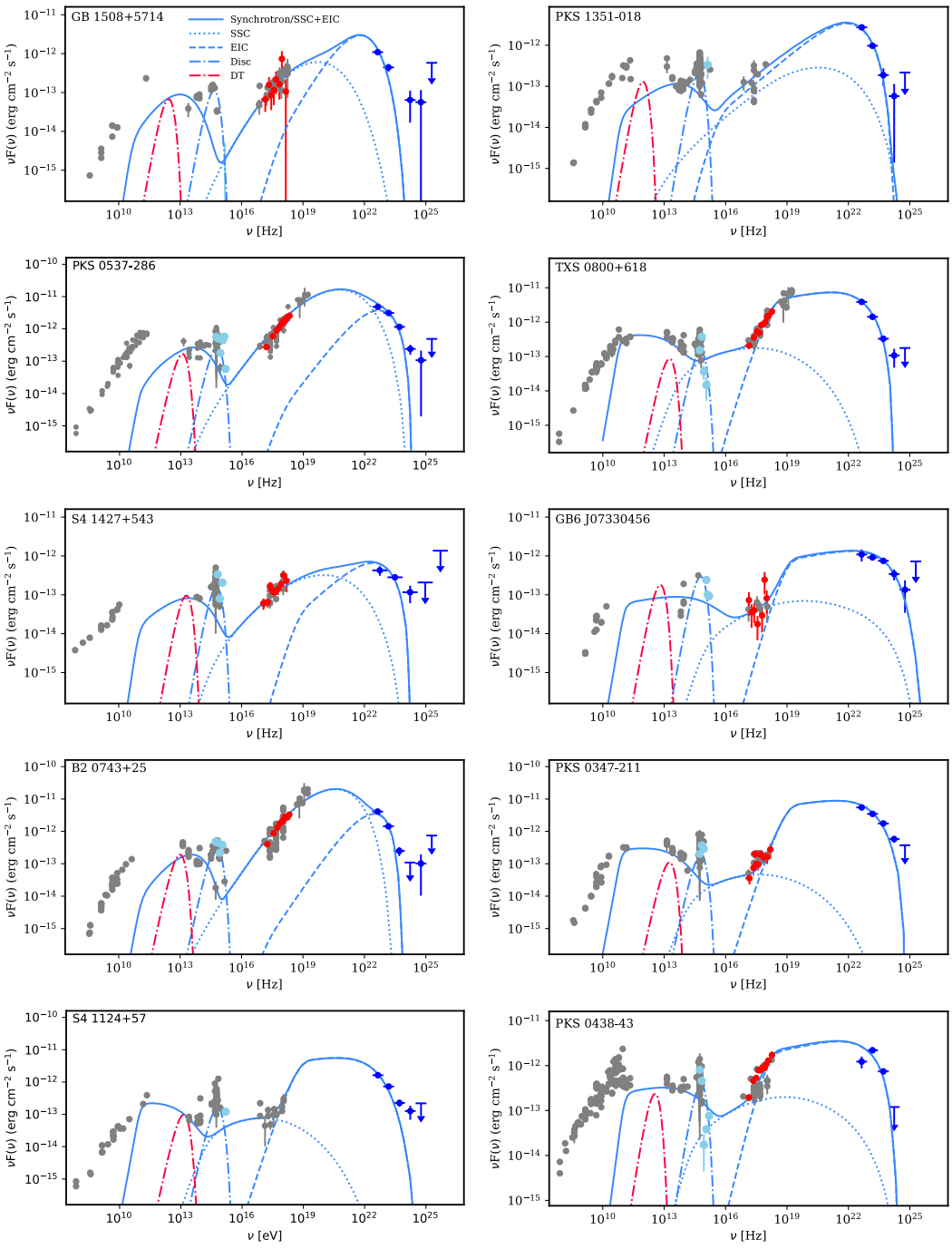

Figure 4.6 Modeling of the broadband SEDs of the considered sources. The Swift UVOT, XRT and *Fermi* data obtained here are shown with cyan, red and blue, respectively, while the archival data are in gray.

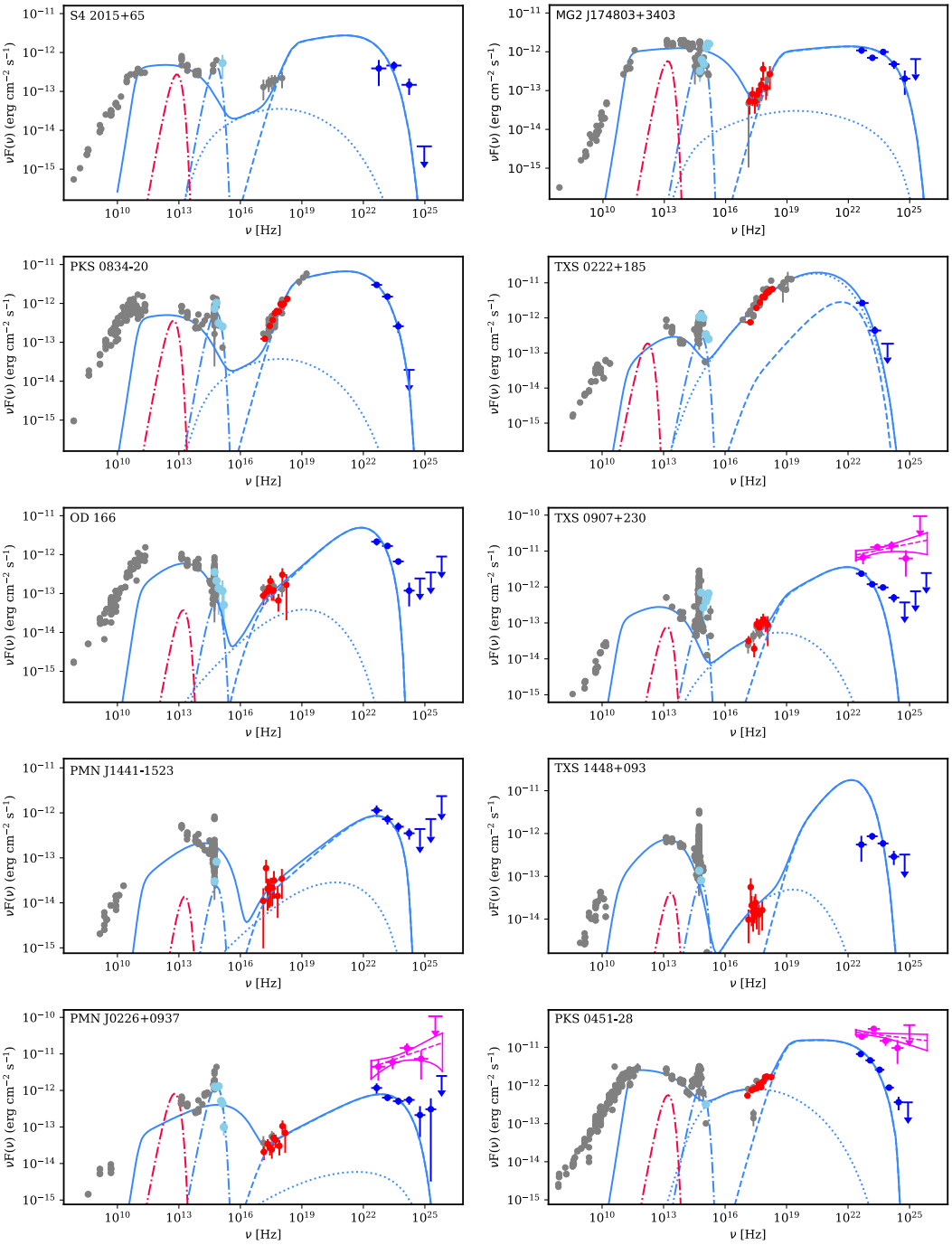

Figure 4.6 (Continued)

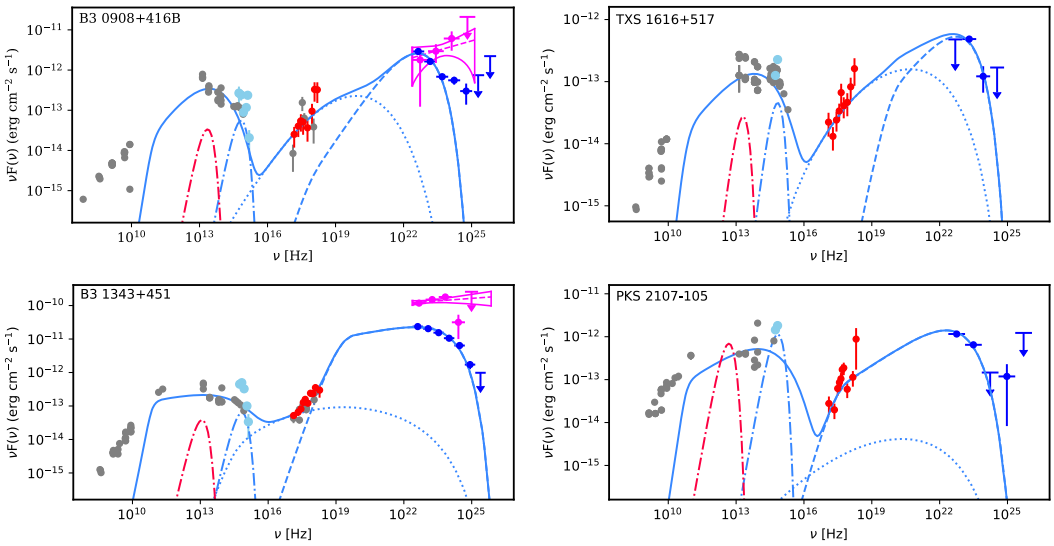

Figure 4.6 (Continued)

necessary for understanding the physics of their jets. The currently proposed models can explain a single SED snapshot, but they cannot self-consistently explain the dynamical evolution of the radiation and origin of the flares. The flares are most likely caused by changes in the radiating particles or in the emission region [e.g., 122], and their origin can be investigated only with contemporaneous multiwavelength data. During the γ-ray flaring of the considered sources (Figs. 4.2 and 4.3), contemporaneous Swift data are available only for PKS 0438-43 and TXS 0800+618. However, the Swift observations in these periods show that the X-ray photon index and flux did not change, being the same as those given in Table 4.3, whereas in the optical/UV bands these sources were detected only in one or two UVOT filters with large uncertainties in the flux estimation. So, it is not clear whether or not the low energy component changed or remained the same during the γ-ray flares. This introduces uncertainties for the theoretical modeling and does not allow to model the SEDs of these two objects during their γ-ray flaring. Moreover, as there are no multiwavelength data during the γ-ray flares of the other sources and our goal is to constrain the main physical parameters of distant blazar jets, only the averaged multiwavelength SEDs have been used in the modeling which represent the typical state of the sources.

To understand the origin of the broadband emission of the considered sources, we have used a simple one-zone leptonic model. In this model, the emission region is assumed to be a spherical blob of radius of R moving in the blazar jet with a bulk Lorentz factor of Γ_j at a viewing angle of θ. The emitting

region is filled with a uniformly tangled magnetic field B and with a homogeneous population of relativistic electrons (and positrons), the nonthermal energy distribution of which is described by a power-law with an exponential cut-off at higher energies as:

$$N(\gamma) \sim \gamma^{-\alpha} exp(-\gamma/\gamma_{cut}) \qquad \gamma > \gamma_{min} \tag{4.6.1}$$

where γ is the Lorentz factor of electrons in the blob rest frame, and α is the power-law index. γ_{min} and γ_{cut} are the Lorentz factors corresponding to the minimum and cutoff energy of the electron distribution in the emission region. The total energy of the electrons in the emitting region is defined as $U_e = m_e\, c^2 \int \gamma N_e(\gamma) d\gamma$. The energy distribution of electrons given by Eq. 4.6.1 is formed when the emitting particles are accelerated with a limiting process at higher energies (e.g., cooling or limited efficiency of the acceleration process). The power-law index (α) defines the properties of the acceleration mechanism [e.g., 91, 55, 156, 53], and γ_{cut} allows constraining the cooling process of the particles and the state of plasma in the jet [22, 143].
In this interpretation, the parameters of the emitting region are the radius, Doppler factor ($\Gamma = \delta$, for small viewing angles), and magnetic field. The magnetic field is a free parameter during the fitting (assuming its density $B^2/8\pi$ scales with U_e), while in principle a constraint on the other two parameters can be derived from the data. For example, a lower limit on δ can be imposed using high-resolution radio data or the emitting region size can be constrained from $R \leq \delta \times c \times t/(1+z)$, provided the minimum variability time is known. Unfortunately, both constraints cannot be assessed for all the sources given in Table 4.1, so both parameters have been left free during the fitting. In this case, R is constrained from the observed Compton Dominance (CD- the IC to the synchrotron peak luminosities ratio) and from polynomial fitting of the data (see the documentation of jetset [3]).
In the modeling it is assumed that the low-energy peak (from radio to optical/UV) is due to synchrotron emission from ultrarelativistic electrons in the jet with an energy distribution as given by Eq. 4.6.1. Instead, the HE peak is due to the IC scattering of internal [SSC; 66, 29, 104] or external photons [EIC; 26, 151, 69]. The IC scattering of external photons is considered, since the SEDs of FSRQS are better explained by EIC, as shown by the previous studies [e.g., 12, 6, 98, 83, 62], and the CD is evident in the SEDs of the considered sources (Fig. 4.6). Localization of the emission region in the jet is an open question and along the jet, depending on the distance from the central black hole, different photon fields can be dominant for the IC scattering [153]. In this paper we assume that the emitting region is outside the broad-

[3] https://jetset.readthedocs.io/en/latest/

line region (BLR) where the dominant photon field is the IR emission from the dusty torus. **(author?)** [152] showed that in MeV blazar SEDs the shift of the peak of the HE component to lower energies is most likely due to the comptonization of IR photons from the dusty torus. The IR radiation from the dusty torus is assumed to have a blackbody spectrum with a luminosity of $L_{IR} = 0.6\, L_{disc}$ [see 12] where L_{disc} is the accretion disk luminosity, which fills a volume that for simplicity is approximated as a spherical shell with a radius of $R_{IR} = 2.5 \times 10^{18}\, (L_d/10^{45})^{1/2}\, cm$ [116] with the energy density of $u_{IR} = 0.6\, L_d / 4\pi R_{IR}^2\, \delta^2$ in the co-moving frame of the jet. In **(author?)** [68] and **(author?)** [106], the HE component in the SED of distant blazars was modeled by IC scattering of BLR reflected photons, adopting a smooth broken power-law shape of the emitting electrons. We refer the reader to these papers for details on the modeling when BLR reflected photons are considered.
The broadband SEDs have been modeled using the jetset version 1.1.2 numerical leptonic code [161, 160, 108]. The free model parameters (those of the emitting electrons, δ, R and B) are constrained by using the Minuit optimizer. The emission directly due to accretion emerges primarily in the UV band, showing a UV excess in the SED, which is modeled by adding a blackbody component [73]. Fitting of this excess allows us to estimate the disc photons temperature and luminosity. When the excess UV component is not distinguished, an upper limit is derived by requiring that the disc emission does not exceed the observed nonthermal emission from the jet.

4.6.1 SED modeling results

The SEDs modeling results are presented in Fig. 4.6 and the corresponding parameters in Table 4.5. The archival data from the Space Science Data Center [4] are in gray, while the optical/UV, X-ray, and γ-ray data, obtained here, are shown in cyan, red, and blue, respectively. The radio data are not included in the SED fits but are considered only as upper limits. The observed radio emission is assumed to originate from a different and extended region. The hard γ-ray emission spectra of TXS 0907+230, PMN J0226+0937, PKS 0451-28, B3 0908+416B, and B3 1343+451 are in magenta, showing that the γ-ray flux increases and their spectra extend to higher energies. As high redshift blazars are considered ($z > 2.5$), their optical/UV flux could be affected by absorption of neutral hydrogen in intervening Lyman-α absorption systems. Following **(author?)** [68] this was corrected using the mean attenuation from **(author?)** [64] which was computed for six wavelengths approximately centred in the UVOT filters.
The SEDs in Fig. 4.6 contain enough data from radio to HE γ-ray bands to

[4] http://www.ssdc.asi.it

shape both low and high energy peaks. The applied model reproduces the multiwavelength data relatively well for almost all the sources. The γ-ray data of TXS 1448+093 are not well explained by the model because in this case the optical/UV data are clearly constraining the HE tail of the electron distribution and if considering $\alpha > 2.0$ (softer than the estimated spectrum with $\alpha = 1.52 \pm 0.15$), the flux predicted by the model will be lower than the data. Due to the large uncertainties in the S4 2015+65 γ-ray data the modeling is difficult, so the best possible one is shown. The electron power-law index is defined by the X-ray data [through $\alpha = 2\Gamma_X - 1$ relation 140] and depending on whether the SSC or EIC component is dominating in the X-ray band, different values for α are obtained. When the X-ray spectrum is hard and the SSC component is dominating, the energy distribution of the emitting electrons has a hard spectrum as well. For example, for GB 1508+5714, PKS 0537-286, B2 0743+25, TXS 0222+185 and B3 0908+416B, $\alpha = 1.17 \pm 0.07$, 1.33 ± 0.07, 1.13 ± 0.19, 1.62 ± 0.05 and 1.31 ± 0.25 were estimated which shows that the emission is due to newly accelerated electrons. The X-ray emission from S4 1427+543 and TXS 1616+517 is also dominated by the SSC component but because of large uncertainty in the X-ray photon index and flux estimations, correspondingly $\alpha = 2.04 \pm 0.10$ and 2.09 ± 0.09 have been obtained. On the contrary, when the emission in the X-ray and γ-ray bands is only defined by the EIC component then $\alpha > 2.2$; e.g., $\alpha = 2.75 \pm 0.04$ and 2.70 ± 0.06 are correspondingly estimated for TXS 0800+618 and PKS 0834-20. Correspondingly, γ_{min} and γ_{cut} are in the range of $2.58 - 93.28$ and $(1.01 - 15.73) \times 10^3$ (excluding TXS 1448+093). The SSC bump in the X-ray band is sensitive to γ_{min} values [73, 158, 173] and those estimated here are well within the range usually estimated for the FSRQs [see Fig. 4 in 173]. As expected [40], lower values of γ_{min} are estimated when the X-rays are produced only by the EIC component: e.g., $\gamma_{min} = 2.68 \pm 0.36$ and 2.58 ± 0.15 are correspondingly estimated for PKS 1351-018 and OD 166. The HE tails of both synchrotron and IC components are well defined by the optical/UV and γ-ray data, respectively, allowing precise estimation of $\gamma_{cut} = (1.01 - 15.73) \times 10^3$. γ_{cut} is in a strong dependence on α, and its highest value, $(15.73 \pm 1.60) \times 10^3$ was estimated when $\alpha = 2.80 \pm 0.04$ (the SED of GB6 J0733+0456 in Fig. 4.6). Meanwhile, when $\alpha = 2.2 - 2.5$, the highest γ_{cut} is $(8.67 \pm 0.48) \times 10^3$ for B3 1343+451.
The modeling shows that the magnetic field in the emitting region is within $0.10 - 1.74$ G. The highest values of 1.74 ± 0.12, 1.68 ± 0.14, 1.45 ± 0.09 and 1.15 ± 0.05 G are estimated for PMN J0226+0937, PMN J1441-1523, MG2 J174803+3403, and OD 166, respectively. The estimated Doppler factor is from $\delta = 10.00$ to $\delta = 27.42$ with a mean of $\delta = 19.09$. Although, these are higher than the average values estimated for FSRQs [e.g., 71, 126], they are well within the range of physically realistic values [e.g., see 95]. The emitting region size is within $R = (0.70 - 9.48) \times 10^{16}$ cm except for TXS 0800+618 and S4 2015+65

for which $R = 1.55 \times 10^{17}$ cm and 1.35×10^{17} cm, respectively. The values estimated for R are consistent with the γ-ray flux variation in a day or several day scales and suggest that the multiwavelength emission is produced in the sub-parsec scale regions of the jet.
The energetics of the considered sources can be estimated using the modeling results. First, the available data allows a straightforward estimation of the disc luminosity of GB 1508+5714, PKS 1351-108, PKS 0537-286, TXS 0800+618, S4 1427+543, GB6 J0733+0456, B2 0743+25, PKS 0347-211, S41124+57, PKS 0438-43, S4 2015+65, PKS 0834-20, TXS 0222+185, TXS 0907+230, PMN J0226+0937, PKS 0451-28 and PKS 2107-105, under the assumption that the disc has a black body spectrum. The estimation shows that $L_d \simeq (1.09 - 10.94) \times 10^{46}\, erg\, s^{-1}$ with a highest value of $L_d \simeq 1.09 \times 10^{47}\, erg\, s^{-1}$ estimated for PMN J0226+0937. Such high luminosities are obtained as very powerful blazars are considered here, and they are of the same order as those usually estimated for bright FSRQs [117] and distant blazars [68, 127]. The jet power in the form of the magnetic field (L_B) and relativistic electrons (L_e) is calculated as $L = \pi R^2 c\, \Gamma^2\, U_i$, where U_i is either electron (U_e) or magnetic field (U_B) energy density, using the parameters from Table 4.5. The corresponding values are given in Table 4.5, showing that L_e is in the range of $(0.03 - 13.49) \times 10^{45}\, erg\, s^{-1}$ while L_B in $(0.24 - 434.69) \times 10^{44}\, erg\, s^{-1}$. L_B and L_e are of the same order with $L_e/L_B = 2.92$ and 0.61 for PKS 0834-20 and PMN J1441-1523 respectively, while for MG2 J174803+3403, OD 166, TXS 1448+093, PMN J0226+0937, PKS 2107-105 $L_B/L_e = 3.7 - 36.0$. For the other sources of Table 4.5, L_e exceeds L_B, the largest deviation of $L_e/L_B \geq 1800$ being found for PKS 0537-286, B2 0743+25 and TXS 0222+185, which are the only sources when the hard X-ray emission above the Swift XRT band is modeled with a SSC component and the EIC is dominating at higher energies. However, we note that the luminosities can be higher when the SEDs in the flaring periods are modeled.

4.7 Discussion and Conclusion

Fermi has detected MeV/GeV emission from $\sim$ 2500 blazars, which are bright emitters across the whole electromagnetic spectrum. *Fermi* has sufficient sensitivity to detect blazars farther than $z = 2.0$, which are among the most powerful objects in the Universe. The distant objects ($z > 2.0$) represent a small fraction of the total observed sources (3.75 %), but their investigation is crucial for the study of the powerful relativistic outflows and measurement of the EBL photon density. We selected the most distant blazars ($z > 2.5$) from 4FGL and studied their multiwavelength emission properties by analyzing *Fermi* , Swift XRT and UVOT data. Also, the origin of their multiwave-

length emission is investigated through theoretical modeling of the broad-band SEDs.
In the X-ray and γ-ray bands, the spectra of the considered sources have different properties; except for TXS 1448+093, the X-ray spectrum of the other sources is hard with $\Gamma_X = 1.01 - 1.86$ while in the γ-ray band $\Gamma_\gamma > 2.2$. Thus, the X-ray and γ-ray data are determining that the second peak in the SED is within $10^6 - 10^8$ eV. The γ-ray flux of the considered sources is from 4.84×10^{-10} to 1.50×10^{-7} $photon\ cm^{-2}\ s^{-1}$, and in the $\Gamma_\gamma - L_\gamma$ plane, they occupy the area more typical for bright blazars, which is natural, since the sources at large distances should be powerful enough to be detected. The two BL Lacs included in the sample, 87GB 214302.1+095227 and MG1 J154930+1708, are relatively faint, $\simeq (0.48 - 1.37) \times 10^{-9} photon\ cm^{-2}\ s^{-1}$, although it is already unusual to observe BL Lacs at large distances.
In the $F_X - \Gamma_X$ plane the considered sources occupy the region of hard X-ray spectra ($\Gamma_X < 2.0$) and a flux from 7.94×10^{-14} $erg\ cm^{-2}\ s^{-1}$ to 1.17×10^{-11} $erg\ cm^{-2}\ s^{-1}$. PKS 0451-28, TXS 0222+185, PKS 0834-20, PKS 0537- 286, TXS 0800+618, B2 0743+25 and PKS 0438-43 are separated from the others with a comparably high X-ray flux $F_{X-ray} \geq 2.13 \times 10^{-12}$ $erg\ cm^{-2}\ s^{-1}$. In the X-ray band, statistically significant flux variation is found for PKS 0438-43 and B2 0743+25 while there is an indication of variability for TXS 0222+185; during the bright X-ray periods, their flux exceeds 10^{-11} $erg\ cm^{-2}\ s^{-1}$.
The γ-ray flux variability can be investigated based on the available data. The most distant flaring blazars are MG3 J163554+3629 and PKS 0537-286 at $z = 3.65$ and $z = 3.10$, respectively. Though γ-ray flux amplification is observed in the 30-day bin light curve of MG3 J163554+3629, the γ-ray flares are more drastic and evident for PKS 0537-286. The adaptively binned light curve PKS 0537-286 shows several bright γ-ray flaring periods with a maximum flux of $(1.29 \pm 0.26) \times 10^{-6}$ $photon\ cm^{-2}\ s^{-1}$ above 100 MeV, observed on MJD 57879.2 in a time bin having a width of ~ 16.0 hours. For the distance of PKS 0537-286, such flux amplification can be useful for investigation of the $\gamma\gamma$ attenuation, but the photon index is $\Gamma_\gamma = 2.64 \pm 0.27$, so the flare is dominated by sub-GeV photons. The γ-ray flux of B3 1343+451 increases in sub-day scales and that of PKS 0347-211 ($z = 2.94$) and PKS 0451-28 ($z = 2.56$) in day scales. B3 1343+451 is among the top 30 bright blazars observed by *Fermi* , showing multiple periods of enhanced γ-ray emission when the average luminosity of $(2 - 4) \times 10^{48}$ $erg\ s^{-1}$ increased up to 1.5×10^{50} $erg\ s^{-1}$. The peak γ-ray flux of $(1.82 \pm 0.45) \times 10^{-6}$ $photon\ cm^{-2}\ s^{-1}$ above 100 MeV was observed on MJD 55891.7 which is ≥ 36.4 times higher than the γ-ray flux in quiescent state. The $\chi 2$ test showed that the γ-ray emission of B3 0908+416B, TXS 0800+618, PKS 0438-43, OD 166 and TXS 0907+230 is variable in week scales while that of MG3 J163554+3629, GB6 J0733+0456, B2 0743+25, PMN J1441-1523 and TXS 1616+517 in month scales.

The γ-ray photon index of B3 1343+451, PKS 0451-28, B3 0908+416B and TXS 0907+230 varies in time, and their γ-ray emission sometimes appears with a hard γ-ray spectrum. The averaged γ-ray photon index of these sources determines that the peak of the HE component to be below 10^8 eV whereas the hard γ-ray spectrum indicates that the peak is shifted to higher energies. During the flares, different processes can cause the shift of the low-energy or HE peaks. For example, both components will be shifted to HEs when the particles are effectively re-accelerated, resulting in higher electron cutoff energy (γ_{cut}). It is expected that only the HE component will increase when due to the changes in the location of the emitting region the external photon fields are starting to dominate [122]. In order to understand the origin of the change in the emission components, extensive multiwavelength observations are required which is not the case for the sources considered here. We note that such changes have already been observed in the previous studies of blazars [e.g., 47, 12, 6, 145].

The main parameters characterizing the jets of the considered sources are derived by modeling the multiwavelength SEDs. The CD observed in the spectrum of almost all the considered sources implies that the electrons are loosing energy mainly by interacting with the external photons. In the framework of the single-zone scenario, the observed X-ray and γ-ray data are satisfactorily explained taking into account IC scattering of synchrotron and IR photons which in its turn allows to constrain the parameters of the emitting electrons. The power-law index of the electrons is from ~ 1.13 to 2.90, which is within the range expected from the standard particle acceleration theories. For example, in the diffuse shock particle acceleration, the formed particle spectra can be from very hard (-1) to very steep, depending on the shock speed, nature of particle scattering, magnitude of turbulence, shock field obliquity, and other parameters [156]. On the other hand, the optical/UV and γ-ray data strongly constrain the cut-off energy of electrons; the particles are effectively accelerated up to $\sim 10^{12}$ eV. The cooling of emitting particles defines the cut-off energy formed when the acceleration and cooling time scales are equal. Considering the electrons are mostly cooling by interacting with IR photons, and equating the radiative cooling time $t_{cool} \sim \frac{3\, m_e c}{4\sigma_T\, u'_{IR}\, \gamma'_e}$ with the electron acceleration time $t_{acc} \simeq \eta_0 \frac{m_e c \gamma'_e}{eB}$ [135], one gets that for 10^{12} eV electrons these timescales are equal when $\eta^{-1} = 5 \times 10^{-4}$. In other words, the maximum electron energy, if limited solely by the radiative energy losses, might be expected to be much higher than that observed, since often $\eta^{-1} \geq 10^{-2}$ is expected [e.g., 86]. Therefore the cutoff is most likely limited by the physical size of the emitting zone. For a given set of parameters, R, B, and δ, γ_{min} is < 93 and lower values of γ_{min} are estimated when the X-rays are produced only by EIC. This shows that the process responsible for the

particle acceleration picks up almost all electrons.
The total jet luminosity (defined as $L = L_e + L_B$) is $\leq 1.41 \times 10^{46}\, erg\, s^{-1}$ which is of the same order as that usually calculated for blazars [74]. Thus, the jet power of distant and nearby blazars do not differ substantially. The estimated disc luminosity is within $L_d \simeq (1.09 - 10.94) \times 10^{46}\, erg\, s^{-1}$, more typical for powerful blazars. The disc and jet luminosities are of the same order for TXS 0800+618 and TXS 0222+185 ($L_{disc}/L_{jet} = 1.17 - 2.44$) while for the others L_{disc} is higher than L_{jet}. However, we note that the protons with unknown content in jet are not included in the computation of L_{jet}, so in principle higher L_{jet} are expected which could be of the same order as L_{disc} [105]. Yet, when the accretion disc luminosity and temperature are well measured, an approximate value of the black hole mass can be derived following **(author?)** [65, 72]. In general, the black hole mass can be well estimated from the optical spectroscopy [149] or from fitting the blue bump at the optical/UV band [36, 71]. The maximum temperature (and hence the $\nu F\nu$ peak of the disc luminosity) of the standard multi-colour accretion disc temperature profile occurs at 5 R_s where R_s is Schwarzschild radius. Taking into account that the peak temperature scales as $T_{disc} \sim (L_{disc}/R_s)^{1/4}$ [65], R_s can be estimated from which the black hole mass can be derived. The black hole mass estimated for the sources with a clear blue-bump in their SED is in the narrow range of $(1.69 - 5.35) \times 10^9\, M_\odot$ where the highest black hole mass of $5.35 \times 10^9\, M_\odot$ is estimated for PMN J0226+0937 which has also the highest disc luminosity. The virial black hole mass of GB 1508+5714, PKS1351-018, S4 1427+543 and B2 0743+25 is also estimated in the quasar catalog of **(author?)** [150] and is $(3.23 \pm 0.40) \times 10^8\, M_\odot$, $(8.91 \pm 0.64) \times 10^8\, M_\odot$, $(1.80 \pm 0.17) \times 10^8\, M_\odot$ and $(3.89 \pm 0.26) \times 10^9 M_\odot$, respectively. In the case of B2 0743+25, both methods produce similar results, $3.06 \times 10^9\, M_\odot$ and $(3.89 - 0.26) \times 10^9 M_\odot$, while for the other sources the masses obtained using optical spectroscopy are slightly lower. Such differences are expected, since both methods rely on a fitting or approximations. For the considered sources, the Eddington luminosity is within $(2.12 - 5.87) \times 10^{48}\, erg\, s^{-1}$, and the ratio L_{disc}/L_{Edd} ranges from 0.05 to 0.16 [e.g., see 74].

4.8 Summary

The origin of the multiwavelength emission from distant blazars ($z > 2.5$) has been investigated using the *Fermi* data accumulated in 2008-2018 and Swift XRT/UVOT data observed in the last fifteen years. The main results are summarized as follows:

i) Twenty-six out of the thirty-three considered sources are FSRQs, five

BCUs, and only two are BL Lacs. The two BL Lacs are also the faintest objects in the sample with a flux of $(0.48 - 1.66) \times 10^{-9}$ *photon* $cm^{-2}\, s^{-1}$) while the others have a flux from 2.73×10^{-9} *photon* $cm^{-2}\, s^{-1}$ to $\sim 1.50 \times 10^{-7}$ *photon* $cm^{-2}\, s^{-1}$.

ii) Except for the two BL Lacs, the photon index of all the considered sources ranges from 2.18 to 3.05. Only, the γ-ray indexes of B3 1343+451, PKS 0451-28, B3 0908+416B and TXS 0907+230 are found to vary in time. The hardest γ-ray spectra of B3 1343+451, B3 0908+416B and TXS 0907+230 are with indexes of 1.73 ± 0.24, 1.84 ± 0.25, and 1.72 ± 0.15, respectively, while that of PKS 0451-28 - with 2.06 ± 0.07.

iii) The Swift XRT observations show a significant X-ray emission only from the FSRQs considered here. Only a few counts have been detected from the other sources, even if some of them have been observed by Swift several times. The X-ray photon index of distant FSRQs is $\Gamma_X = 1.1 - 1.8$ and the flux is spanning from $\sim 5 \times 10^{-14}$ *erg* $cm^{-2}\, s^{-1}$ to 10^{-11} *erg* $cm^{-2}\, s^{-1}$.

iv) The brightest X-ray source in the sample is TXS 0222+185 ($z = 2.69$) with a flux of $(1.19 \pm 0.04) \times 10^{-11}$ *erg* $cm^{-2}\, s^{-1}$. The X-ray emission from only PKS 0438-43, B2 0743+25 and TXS 0222+185 showed a substantial flux increase in some observations, whereas the X-ray emission from other sources is relatively constant in different years.

v) The γ-ray variability of the considered sources has been investigated using the data accumulated for ten years. Fourteen sources from the sample show a variable γ-ray emission on short and long timescales. The γ-ray flux of B3 1343+451 ($z = 2.53$) and PKS 0537-286 ($z = 3.10$) increases in sub-day scales, that of PKS 0347-211 ($z = 2.94$) and PKS 0451-28 ($z = 2.56$) in day scales. The γ-ray emission of B3 0908+416B, TXS 0800+618, PKS 0438-43, OD 166 and TXS 0907+230 is variable in a week scale while that of MG3 J163554+3629, GB6 J0733+0456, B2 0743+25, PMN J1441- 1523 and TXS 1616+517 in a month scale. The most distant γ-ray blazar flaring on short time scales is PKS 0537-286 ($z = 3.10$) when its flux increased up to $(1.29 \pm 0.26) \times 10^{-6}$ *photon* $cm^{-2}\, s^{-1}$ above 100 MeV within a time bin having a width of $\sim$ 16.0 hours. The γ-ray flux of B3 1343+45 increased significantly from its average level in multiple periods with a maximum flux of $(1.82 \pm 0.45) \times 10^{-6}$ *photon* $cm^{-2}\, s^{-1}$ above 100 MeV, accompanied by moderate hardening of the spectra.

vi) In the $\Gamma_\gamma - L_\gamma$ plane, the majority of the considered sources occupy the narrow range of $\Gamma_\gamma = 2.2 - 3.1$ and $L_\gamma = (0.10 - 5.54) \times 10^{48}$ *erg* s^{-1},

which is more typical for the brightest blazars. However, during γ-ray flares, the luminosity of variable sources is significantly beyond this boundary, changing within $(10^{49} - 10^{50})\ erg\ s^{-1}$. For example, the luminosity of B3 1343+451 increases $\sim$ 36.4 times and corresponds to $L_\gamma = 1.5 \times 10^{50}\ erg\ s^{-1}$, being among the highest values so far observed in the γ-ray band.

vii) The SEDs were modeled within a one-zone leptonic scenario, considering the IC scattering of both synchrotron and IR photons from the dusty torus. The X-ray and γ-ray data allowed to constrain the peak of the HE component (within $10^6 - 10^8$ eV) as well as the power-law index and cut-off energy of the radiating electrons; the index and the cutoff energy are within the range of $1.13 - 2.90$ and $(1.01 - 15.73) \times 10^3$, respectively. The radius of the emitting region is estimated to be ≤ 0.05 pc while the magnetic field and the Doppler factor are correspondingly within $0.10 - 1.74$ G and $10.00 - 27.42$.

viii) The jet luminosity is estimated to be $\leq 1.41 \times 10^{46}\ erg\ s^{-1}$, which is of the order of the values usually obtained for blazars. For all the sources, expect for TXS 0800+618 and TXS 0222+185 for which $L_{disc}/L_{jet} = 1.17 - 2.44$, the jet luminosity is lower than that of the disc $L_d \simeq (1.09 - 10.94) \times 10^{46}\ erg\ s^{-1}$ which is estimated by fitting the UV excess. The black hole masses are estimated to be within $(1.69 - 5.35) \times 10^9\ M_\odot$ so the disc luminosity is 5-16% of the Eddington luminosity.

5 Broadband Study of High-Synchrotron-Peaked BL Lac Object 1ES 1218+304

5.1 Introduction

Active galactic nuclei (AGNs) with a bolometric luminosity of up to $10^{48}\,erg\,s^{-1}$ are the most powerful non-explosive sources in the Universe. Among AGNs, blazars are the most extreme class dominated by nonthermal emission extending from radio to Very High Energy (VHE; $>$ 100 GeV) γ-ray band. The blazar features are best described when assuming that the relativistically moving plasma in the jet is closely aligned with the line of sigh of the observer [163]. The observations in various bands provide different windows on blazar physics, allowing to investigate the accretion disc, innermost jet (sub-parsec) as well as the knots and hotspots of large-scale jets. Most recently, the observation of VHE neutrinos from TXS 0506+056 [85, 84] opened another window for studying the physics of blazar jets. Combination of electromagnetic and neutrino observations could provide most detailed information on the physics at work in the jets (e.g., for TXS 0506+056 [17, 61, 41, 90, 114, 94, 166, 119, 141, 137] and [142]).
Commonly, blazars are divided into two subclasses: flat-spectrum radio quasars (FSRQs) and BL Lacertae objects [163]. The optical spectrum of FSRQs reveals strong broad emission lines, while that of BL Lacs has weak or no lines. The spectral energy distribution (SED) of blazars in $\nu F\nu$ representation has two components [e.g., 118] and is characterized by two broad peaks: the low energy component commonly explained by synchrotron emission of relativistic electrons, peaks between the IR and the X-ray bands. When the synchrotron peak (ν_s) is $\nu_s < 10^{14}$ Hz in the rest-frame, blazars are called low synchrotron peaked (LSP) sources, and when $10^{14} < \nu_s < 10^{15}$ Hz and $\nu_s > 10^{15}$ Hz are intermediate synchrotron peaked (ISP) and high synchrotron peaked (HSP) sources, respectively [77, 1]. In this division, FSRQs are almost exclusively LSPs.
There are various models explaining the second peak in the SED. In the leptonic scenarios, this is explained as inverse Compton (IC) scattering of pho-

tons provided by the synchrotron emission of the jet itself [i.e., synchrotron self Compton (SSC) 103, 29, 66] or produced external to the jet [151, 49]. The most widely used sources of external seed photons are disc photons reflected from broad line region (BLR) clouds [151] or IR photons emitted from the dusty torus [27, 70]. Since the BLR lines are weak or absent in BL Lacs their SEDs are usually modeled using SSC while those of FSRQs by external IC mechanism. In the alternative hadronic scenarios, the second component is modeled by proton synchrotron emission [e.g., 112], photopion production [100, 102, 112, 113, 33] or pp interaction [48, 18, 24, 23, 25].
The synchrotron peak location is defined by the maximum energy at which the electrons are accelerated. In this context, HSPs are not the highest-energy end of the blazar sequence, and **(author?)** [46] found objects with a hard synchrotron X-ray spectrum of at least up to $\sim$ 100 keV. These extreme synchrotron BL Lacs or extreme HSPs (EHSPs) show a synchrotron peak energy above 2.4×10^{17} Hz (1 keV), an order of magnitude higher than that of standard HSPs. For example, during the flares of Mkn 501 the synchrotron peak reached $\sim$ 100 keV [128]. Due to this shift, in the optical band the emission from EHSPs is generally dominated by the thermal emission of the giant elliptical host galaxy. The radio properties of EHSPs are in general similar to those of HSPs but rather with a low flux. In addition to extreme synchrotron BL Lacs, there are BL Lacs extreme in γ-rays which after extragalactic background light (EBL) correction demonstrate a very hard intrinsic photon index of up to and beyond 1 TeV [31, 157]. There is no clear relation between extreme synchrotron and TeV blazars and these two extreme behaviors should not necessarily appear together. Hard spectral photon indexes above 1 TeV due to similar hard index of the emitting particles represent major difficulties for current particle acceleration and emission theories. These extreme blazars are also discussed as possible sources of VHE neutrinos and cosmic rays [120, 133].
The hard High Energy (HE; $>$ 100 MeV) γ-ray spectrum of HSPs implies that particles are efficiently accelerated up to VHEs in their jets, so their detailed study is interesting from the theoretical point of view. One of such HSPs, is at $z = 0.182$ [164] which has been for the first time observed at VHEs by MAGIC [15] and then by VERITAS telescopes [7]. The observed $\sim$ 160 GeV and $\sim$ 1.8 TeV emission is described with a hard γ-ray photon index of 1.86 ± 0.37 after EBL correction [7]. Next, the VERITAS observations during the active state in 2009 provided the first evidence of variability of VHE γ-ray emission of with a flux doubling time scale of $\leq$ 1 day [8]. In the HE γ-ray band, appears with a hard photon index of 1.72 ± 0.02, as observed by Fermi Large Area Telescope (*Fermi*) [5], with the emission extending beyond 100 GeV well in agreement with the data in the VHE γ-ray band. was identified as an X-ray source in the early observations [168] and since then it was always observed

with X-ray telescopes. Considering the unusually hard VHE γ-ray spectra of for its redshift, its observations were also used to constrain the EBL absorption density [e.g., 92] or extragalactic magnetic field [159].
The multiwavelength observations of over years provided a large amount of data in different bands. First, more than eleven years of *Fermi* observations will allow detailed temporal and spectral analyses of γ-ray data which combined with MAGIC/VERITAS data provides the γ-ray spectrum in the large energy range from 100 MeV to $\sim$ 1 TeV. Moreover, using the new PASS 8 event selection and instrument response function, the spectrum can be investigated with improved statistics at higher energies, which is crucial for identifying the peak of the HE component. Frequent observations of with Neil Gehrels Swift Observatory ([63], hereafter Swift) provided unprecedented data both in the optical/UV and X-ray bands, allowing to perform a detailed investigation of the flux variation in these bands. This broadband coverage allows to constrain the SED of in different periods, which is then used for theoretical modeling. Together with Swift, the NuSTAR observation will shape the peak of the low energy component, which in turn allows to derive the main parameters characterizing the jet of (emitting electron distribution, magnetic field, jet power, etc.). belongs to the group of blazars that exhibit hard γ-ray spectrum from MeV/GeV to TeV band, which implies the emission is most likely produced from fresh accelerated electrons allowing to test various acceleration and cooling processes for the emitting particles. The combination of this with the available data, makes an ideal target for exploring the physics of blazar jets.
The purpose of this paper is to investigate the origin of broadband emission from by analyzing the most recent available data. In Section 5.2 the γ-ray data extraction and analyses are presented and discussed while X-ray and optical data analyses are in Section 5.3. The origin of broadband emission as well as the SED modeling are given in Section 5.4. The time dependent formation of emitting electron spectrum is discussed in Section 5.5. The discussions and conclusions are given in Section 5.6.

5.2 Fermi-LAT data extraction and analyses

Fermi is a pair-conversation telescope sensitive to $>$ 100 MeV γ-rays [20]. By default it operates in the survey mode scanning the entire sky every three hours. Operating since 2008, *Fermi* has provided a most detailed and deeper view of the γ-ray sky.
In the current study, γ-ray data from the observation of from August 2008 to April 2020 were obtained from the data portal and analyzed using the stan-

dard analysis procedure provided by the *Fermi* collaboration. The events in the energy range from 100 MeV to 600 GeV within a circular region of 11° radius centered on the γ-ray position of were analyzed using Fermi ScienceTools (1.2.1) package with P8R2_SOURCE_V6 instrument response functions. A zenith angle cut of 90° was applied to reduce the contamination due to the γ-rays from the Earth's limb. The model file containing the spectral parameters of all known γ-ray emitting sources located within a 11°+5° region was generated by make4FGLxml.py script based on the fourth *Fermi* source catalog of γ-ray sources (4FGL) [5]. The Galactic and extragalactic diffuse γ-ray emission was parametrized using gll_iem_v07 and iso_P8R3_SOURCE_V2_v1 models. The parameters of all sources within the 11° region around as well as the normalization of diffuse components were left free to vary during the fitting while the spectral parameters of all other sources were fixed to their values given in the 4FGL.
The data from a $15.5° \times 15.5°$ square region are divided into a spatial pixel size of $0.1° \times 0.1°$ and into 38 logarithmically equal energy bins. The best match between the model and the data is obtained by the binned likelihood analysis method implemented in gtlike tool. In the considered $\sim$ 11.7 years, is detected with an overall significance of 77.2σ ($\sigma = \sqrt{TS}$ where $TS = 2(logL_1 - logL_0)$ and L_1 and L_0 are the maximum likelihood values obtained when fitting the observed data using the null and alternative hypotheses, respectively). The best fit results a relatively hard γ-ray photon index of 1.71 ± 0.02 with a γ-ray flux of $(1.89 \pm 0.09) \times 10^{-8} photon\ cm^{-2}\ s^{-1}$ in the energy range from 100 MeV to 600 GeV. The SED of generated by running the gtlike tool separately for ten energy bands is shown in Fig. 5.3.

The γ-ray light curve is generated to investigate the flux and photon index variation in time. The $>$ 500 MeV events were only considered in the unbinned likelihood analyses, since, due to the hard spectrum of during short periods the number of photons is not enough at lower energies. The model file obtained from the binned likelihood analyses was used for the light curve calculations fixing the photon indexes of all background sources allowing only their normalization to vary. The normalization of both background models was fixed as no variability is expected from them. When the source detection significance is $TS < 4$, only upper limit is computed.
Fig. 5.1 panels a) and b) show the change of the γ-ray flux and photon index calculated for 20 day intervals, respectively. Despite the increase of the γ-ray flux in some periods, no high-amplitude flares are observed. This is in agreement with the results of 4FGL where was flagged as variable source [i.e., the variability index over two-month intervals is 95.6 5]. The hard γ-ray photon index of implies that the emission is mostly at higher energies where the number of observed photons is low, so no comprehensive vari-

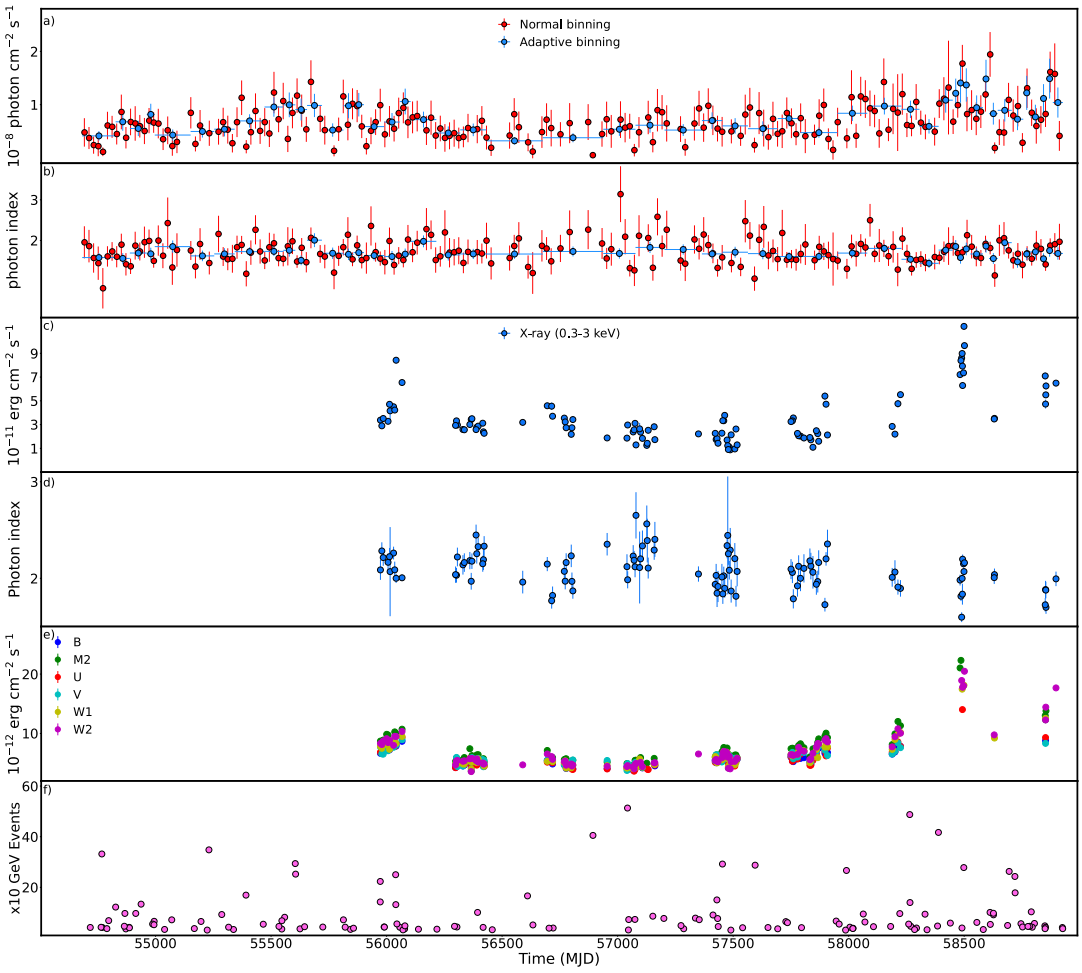

Figure 5.1 Multiwavelength light curve of during 2008-2020. a) and b) γ-ray flux and photon index computed for normal and adaptively time binning. c and d Swift XRT measured X-ray flux and photon index variation in time. e) Swift UVOT measured UV/optical fluxes in V, B, U, W1, M2, and W2 bands. f) The arrival time of HE photons from the direction of .

ability studies (e.g., short time scale variation) are possible. Next, using the adaptive binning algorithm [97], the γ-ray light curve is computed. In this method, the time bins have been optimized to have a fractional uncertainty of 20 % above the optimal energy of $E_{opt} = 394.1$ MeV [for the calculation of E_{opt} see 97]. The light curve generated by this strategy allows us to search variability, which is sometimes not visible in the regular time binning [130, 145, 21, 172, 144, 62, 132]. The flux and photon index calculated by adaptive binning method shown in light blue correspondingly in Fig. 5.1 a) and b). The photon index is relatively stable, being always below 2.0, which is natural, as HSPs usually have a hard γ-ray photon index but the γ-ray flux is sometimes above its average level. Despite large uncertainties, an increases in the flux had been observed around MJD 55578, 55879, 56080 and after 58000. For example, on MJD 58869.84 ± 13.82 the flux above $E_{opt} = 394.1$ MeV was $(1.49 \pm 0.37) \times 10^{-8} photon\ cm^{-2}\ s^{-1}$ with a photon index of 1.75 ± 0.15, with a 10.2σ detection significance. It corresponds to a flux of $(3.89 \pm 0.84) \times 10^{-8} photon\ cm^{-2}\ s^{-1}$ above 100 MeV. Or on MJD 58594.42 ± 12.95 and 56080.57 ± 23.54, the γ-ray flux and photon index were $(5.15 \pm 1.05) \times 10^{-8} photon\ cm^{-2}\ s^{-1}$ and 1.86 ± 0.16, and $(2.87 \pm 0.55) \times 10^{-8} photon\ cm^{-2}\ s^{-1}$ and 1.66 ± 0.13, respectively. Therefore, even if the flux is above its average level ($\sim$ 2 times), the photon index does not change substantially. However, in normal binning, the hardest photon index of 1.30 ± 0.17 was observed from MJD 58262 to 58282 when the detection significance was 10.1σ. The spectrum in this period was investigated further. The source emission above 1 GeV can be described by the 1.39 ± 0.16 photon index and the emission extending up to $\sim$ 200 GeV with a flux of $(5.09 \pm 1.47) \times 10^{-9} photon\ cm^{-2}\ s^{-1}$.
is also a source of VHE photons due to its relatively hard photon index. Using the output model file obtained after running gtlike, with the gtsrcprob tool, the probability of VHE events from the direction of is computed. The distribution of highest-energy events ($>$ 30 GeV) is presented in Fig. 5.1 (f). Interestingly, there are many $>$ 100 GeV photons within the inner region around with a high probability of being associated with it. For example, the 169.2, 178.4 and 487.4 GeV events with probabilities of 0.99996, 0.99993 and 0.99988, respectively, were observed within a circle of 0.015°, 0.024° and 0.035°, respectively. The highest energy event of 513.2 GeV has been detected on MJD 57042.8 within a circle of 0.18° around with the 0.99496 probability to be associated with it.

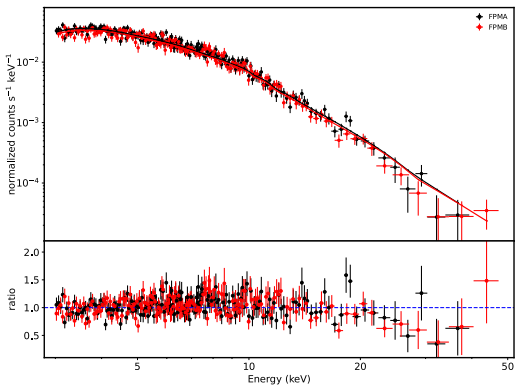

Figure 5.2 Upper panel: NuSTAR spectra (FPMA in black and FPMB in red) and the best fit model. Lower panel: the ratios (data/model) for power-law model.

5.3 X-ray and optical/UV observations

The X-ray emission from is investigated by analyzing the data collected by Swift XRT [63] and NuSTAR [81]. This provides X-ray data in a large energy range of $0.3 - 70$ keV which is important, as for HSPs this range corresponds to the highest energy tail of the low energy component.

5.3.1 Swift XRT

Swift observed 116 times between 2008 and 2020. All XRT data are analyzed using the Swift XRTPROC pipeline, which is an automatic script for downloading and analyzing XRT data. The script first presented in **(author?)** [80] and further updated in the context of the Open Universe initiative [76], is based on the official XRT Data Analysis Software (XRTDAS). For the source region, photons were counted over a circular region of 47 arcsec (20-pixel) radius centered on the source position, while for the background region a larger annulus was used, with inner and outer radii of 120 and 200 arcsec, correspondingly, centered on the source and selected to avoid any contaminating sources. The count rate in some observations was above 0.5 $count\ s^{-1}$, so the data is significantly affected by the pileup in the inner part of the point-spread function [110]. This effect was removed by excluding the events within a 3-pixel radius circle centered on the source position. In this case, the source count selection radius was increased to 70 arcsec. The individual spectra were fitted with XSPEC12.10.1 adopting an absorbed power-law and log-parabola models, applying Cash statistics on ungrouped data.
The 0.3-3, 0.5-2, 2-10, 3-7 keV X-ray fluxes as well as the 0.3-10 keV pho-

ton index are computed for each observation. In the X-ray band, the flux gradually increases around MJD 58500 with the highest 0.3-3 keV X-ray flux of $(1.13 \pm 0.02) \times 10^{-10}\, erg\, cm^{-2}\, s^{-1}$ on MJD 58499.1, which is by a factor of $\sim$ 5.6 higher than the mean X-ray flux ($(2-3) \times 10^{-11}\, erg\, cm^{-2}\, s^{-1}$). It should be noted that from MJD 58482 to 58501, was in an active X-ray emission state, when the 0.3-3 keV flux changed in the range of $(6.29 - 9.65) \times 10^{-11}\, erg\, cm^{-2}\, s^{-1}$. Similar increases are also observed in the other considered intervals for the flux computation. The X-ray photon index varies as well, being of the order of $(2.1 - 2.2)$ for most of the time, but on MJD 58489.1 it was 1.60 ± 0.05 which is the hardest index recorded for this source (corrected for pile-up effect). There are thirty-four periods with a photon index of < 2.0 and six with < 1.8. Fig. 5.3 shows the XRT spectra when was in a bright (Obsid 30376106), moderately bright (Obsid 30376101), and average (Obsid 30376042) X-ray emitting states, as well as when the X-ray emission is with the hardest X-ray photon index (Obsid 30376099).

5.3.2 NuSTAR

NuSTAR is a hard X-ray focusing satellite comprised of two Focal Plane Modules (FPMs): FPMA and FPMB, providing continuous coverage over a broad bandpass of 3-78 keV [81]. was observed by NuSTAR on MJD 57349 with a net exposure of 49.5 ksec. The NuSTAR data were processed with the NuSTARDAS software package available within HEASOFT package using the latest version of the calibration database (CALDB). The event file is cleaned and calibrated using nupipeline tool. The spectra of in the energy range of 3-79 keV is extracted from a circular region of $50''$ radius centered at the source position whereas the background counts are extracted from a circle of $80''$ from a nearby region on the same chip and avoiding source contamination. The spectra were binned so as to have at least 30 counts bin^{-1} and fitted assuming an absorbed power-law model.
Initially, the energy range from 3 to 79 keV have been considered for the fit. However, the count rate rapidly decreases above 50 keV and the background starts to dominate. Thus, the source parameters are estimated in the energy range 3-50 keV. The best fit resulted in $\Gamma_{X-ray} = 2.56 \pm 0.028$ and $F_{X-ray} = (1.21 \pm 0.02) \times 10^{-11}\, erg\, cm^{-2}\, s^{-1}$ with $\chi^2/d.o.f = 1.04$ for 364 degree of freedom. The spectra of FPMA and FPMB are shown in Fig. 5.2 with black and red, respectively. The high energy tail of X-ray spectra cannot be fitted satisfactorily by a simple power-law, and the model deviates from the data. Thus, an additional fit with a log-parabola is performed. The best-fit spectral parameters of the log-parabola fit are: $\alpha = 2.22 \pm 0.10$, $\beta = 0.45 \pm 0.13$ and $F_{X-ray} = (1.14 \pm 0.02) \times 10^{-11}\, erg\, cm^{-2}\, s^{-1}$ with $\chi^2/d.o.f = 0.94$.

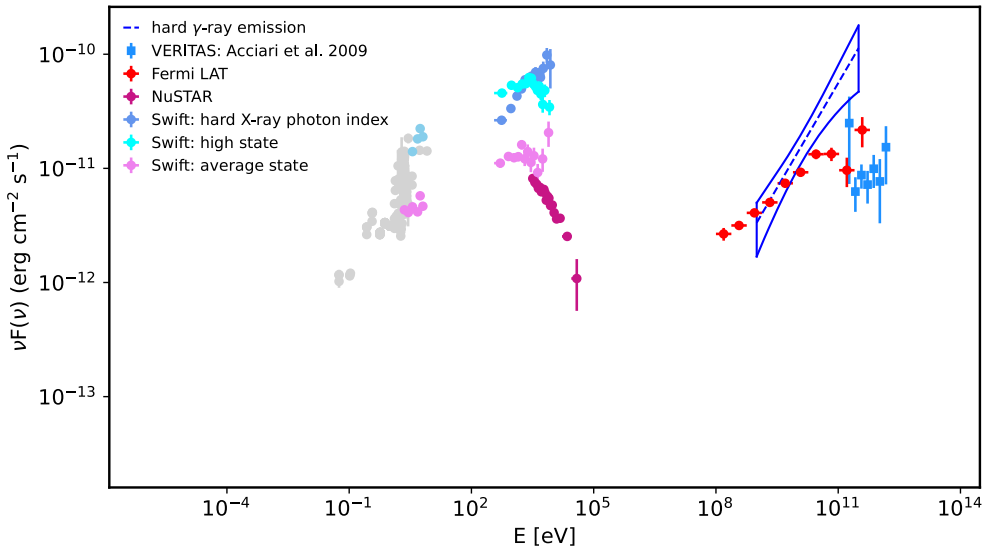

Figure 5.3 Multiwavelength SED of for different periods. The red data corresponds to the *Fermi* spectrum averaged over 11.7 years, and the blue bowtie shows the spectrum during the hard emission period. The UVOT data in light blue corresponds to the highest flux in U, W1, M2 and W2 filters observed around MJD 58490. The archival data from SSDC are in gray. VHE γ-ray data from the VERITAS observation are in light blue squares.

5.3.3 Swift UVOT

was also observed with the UVOT instrument of Swift observatory. UVOT provides observations in three optical (V,B,U) and three UV (W1,M2,W2) filters [138]. All the data available from the observations of were downloaded from the Swift archive and reduced using the HEAsoft version 6.26 with the latest release of of HEASARC CALDB. Source counts were extracted using a $5''$ radius for all single exposures and all filters, while the background was estimated from different positions from a region with $20''$ radius not being contaminated with any signal from the nearby sources. uvotsource tool was used to derive the magnitudes which were converted to fluxes using the conversion factors provided by [129]. Then, the fluxes were corrected for extinction using the reddening coefficient $E(B-V)$ from the Infrared Science Archive [1].

The flux measured for all six filters (V, B, U, W1, M2, and W2) is sown in Fig. 5.1 e). The light curve shows that like in the X-ray band, also the optical/UV flux shows few active periods. In the average state the flux in all filters is around $(3-5.5)\times10^{-12}\,erg\,cm^{-2}\,s^{-1}$, which around MJD 56035, 57870 and 58200 moderately increases up to $\sim(8-9)\times10^{-12}\,erg\,cm^{-2}\,s^{-1}$. Strong brightening of the optical/UV flux was observed after MJD 58482 when the flux reached $\simeq 10^{-11}\,erg\,cm^{-2}\,s^{-1}$; the absolute highest fluxes of $(2.23\pm0.05)\times10^{-11}\,erg\,cm^{-2}\,s^{-1}$ and $(2.05\pm0.04)\times10^{-11}\,erg\,cm^{-2}\,s^{-1}$ were observed in M2 and W2 filters on MJD 58486.10 and 58501.20, respectively. Fig. 5.3 shows the UVOT spectra for the average state (Obsid 30376044, pink) state and when the highest flux in U, W1, M2 and W2 filters were observed around MJD 58490 (light blue).

5.4 The Origin of Broadband Emission

The multiwavelength dataset analyzed in this paper allows to build broadband SEDs of in different emission states. The resulting broadband SED of is shown in Fig. 5.3, displaying the standard double peaked structure. Archival data are extracted from SSDC SED Builder tool [2] and are shown in gray. The Swift UVOT/XRT data from different states of the source are shown together with the NuSTAR spectrum. In the average state (pink), the 0.3-10 keV X-ray photon index is ≥ 2.0 which softens to 2.56 ± 0.028 in the 3-50 keV band. In the bright state (cyan), the photon index is 2.07 ± 0.03 but it can be as hard as 1.60 ± 0.05 on MJD 58489.1 (dark blue circle). In the γ-ray band, in addition to the γ-ray spectra averaged over $\sim$ 11.7 years, the spectrum in the

[1] http://irsa.ipac.caltech.edu/applications/DUST/
[2] https://tools.ssdc.asi.it/SED/

period of the hardest γ-ray emission (1.39 ± 0.16) is shown with a bow-tie. Even though the γ-ray light curve reveals periods when the flux moderately increases, their duration ($\sim$ 20-30 days) and the low amplitude ($\sim 1.5 - 2.0$) do not impact the averaged γ-ray spectra in Fig. 5.3. To demonstrate this, the γ-ray data analysis was performed limiting the time up to MJD 58500 which resulted in $(1.86 \pm 0.11) \times 10^{-8} photon\ cm^{-2}\ s^{-1}$ and 1.71 ± 0.02, in agreement with the results obtained for $\sim$ 11.7 years. The VHE γ-ray data are from the VERITAS observations after EBL correction [7].
The multiwavelength SED in Fig. 5.3 shows dramatic changes in the spectrum of , especially in the X-ray band. In the quiescent state, the NuSTAR spectrum is a continuation of that of XRT and they together constrain the HE tail of the synchrotron component. Moreover, in quiescent state, the synchrotron and IC peaks have similar luminosity but unlike the HE peak which is relatively stable, the X-ray flux increases substantially (cyan data) and the low energy peak luminosity clearly dominates over that at HEs. In the active state, apart from the flux increase, the X-ray spectrum also hardened, shifting towards HEs (light blue data). Such an X-ray spectrum cannot be associated with the synchrotron component dominating at lower energies, being most likely due to another component. For example, this hard X-ray emission can be due to Comptonization of disc photons in the jet [39]. However, the origin of this X-ray emission cannot be investigated because of the absence of contemporaneous multiwavelength data. This change of X-ray spectrum will be further discussed in Section 5.6. The HE γ-ray data clearly demonstrate that the peak of the second component is above $10^{11} - 10^{12}$ eV which cannot be constrained even when VHE γ-ray data are considered because of the large uncertainty in the measurement of the VHE γ-ray photon index (1.86 ± 0.37). However, independently of the VHE γ-ray data, the constraint on the synchrotron spectrum and hence on the distribution of emitting electrons will allow to shape the second component.
The SED of in Fig. 5.3 is modeled in order to gain further insight of the physical processes at work in its jet. The broadband spectrum of in the quiescent state is modeled within a simple one zone leptonic scenario as a large amount of data is available. In this model, the low energy data are interpreted by synchrotron emission of relativistic electrons while the HE component - as SSC radiation from a compact emitting region [30, 67, 107, 44]. It is assumed that this emission region is a spherical blob moving relativistically along the axis of the jet with a Lorentz factor of Γ and because of this, the emission will be strongly Doppler boosted in the observer frame by a factor of $\delta = (\Gamma(1 - \beta cos\theta))^{-1}$ where θ is the angle between the direction of observation and the axis of the jet. For a small viewing angle $\Gamma \simeq \delta$. It is assumed that the blob is filled with an electron (or electron/positron) population in an isotropic magnetic field. For the electron energy distribution we consider a

broken power-law (BPL) function in the form of

$$N_e(\gamma) = \begin{cases} N_0 \left(\gamma\right)^{-\alpha} & \gamma_{\rm min} \leqslant \gamma \leqslant \gamma_{\rm br} \\ N_0 \left(\gamma_{br}\right)^{\alpha_1-\alpha} \left(\gamma\right)^{-\alpha_1} & \gamma_{\rm br} \leqslant \gamma \end{cases} \tag{5.4.1}$$

where N_0 defines the total electron energy $U_e = \int_{\gamma_{min}}^{\gamma_{max}} \gamma\, N_e(\gamma) d\gamma$, α and α_1 are the low and high indexes of electrons, correspondingly below and above the break energy γ_{br}. γ_{min} is the minimum energy of electrons in the jet frame. The electron distribution given by Eq. 5.4.1 is a result of injection and cooling of particles [87]. As an alternative, a power-law with an exponential cut-off (PLEC) distribution of particles is assumed:

$$N_e(\gamma) = N_0 \gamma^{-\alpha}\, exp(-\gamma/\gamma_{cut}) \tag{5.4.2}$$

where γ_{cut} is the highest energy cut-off in the electron spectrum. This electron distribution is naturally formed when the acceleration is limited by cooling or dynamical time scales (e.g., **(author?)** [170, 174, 143, 22]). In the next section, time dependent formation of these spectra is discussed in the context of particle acceleration and cooling.

The emitting region is characterized by the electron energy distribution (α, α_1, $\gamma_{br/cut}$), magnetic field, Doppler boosting and its size. The upper limit on the size of the emission region can be derived from the relation $R \leq \delta\, c\, t_{var}$, where the variability time t_{var} can be inferred from the γ-ray light curve when the flare rise or decay time can be estimated. In the HE γ-ray band, did not show prominent flares, while in the VHE γ-ray band, the flux doubling time was observed to be $t_{var} \leq 1$ day [8] which limits the emission region size by $R \leq 2.19 \times 10^{15} \times \delta\, cm$. Assuming a typical value for $\delta = 25$, the emission region size would be $R \simeq 5.5 \times 10^{16}\, cm$. Also, following **(author?)** [139], for the same $R \simeq 5.5 \times 10^{16}\, cm$ the data is modeled considering $\delta = 80$.

In the fit, the model free parameters and their uncertainties are estimated using the Markov chain Monte Carlo (MCMC) method in two approaches. Initially, the spectral model parameters have been derived through MCMC sampling of their likelihood distributions using a modified version of naima package [e.g., 145, 62]. Then, the fitting is done with the open source package JetSet [108, 161, 160], initially optimizing the parameter space with Minuit minimizer, then applying MCMC sampling centered on the best fit values. Both methods produce similar results.

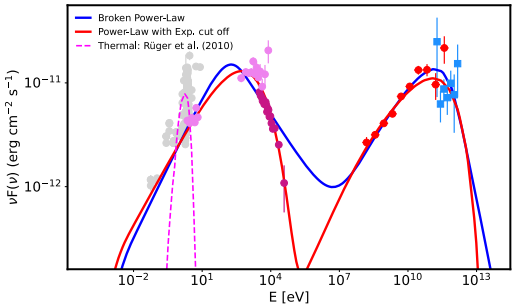

Figure 5.4 Broadband SED of modeled using a one-zone model. The red curve shows the emission assuming a power-law with an exponential cutoff distribution for the emitting electrons while that using a broken power-law is in blue.

5.4.1 Broadband SED fitting

The SED modeling results are shown in Fig. 5.4 with the corresponding parameters listed in Table 5.1. In addition to the synchrotron/SSC component, a thermal component (a blackbody with a temperature of $T = 4500$ K) from **(author?)** [139] is shown in magenta. This corresponds to the thermal emission of the host galaxy, showing that the UVOT data in the average state are likely dominated by the nonthermal emission from the jet rather than by thermal emission from the host galaxy. It can be seen that the data up to the X-ray band (including NuSTAR) are explained by synchrotron radiation of electrons. The SSC component is dominant above ~ 1 MeV and it describes the data up to the VHE γ-ray band. When the BPL distribution of electrons is considered (blue line in Fig. 5.4), the data can be modeled when $\alpha = 2.09 \pm 0.06$ changes to 3.67 ± 0.10 at the break energy of $(1.72 \pm 0.31) \times 10^5$. So, the index change is significantly different from that expected when the electrons undergo radiative losses effectively ($\Delta\alpha = 1$). The archival data allows to put a limit on the γ_{min} to be $(5.69 \pm 0.05) \times 10^2$: for larger γ_{min} the synchrotron component will decline in the low energy band which is in disagreement with the observed data. The magnetic field is estimated to be $(1.58 \pm 0.21) \times 10^{-2}$ G and the emission region is particle-dominated with an equipartition ratio between the particle energy density U_e and magnetic field energy density U_B of $U_e/U_B \simeq 2.1 \times 10^2$.
The modeling with a PLEC distribution of electrons better explains the SED (red line in Fig. 5.4); the goodness of fit (reduced χ square) is $\chi^2 = 0.90$. The power-law index is 2.19 ± 0.04 not substantially different from that estimated in the previous case. The synchrotron peak and NuSTAR spectrum allowed to measure the cut-off energy with a high accuracy, $\gamma_{cut} = (4.73 \pm 0.34) \times 10^5$, which in its turn constrains the HE component which decreases above $\sim 10^{12}$

Table 5.1 Parameters of the models in Fig. 5.4.

	PLEC ($\delta = 80$)	BPL ($\delta = 80$)
α	2.19 ± 0.04 (2.31 ± 0.03)	2.09 ± 0.06 (2.43 ± 0.02)
α_1	–	3.67 ± 0.10 (4.37 ± 0.15)
$\gamma_{min} \times 10^2$	4.55 ± 0.04 (5.07 ± 0.10)	5.69 ± 0.05 (1.67 ± 0.03)
$\gamma_{cut/break} \times 10^5$	4.73 ± 0.34 (9.57 ± 0.82)	1.72 ± 0.31 (7.47 ± 0.79)
$B[G] \times 10^{-2}$	1.53 ± 0.09 (0.16 ± 0.07)	1.58 ± 0.21 (0.17 ± 0.01)
$U_e[erg\ cm^{-3}]$	2.68×10^{-3} (2.24×10^{-3})	2.15×10^{-3} (3.77×10^{-3})
$U_B[erg\ cm^{-3}]$	9.31×10^{-6} (9.92×10^{-8})	9.96×10^{-6} (1.13×10^{-7})
$L_e[erg\ s^{-1}]$	7.64×10^{43} (6.39×10^{43})	6.11×10^{43} (1.07×10^{44})
$L_B[erg\ s^{-1}]$	2.65×10^{41} (2.83×10^{39})	2.84×10^{41} (3.23×10^{39})

eV. A relatively high value of the minimal energy of the radiating electrons, $\gamma_{min} = (4.55 \pm 0.04) \times 10^2$ is obtained which is not exceptional for blazar modeling, and high γ_{min} is often used to describe the emission from HSPs [e.g., 4, 19, 99]. The magnetic field is mostly constrained by fitting the low energy component; the synchrotron component depends on the product of B and N_e, so $B = (1.55 \pm 0.09) \times 10^{-2}$ G is the same as in the previous case. Again, the electron energy density is higher than that of the magnetic field, $U_e/U_B \simeq 2.9 \times 10^2$.

The modeling parameters when $\delta = 80$ are given in Table 5.4 in the brackets. As compared with the modeling when $\delta = 25$, a noticeable difference in this case is that the electron distribution is with a softer power-law index ($\alpha = 2.31$ and 2.43) and the magnetic field is lower ($\simeq (1.6 - 1.7) \times 10^{-3}$ G). As the peak of the low energy component is well defined by the data, when increasing the Doppler factor (and hence the luminosity), a lower magnetic field would be required to explain the same data. This, in its turn increases the particle dominance and now $U_e/U_B > 10^4$.

The jet power in the form of magnetic field and particles is given in Table 5.1. The luminosities have been computed for a pure electron/positron jet, since the proton content is not well known, and these can be considered as the lower limit. The absolute jet power ($L_{jet} \simeq 8 \times 10^{43} erg\ s^{-1}$) is significantly below the Eddington luminosity for a $5.6 \times 10^8\ M_\odot$ black hole mass ($L_{Edd} = 7.3 \times 10^{46}\ erg\ s^{-1}$) estimated from the properties of the host galaxy in the optical band [139].

5.5 Time dependent formation of electron spectrum: Electron cooling

The multiwavelength modeling presented in the previous section allowed to put a constraint on the parameters of emitting electrons. These parameters contain valuable information on the processes taking place in the jet of . For example, the power-law index of the emitting electrons mostly defined by the acceleration mechanisms could be used to test the process by which the particles gain energy. On the other hand, the break or cutoff energy allows to evaluate the electron radiation cooling or dynamical timescales, which helps to understand the particle interaction processes. Thus, the parameters reported in Table 5.1 can be used for further exploring the physics of jet.
The spectra given in Eqs. 5.4.1 and 5.4.2 are ad-hoc assumption of emitting particles used for modeling the SED. However, the formation of the particle spectrum is governed by the injection and cooling of electrons. To calculate the temporal evolution of the electron distribution $[N_e(\gamma, t)]$, it is necessary to solve integro-differential equations, describing the losses and injection of relativistic electrons in the emitting region [87]. In this case the kinetic equation has the following form

$$\frac{\partial N_e(\gamma,t)}{\partial t} = \frac{\partial}{\partial \gamma}\left(\dot{\gamma} N_e(\gamma,t)\right) - \frac{N_e(\gamma,t)}{t_{esc}} + Q(\gamma,t)\,, \tag{5.5.1}$$

where $\dot{\gamma} = d\gamma/dt$ is the radiation loss term, t_{esc} is the characteristic escape time and $Q(\gamma, t)$ is the rate of electron injection. The emitting region electrons can loose energy by synchrotron and SSC processes, so $\dot{\gamma} = -4/3\,\sigma_T\, cU'\,\gamma^2$ where U' is either the energy density of the magnetic field ($U'_B = B^2/8\pi$) or the density of synchrotron radiation (U'_s). The latter can be approximated by $U'_s \simeq L'_{syn}/4\pi\, R^2\, c$ where $L'_{syn} = \int \partial L_{\nu,syn}/\partial\nu\, d\nu$ is the total synchrotron luminosity in the jet frame. The modeling shows that $L_{syn} = 5.74 \times 10^{41}\, erg\, s^{-1}$ so $U'_s \simeq L_{syn}/4\pi\, R^2\, c\, \delta^3 \simeq 3.2 \times 10^{-8}\, erg\, cm^{-3}$ which is significantly less than $U'_B = 9.31 \times 10^{-6}\, erg\, cm^{-3}$. This implies that the electrons are predominantly cooled through interaction with the magnetic field. However, usually U'_s should be taken into account, considering the non-linear effects in the particle cooling which is particularly strong when the emission is produced in a very compact region $\sim 10^{15}\, cm$. In this case, also due to the narrow distribution of synchtron photons (low energy component in Fig. 5.4), its density is lower than that of the magnetic field. Accordingly, the radiation loss term in Eq. 5.5.1 is replaced by pure synchrotron cooling.
In the case of no escape ($t_{esc} \to \infty$), that is all the particles cool inside the emitting region, a BPL spectrum of the electrons will be formed when the

power-law index changes as $\alpha_1 - \alpha = 1$. The break energy will be defined by equating the cooling time with the evolution time of the system. In Fig. 5.5 the evolution of the spectrum when the particles are constantly injected ($t_{inj} >> t_{cool}$) into the emitting region with $Q(\gamma) \sim \gamma^{-2.09}$ is shown for different dynamical time scales; the red gradient shows the spectrum with increasing time. After the system evolves up to $\sim 1.80 \times 10^7$ sec, a break at 1.72×10^5 will be formed in the spectrum; for shorter times the break is at higher energies. However, as expected, the transition at the break energy is smooth ($2.09 \rightarrow 3.09$) which cannot explain the estimated electron spectrum obtained from the data modeling (blue spectrum in Fig. 5.5). A steep electron spectrum is required after the break to explain the X-ray data; the NuSTAR spectrum completely defines the power-law index of the electrons after the break to be $2 \times \Gamma_{X-ray} - 1 = 4.12$. It means that the power law index of electrons before the break should be 3.12 but in that case their γ-ray emission will be nearly flat ~ 2.06 in disagreement with the data ($\sim E_\gamma^{-1.76}$). The electron power-law indexes before and after the break are rather well defined by the X-ray and γ-ray data, so when changing the values of α and α_1 reported in Table 5.1 to get a cooling break, the data will not be satisfactorily reproduced. When assuming a constant injection of particles with their escape timescale depending on the energy ($\sim \gamma^\epsilon$), more gradual transition will be achieved at the cooling break when $\epsilon \neq 0$, but again a component with a softer spectrum cannot be formed. Most likely, this break is due to the characteristics of the acceleration processes and for an unknown reason the change in the electrons spectrum is $\Delta\alpha > 1$. Or alternatively, the inhomogeneities in the emitting region could also cause a stronger change in the emitting electron spectrum, which might produce BPL spectrum of electrons with $\Delta\alpha > 1$ [134].
In the case the electrons can escape from the emitting region, a standard BPL spectrum will be formed again, only the break will correspond to the electron energy at which the escape and cooling timescales are equal ($t_{esc} = 3m_e\, c/4\sigma_T U_B\, \gamma_{br}$). For example, a BPL spectrum at $\gamma_{br} = 1.72 \times 10^5$ can be formed when $t_{esc} = 9.83R/c$. However, the transition at the break is again not sharp enough to explain the observed data.
Alternative to BPL, a PLEC spectrum can be formed as a result of time averaging of the injected particle spectrum, i.e., after the abrupt power-law injection of the particles ($t_{inj} < t_{cool}$) they start to cool in the emitting region. In time, the HE tail of the particle distribution steepens and a cut-off will be formed. In order to demonstrate this, it is assumed that the $Q(\gamma) \sim \gamma^{-2.19}$ injection of the particles stops at $R/10\, c$ and then the electron distribution evolution up to $10\, R/c$ is followed by setting $t_{esc} = 1.5R/c$ and $B = 1.53 \times 10^{-2}$ G. The blue gradient in Fig. 5.5 corresponds to the electron spectrum calculated for different time intervals. Initially, only the HE electrons ($\gamma > 10^6$) cool or escape the region, declining the injected electron spectrum only at higher

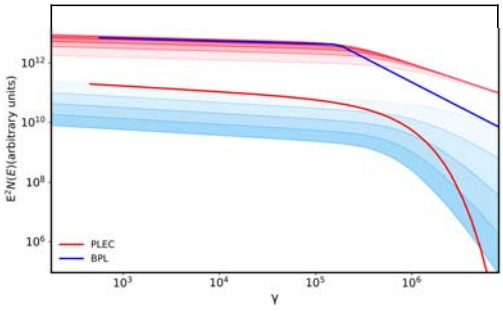

Figure 5.5 Time evolution of electron spectra considering different initial injection rates. The BPL and PLEC spectra in arbitrary units are shown in blue and red, respectively.

energies. Then, with the time the cut-off energy moves to lower energies and after $\sim 3-4\,R/c$ the break is at the same level as that estimated from the data modeling (1.58×10^5). In principle, by changing the parameters (injection and escape times, etc.), it is possible to satisfactorily reproduce the PLEC spectrum of electrons with the parameters given in Table 5.1. It should be noted that such an exponential cut-off will be also formed in the case of an episodic injection with an energy dependent escape.

5.6 Discussions and Conclusions

The HSP blazars having the second peak in the SED toward the higher energies are extremely interesting sources for HE and VHE γ-ray observations. For HSPs, the X-ray spectrum limits the synchrotron component below keV/MeV band and the γ-ray emission is due to IC scattering. In the γ-ray band, HSPs appear with a moderately hard photon index (< 2.0) with a mean of 1.81 ± 0.08 [13], so the emitting particles are accelerated to much higher energies as compared with LSPs or ISPs. This implies the multiwavelength observations have potential not only for investigation of the emission features in different bands but also for testing various acceleration and emission scenarios in the blazar jets.
The γ-ray emission from is investigated during more than eleven years, from August 2008 to April 2020. Its long time-averaged γ-ray spectrum is hard with a photon index of 1.71 ± 0.02 and with a flux of $(1.89 \pm 0.09) \times 10^{-8}\, photon\ cm^{-2}\, s^{-1}$. The emission extends up to ~ 600 GeV with a detection significance of 77.2σ. The sub-GeV source photons are relatively less, which prevents detailed variability studies in short time scales. Although the adaptively binned light curve shows several periods (e.g., on MJD 58869.84 ± 13.82, 58594.42 ± 12.95

and 56080.57 ± 23.54) when the flux moderately increased as compared to its average level. During these periods the data accumulation of 20-30 days is enough to reach the required uncertainty of 20 % (usually $> (100 - 150)$ days are required). The photon index of the source is relatively constant with the hardest and softest values being 1.44 ± 0.11 and 2.01 ± 0.17, respectively. The hard emission observed in MJD 58272 ± 10 extends up to $\sim$ 200 GeV with a flux of $(5.09 \pm 1.47) \times 10^{-7} photon\ cm^{-2}\ s^{-1}$ and photon index of 1.39 ± 0.16 above 1 GeV. In general, the spectrum measured by *Fermi* agrees well with that non-simultaneously measured by VERITAS at VHE γ-rays (after EBL correction).

As a bright source in the X-ray band, shows interesting features in the 0.3-10 keV band. First of all, an X-ray flux amplification in different observations is found with a highest X-ray flux of $(1.13 \pm 0.02) \times 10^{-10}\, erg\ cm^{-2}\, s^{-1}$. In the hard X-ray band, as observed by NuSTAR, the spectrum is soft with 2.56 ± 0.028 photon index. In the quiescent state, the Swift XRT and NuSTAR measured spectra are in a good agreement, allowing to measure the spectrum in the broad band of 0.3-50 keV. Yet, the Swift XRT observations reveal interesting modification of the X-ray photon index in some observations. It is mostly above 2.0, as expected for HPS, but there are periods when the photon index hardens to ≤ 1.80. In Fig. 5.6 eight periods when such hard photon index is observed are presented together with Swift UVOT and NuSTAR data where the modification of X-ray spectra is evident. In the quiescent state, the nearly flat spectrum measured by Swift XRT and the soft X-ray photon index obtain by NuSTAR clearly imply that the synchrotron peak is $< 10^{17}$ Hz. However, in the specific periods shown in Fig. 5.6, the position of the synchrotron peak moves above 10^{17} Hz and shows characteristics similar to EHSPs. This peak frequency shift is more evident and drastic for the periods highlighted in the lower panel of Fig. 5.6. It should be noted that the optical/UV flux did not change substantially, but not always all the filters are available for detailed investigation. During the observations on MJD 57760 and 57897 the UVOT data could either correspond to the peak of the host galaxy emission (thus appear with a nearly flat spectrum) or be due to the synchrotron emission from the jet electrons but from a different component that produces hard X-ray emission. However, due to the lack of data no definite conclusion can be drawn. Such temporary extreme behavior of HPSs has already been observed for Mrk 501 [128] and 1ES 2344+514 [78]. In these extreme periods, the high counts ($\geq$ 280) allowed precise estimation of the photon index which was 1.60 ± 0.05 and 1.70 ± 0.07 on MJD 58489 and 58854, respectively, and being within $1.72 - 1.84$ for the other periods. Also, the MAGIC and VERITAS observations of reveal an exceptional hard photon index in the TeV band (< 2.0), though not simultaneous with the X-ray observations, which shows might have features similar to those of BL Lacs extreme

in the γ-ray band. Along with these features also in the γ-ray band does not show a short time scale variability compatible with the behaviour of EHSPs. Yet, in the γ-ray band some of VHE photons from the direction of were observed around those extreme X-ray periods. For example, VHE events with $E_\gamma = 292.0$, 278.1 and 150.3 GeV were observed on MJD 57453.7, 58498.3 and 57429.6, respectively, within a circle of $< 0.1^\circ$ around and with a $> 3.0\sigma$ probability to be associated with it. These periods overlap with some highlighted in Fig. 5.6. The are also > 100 GeV events emitted close to the periods in Fig. 5.6 which come from a bit larger circular region or with a smaller probability of association with . However, considering is the only source in the ROI with emission extending above tens of GeV, these photons are most likely also associated with it. This shows that during the extreme X-ray emission periods of , also GeV/TeV photons were efficiently produced which hints at possible transition of to an extreme BL Lac from the viewpoint of both synchrotron peak and VHE γ-ray photon index. It is expected that such extreme periods are hidden in the spectrum of HSP blazars and sometimes the transition of the synchrotron peak to higher frequencies is possible.

The quiescent state SED is modeled within a one-zone leptonic scenario. The synchrotron/SSC model well explains the observed data and can reproduce both low and HE peaks. The low energy photons with a peak at $\nu_{sync} \simeq 7 \times 10^{16}$ Hz, well constrained by XRT and NuSTAR data, are IC up scattered to higher energies $4/3\, \gamma^2_{cut/br}\, \nu_{sync} \simeq 10^{27}$ Hz, explaining the second peak. The derived magnetic field in the jet emitting region is $B = 1.5 \times 10^{-2}$ G for $R \simeq 5.5 \times 10^{16}\, cm$, the system being slightly particle dominated $U_e/U_B \simeq 290$ which is in agreement with the SED modeling of other HSPs; usually within the leptonic scenario the HSP SEDs can be modeled when the emitting region is by far out of equipartition. In this case the equipartition is between the magnetic field and nonthermal electron energy density, and it would break when considering the jet protons, the content of which is unknown. The energy density of electrons strongly depends on $\gamma_{min} \sim 500$ which in this case should be considered as an upper limit; in the case when $\leq \gamma_{min}$ the SED can be still described well but when $> \gamma_{min}$, the model starts to drop in disagreement with the observed data. When the modeling infers an extremely out-of-equipartition condition in the jet, additional jet power is required which is however limited by the Eddington accretion rate [e.g., 50]. As an alternative, in highly magnetized environments the combined lepto-hadronic modeling would allow to choose parameters and explain the data when the system is close to the equipartition condition [e.g., modeling of 3C 279 32].

The one-zone SSC model was also used to model the SED in the previous studies [e.g., 139, 167, 45, 154]. For example, in **(author?)** [139], using a time dependent code taking into account cooling of electrons and time evolution

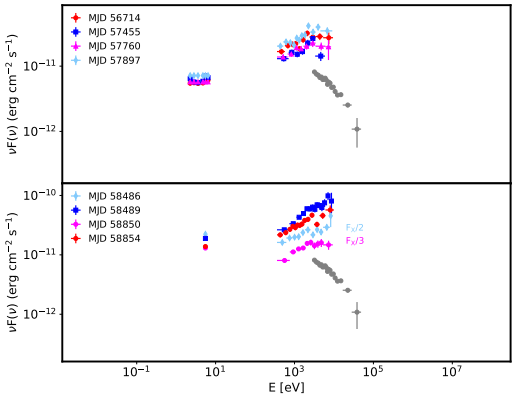

Figure 5.6 Swift UVOT and XRT spectra of during the extreme X-ray emission period as compared with that of NuSTAR (gray).

of photons the SED of was modeled for the electron distribution with $\alpha = 2.1$ and $\gamma_{cut} = 5 \times 10^5$. Or in **(author?)** [154], a log-parabolic distribution function for the electrons can reproduce the observed data for index of 1.8 and curvature parameter of 0.5. Thus, in the previous modelings even if different assumptions were made for the emitting region size and Doppler boosting, the parameters obtained for the emitting electrons do not differ significantly from those obtained here. The energetics (e.g., luminosity or energy density) is different in all modelings as it depends on R and δ the values of which were different. However, like in all the models, here too $U_e/U_B > 10$. As an alternative to leptonic models, the HE bump of can be modeled by the proton synchrotron component when the magnetic field in the region is $B = (3.4 - 454)$ G and the protons are accelerated up to ultra high energies 2.4×10^{19} eV and $(U_e + U_p)/U_B = 2.2 \times 10^{-2}$ [42].

The BPL and PLEC electron spectra were used to model the SED. In general, the spectra of electrons is controlled by several timescales, namely, the cooling time, the injection duration and the escape time. In the continuous injection of particles and in the absence of escape, the traditional cooling break formed in the electron spectrum can not explain the tail of the high energy component which requires much stepper decrease: the cooled electron spectrum above 1.72×10^5 will exceed that obtained from the modeling. The change in the electron spectrum is most likely caused by the nature of the acceleration process. Alternatively, **(author?)** [134] showed that when synchrotron losses are dominating, spectral breaks in the electrons spectrum differing from 0.5 can be naturally formed in inhomogeneous sources. These can be straightforwardly applied to pulsar wind nebulae or knots in large-scale jets, but may be applied also wherever bulk flows of relativistic material are involved, as in the case of relativistic jets. On the other hand, the

time limited power-law injection of electrons which cool in the emitting region will stabilize and form a cutoff in the electron distribution in time. The value of cut-off energy depends on the time for which the system evolves and $\gamma_{cut} = (4.73 \pm 0.34) \times 10^5$ obtained from the SED modeling can be naturally obtained. The required time for dynamical evolution of the system is 3-4 R/c which is in agreement with the absence of flaring activities in γ-ray band in short time scales. In principle, more complicated scenarios for the formation of a curved spectrum are possible, but here a simplified scenario when the curvature is caused by the injection/cooling or energy-independent escape from the emitting region, is discussed.

As a powerful HSP, has always been monitored in various bands; it is still debatable whether is a normal HSP or an extreme blazar. Some of the Swift XRT observations analyzed here appeared with an extremely hard photon index of ≤ 1.8 shifting the X-ray spectrum toward higher frequencies, making an episodic extreme synchrotron blazar. It should be noted that a smooth transition within the blazar classification is emerging in some observations, e.g., a classical FSRQ shows a BL Lac features during the flares [e.g., 47, 147, 38, 79] or HSPs appear as extreme blazars [e.g., 128, 78, 75]. Identification of such hidden periods when HSPs are in an extreme emission state with a large multifrequency coverage can be crucial for understanding the physics of extreme blazars and investigation of the changes in the jet parameters causing their extreme behaviour.

Bibliography

[1] A. A. Abdo, M. Ackermann, I. Agudo, M. Ajello, H. D. Aller, M. F. Aller, E. Angelakis, A. A. Arkharov, M. Axelsson, U. Bach, L. Baldini, J. Ballet, G. Barbiellini, D. Bastieri, B. M. Baughman, K. Bechtol, R. Bellazzini, E. Benitez, A. Berdyugin, B. Berenji, R. D. Bland ford, E. D. Bloom, M. Boettcher, E. Bonamente, A. W. Borgland, J. Bregeon, A. Brez, M. Brigida, P. Bruel, T. H. Burnett, D. Burrows, S. Buson, G. A. Caliandro, L. Calzoletti, R. A. Cameron, M. Capalbi, P. A. Caraveo, D. Carosati, J. M. Casand jian, E. Cavazzuti, C. Cecchi, Ö. Çelik, E. Charles, S. Chaty, A. Chekhtman, W. P. Chen, J. Chiang, G. Chincarini, S. Ciprini, R. Claus, J. Cohen-Tanugi, S. Colafrancesco, L. R. Cominsky, J. Conrad, L. Costamante, S. Cutini, F. D'ammando, R. Deitrick, V. D'Elia, C. D. Dermer, A. de Angelis, F. de Palma, S. W. Digel, I. Donnarumma, E. do Couto e. Silva, P. S. Drell, R. Dubois, D. Dultzin, D. Dumora, A. Falcone, C. Farnier, C. Favuzzi, S. J. Fegan, W. B. Focke, E. Forné, P. Fortin, M. Frailis, L. Fuhrmann, Y. Fukazawa, S. Funk, P. Fusco, J. L. Gómez, F. Gargano, D. Gasparrini, N. Gehrels, S. Germani, B. Giebels, N. Giglietto, P. Giommi, F. Giordano, A. Giuliani, T. Glanzman, G. Godfrey, I. A. Grenier, C. Gronwall, J. E. Grove, L. Guillemot, S. Guiriec, M. A. Gurwell, D. Hadasch, Y. Hanabata, A. K. Harding, M. Hayashida, E. Hays, S. E. Healey, J. Heidt, D. Hiriart, D. Horan, E. A. Hoversten, R. E. Hughes, R. Itoh, M. S. Jackson, G. Jóhannesson, A. S. Johnson, W. N. Johnson, S. G. Jorstad, M. Kadler, T. Kamae, H. Katagiri, J. Kataoka, N. Kawai, J. Kennea, M. Kerr, G. Kimeridze, J. Knödlseder, M. L. Kocian, E. N. Kopatskaya, E. Koptelova, T. S. Konstantinova, Y. Y. Kovalev, Yu. A. Kovalev, O. M. Kurtanidze, M. Kuss, J. Lande, V. M. Larionov, L. Latronico, P. Leto, E. Lindfors, F. Longo, F. Loparco, B. Lott, M. N. Lovellette, P. Lubrano, G. M. Madejski, A. Makeev, P. Marchegiani, A. P. Marscher, F. Marshall, W. Max-Moerbeck, M. N. Mazziotta, W. McConville, J. E. McEnery, C. Meurer, P. F. Michelson, W. Mitthumsiri, T. Mizuno, A. A. Moiseev, C. Monte, M. E. Monzani, A. Morselli, I. V. Moskalenko, S. Murgia, I. Nestoras, K. Nilsson, N. A. Nizhelsky, P. L. Nolan, J. P. Norris, E. Nuss, T. Ohsugi, R. Ojha, N. Omodei, E. Orlando, J. F. Ormes, J. Osborne, M. Ozaki, L. Pac-

ciani, P. Padovani, C. Pagani, K. Page, D. Paneque, J. H. Panetta, D. Parent, M. Pasanen, V. Pavlidou, V. Pelassa, M. Pepe, M. Perri, M. Pesce-Rollins, S. Piranomonte, F. Piron, C. Pittori, T. A. Porter, S. Puccetti, F. Rahoui, S. Rainò, C. Raiteri, R. Rando, M. Razzano, A. Reimer, O. Reimer, T. Reposeur, J. L. Richards, S. Ritz, L. S. Rochester, A. Y. Rodriguez, R. W. Romani, J. A. Ros, M. Roth, P. Roustazadeh, F. Ryde, H. F. W. Sadrozinski, A. Sadun, D. Sanchez, A. Sander, P. M. Saz Parkinson, J. D. Scargle, A. Sellerholm, C. Sgrò, M. S. Shaw, L. A. Sigua, E. J. Siskind, D. A. Smith, P. D. Smith, G. Spandre, P. Spinelli, J. L. Starck, M. Stevenson, G. Stratta, M. S. Strickman, D. J. Suson, H. Tajima, H. Takahashi, T. Takahashi, L. O. Takalo, T. Tanaka, J. B. Thayer, J. G. Thayer, D. J. Thompson, L. Tibaldo, D. F. Torres, G. Tosti, A. Tramacere, Y. Uchiyama, T. L. Usher, V. Vasileiou, F. Verrecchia, N. Vilchez, M. Villata, V. Vitale, A. P. Waite, P. Wang, B. L. Winer, K. S. Wood, T. Ylinen, J. A. Zensus, G. V. Zhekanis, and M. Ziegler.
The Spectral Energy Distribution of Fermi Bright Blazars.
ApJ, 716(1):30–70, June 2010.

[2] A. A. Abdo, M. Ackermann, M. Ajello, A. Allafort, W. B. Atwood, L. Baldini, J. Ballet, G. Barbiellini, M. G. Baring, D. Bastieri, B. M. Baughman, K. Bechtol, R. Bellazzini, B. Berenji, P. N. Bhat, R. D. Blandford, E. D. Bloom, E. Bonamente, A. W. Borgland, A. Bouvier, T. J. Brandt, J. Bregeon, A. Brez, M. S. Briggs, M. Brigida, P. Bruel, R. Buehler, T. H. Burnett, S. Buson, G. A. Caliandro, R. A. Cameron, P. A. Caraveo, S. Carrigan, J. M. Casand jian, E. Cavazzuti, C. Cecchi, Ö. Çelik, E. Charles, A. Chekhtman, A. W. Chen, C. C. Cheung, J. Chiang, S. Ciprini, R. Claus, J. Cohen-Tanugi, V. Connaughton, J. Conrad, L. Costamante, C. D. Dermer, A. de Angelis, F. de Palma, S. W. Digel, B. L. Dingus, E. do Couto e. Silva, P. S. Drell, R. Dubois, C. Favuzzi, S. J. Fegan, J. Finke, P. Fortin, Y. Fukazawa, S. Funk, P. Fusco, F. Gargano, D. Gasparrini, N. Gehrels, S. Germani, N. Giglietto, R. C. Gilmore, P. Giommi, F. Giordano, M. Giroletti, T. Glanzman, G. Godfrey, J. Granot, J. Greiner, I. A. Grenier, J. E. Grove, S. Guiriec, M. Gustafsson, D. Hadasch, M. Hayashida, E. Hays, D. Horan, R. E. Hughes, G. Jóhannesson, A. S. Johnson, R. P. Johnson, W. N. Johnson, T. Kamae, H. Katagiri, J. Kataoka, J. Knödlseder, D. Kocevski, M. Kuss, J. Lande, L. Latronico, S. H. Lee, M. Llena Garde, F. Longo, F. Loparco, B. Lott, M. N. Lovellette, P. Lubrano, A. Makeev, M. N. Mazziotta, W. McConville, J. E. McEnery, S. McGlynn, J. Mehault, P. Mészáros, P. F. Michelson, T. Mizuno, A. A. Moiseev, C. Monte,

M. E. Monzani, E. Moretti, A. Morselli, I. V. Moskalenko, S. Murgia, T. Nakamori, M. Naumann-Godo, P. L. Nolan, J. P. Norris, E. Nuss, M. Ohno, T. Ohsugi, A. Okumura, N. Omodei, E. Orlando, J. F. Ormes, M. Ozaki, D. Paneque, J. H. Panetta, D. Parent, V. Pelassa, M. Pepe, M. Pesce-Rollins, F. Piron, T. A. Porter, J. R. Primack, S. Rainò, R. Rando, M. Razzano, S. Razzaque, A. Reimer, O. Reimer, L. C. Reyes, J. Ripken, S. Ritz, R. W. Romani, M. Roth, H. F. W. Sadrozinski, D. Sanchez, A. Sander, J. D. Scargle, T. L. Schalk, C. Sgrò, M. S. Shaw, E. J. Siskind, P. D. Smith, G. Spand re, P. Spinelli, F. W. Stecker, M. S. Strickman, D. J. Suson, H. Tajima, H. Takahashi, T. Takahashi, T. Tanaka, J. B. Thayer, J. G. Thayer, D. J. Thompson, L. Tibaldo, D. F. Torres, G. Tosti, A. Tramacere, Y. Uchiyama, T. L. Usher, J. Vandenbroucke, V. Vasileiou, N. Vilchez, V. Vitale, A. von Kienlin, A. P. Waite, P. Wang, C. Wilson-Hodge, B. L. Winer, K. S. Wood, R. Yamazaki, Z. Yang, T. Ylinen, and M. Ziegler.
Fermi Large Area Telescope Constraints on the Gamma-ray Opacity of the Universe.
ApJ, 723(2):1082–1096, November 2010.

[3] A. A. Abdo, M. Ackermann, M. Ajello, E. Antolini, L. Baldini, J. Ballet, G. Barbiellini, D. Bastieri, K. Bechtol, R. Bellazzini, B. Berenji, R. D. Blandford, E. D. Bloom, E. Bonamente, A. W. Borgland, A. Bouvier, J. Bregeon, A. Brez, M. Brigida, P. Bruel, R. Buehler, T. H. Burnett, S. Buson, G. A. Caliand ro, R. A. Cameron, P. A. Caraveo, S. Carrigan, J. M. Casandjian, E. Cavazzuti, C. Cecchi, Ö. Çelik, A. Chekhtman, C. C. Cheung, J. Chiang, S. Ciprini, R. Claus, J. Cohen-Tanugi, L. R. Cominsky, J. Conrad, L. Costamante, S. Cutini, C. D. Dermer, A. de Angelis, F. de Palma, E. do Couto e. Silva, P. S. Drell, R. Dubois, D. Dumora, C. Farnier, C. Favuzzi, S. J. Fegan, W. B. Focke, P. Fortin, M. Frailis, Y. Fukazawa, S. Funk, P. Fusco, F. Gargano, D. Gasparrini, N. Gehrels, S. Germani, B. Giebels, N. Giglietto, P. Giommi, F. Giordano, T. Glanzman, G. Godfrey, I. A. Grenier, M. H. Grondin, J. E. Grove, S. Guiriec, D. Hadasch, M. Hayashida, E. Hays, S. E. Healey, D. Horan, R. E. Hughes, R. Itoh, G. Jóhannesson, A. S. Johnson, W. N. Johnson, T. Kamae, H. Katagiri, J. Kataoka, N. Kawai, J. Knödlseder, M. Kuss, J. Lande, S. Larsson, L. Latronico, M. Lemoine-Goumard, F. Longo, F. Loparco, B. Lott, M. N. Lovellette, P. Lubrano, G. M. Madejski, A. Makeev, E. Massaro, M. N. Mazziotta, J. E. McEnery, P. F. Michelson, W. Mitthumsiri, T. Mizuno, A. A. Moiseev, C. Monte, M. E. Monzani, A. Morselli, I. V. Moskalenko, M. Mueller, S. Murgia, P. L. Nolan, J. P. Norris, E. Nuss, M. Ohno, T. Ohsugi, N. Omodei, E. Or-

lando, J. F. Ormes, M. Ozaki, J. H. Panetta, D. Parent, V. Pelassa, M. Pepe, M. Pesce-Rollins, F. Piron, T. A. Porter, S. Rainò, R. Rando, M. Razzano, A. Reimer, O. Reimer, S. Ritz, A. Y. Rodriguez, R. W. Romani, M. Roth, F. Ryde, H. F. W. Sadrozinski, A. Sand er, J. D. Scargle, C. Sgrò, M. S. Shaw, P. D. Smith, G. Spandre, P. Spinelli, J. L. Starck, M. S. Strickman, D. J. Suson, H. Takahashi, T. Takahashi, T. Tanaka, J. B. Thayer, J. G. Thayer, D. J. Thompson, L. Tibaldo, D. F. Torres, G. Tosti, A. Tramacere, Y. Uchiyama, T. L. Usher, V. Vasileiou, N. Vilchez, V. Vitale, A. P. Waite, E. Wallace, P. Wang, B. L. Winer, K. S. Wood, Z. Yang, T. Ylinen, and M. Ziegler.

Gamma-ray Light Curves and Variability of Bright Fermi-detected Blazars.

ApJ, 722(1):520–542, October 2010.

[4] A. A. Abdo, M. Ackermann, M. Ajello, L. Baldini, J. Ballet, G. Barbiellini, D. Bastieri, K. Bechtol, R. Bellazzini, B. Berenji, R. D. Bland ford, E. D. Bloom, E. Bonamente, A. W. Borgland , A. Bouvier, J. Bregeon, A. Brez, M. Brigida, P. Bruel, R. Buehler, S. Buson, G. A. Caliandro, R. A. Cameron, A. Cannon, P. A. Caraveo, S. Carrigan, J. M. Casandjian, E. Cavazzuti, C. Cecchi, Ö. Çelik, E. Charles, A. Chekhtman, J. Chiang, S. Ciprini, R. Claus, J. Cohen-Tanugi, J. Conrad, S. Cutini, A. de Angelis, F. de Palma, C. D. Dermer, E. do Couto e. Silva, P. S. Drell, R. Dubois, D. Dumora, L. Escande, C. Favuzzi, S. J. Fegan, J. Finke, W. B. Focke, P. Fortin, M. Frailis, L. Fuhrmann, Y. Fukazawa, T. Fukuyama, S. Funk, P. Fusco, F. Gargano, D. Gasparrini, N. Gehrels, M. Georganopoulos, S. Germani, B. Giebels, N. Giglietto, P. Giommi, F. Giordano, M. Giroletti, T. Glanzman, G. Godfrey, I. A. Grenier, S. Guiriec, D. Hadasch, M. Hayashida, E. Hays, D. Horan, R. E. Hughes, G. Jóhannesson, A. S. Johnson, W. N. Johnson, M. Kadler, T. Kamae, H. Katagiri, J. Kataoka, J. Knödlseder, M. Kuss, J. Lande, L. Latronico, S. H. Lee, F. Longo, F. Loparco, B. Lott, M. N. Lovellette, P. Lubrano, G. M. Madejski, A. Makeev, W. Max-Moerbeck, M. N. Mazziotta, J. E. McEnery, J. Mehault, P. F. Michelson, W. Mitthumsiri, T. Mizuno, C. Monte, M. E. Monzani, A. Morselli, I. V. Moskalenko, S. Murgia, T. Nakamori, M. Naumann-Godo, S. Nishino, P. L. Nolan, J. P. Norris, E. Nuss, T. Ohsugi, A. Okumura, N. Omodei, E. Orlando, J. F. Ormes, M. Ozaki, D. Paneque, J. H. Panetta, D. Parent, V. Pavlidou, T. J. Pearson, V. Pelassa, M. Pepe, M. Pesce-Rollins, M. Pierbattista, F. Piron, T. A. Porter, S. Rainò, R. Rando, M. Razzano, A. Readhead, A. Reimer, O. Reimer, L. C. Reyes, J. L. Richards, S. Ritz, M. Roth, H. F. W. Sadrozinski, D. Sanchez, A. Sander, C. Sgrò, E. J. Siskind,

P. D. Smith, G. Spand re, P. Spinelli, Ł. Stawarz, M. Stevenson, M. S. Strickman, D. J. Suson, H. Takahashi, T. Takahashi, T. Tanaka, J. G. Thayer, J. B. Thayer, D. J. Thompson, L. Tibaldo, D. F. Torres, G. Tosti, A. Tramacere, E. Troja, T. L. Usher, J. Vandenbroucke, V. Vasileiou, G. Vianello, N. Vilchez, V. Vitale, A. P. Waite, P. Wang, A. E. Wehrle, B. L. Winer, K. S. Wood, Z. Yang, Y. Yatsu, T. Ylinen, J. A. Zensus, M. Ziegler, Fermi LAT Collaboration, J. Aleksić, L. A. Antonelli, P. Antoranz, M. Backes, J. A. Barrio, J. Becerra González, W. Bednarek, A. Berdyugin, K. Berger, E. Bernardini, A. Biland, O. Blanch, R. K. Bock, A. Boller, G. Bonnoli, P. Bordas, D. Borla Tridon, V. Bosch-Ramon, D. Bose, I. Braun, T. Bretz, M. Camara, E. Carmona, A. Carosi, P. Colin, E. Colombo, J. L. Contreras, J. Cortina, S. Covino, F. Dazzi, A. de Angelis, E. De Cea del Pozo, C. Delgado Mendez, B. De Lotto, M. De Maria, F. De Sabata, A. Diago Ortega, M. Doert, A. Domínguez, D. Dominis Prester, D. Dorner, M. Doro, D. Elsaesser, D. Ferenc, M. V. Fonseca, L. Font, R. J. García López, M. Garczarczyk, M. Gaug, G. Giavitto, N. Godinovi, D. Hadasch, A. Herrero, D. Hildebrand, D. Höhne-Mönch, J. Hose, D. Hrupec, T. Jogler, S. Klepser, T. Krähenbühl, D. Kranich, J. Krause, A. La Barbera, E. Leonardo, E. Lindfors, S. Lombardi, M. López, E. Lorenz, P. Majumdar, E. Makariev, G. Maneva, N. Mankuzhiyil, K. Mannheim, L. Maraschi, M. Mariotti, M. Martínez, D. Mazin, M. Meucci, J. M. Mirand a, R. Mirzoyan, H. Miyamoto, J. Moldón, A. Moralejo, D. Nieto, K. Nilsson, R. Orito, I. Oya, R. Paoletti, J. M. Paredes, S. Partini, M. Pasanen, F. Pauss, R. G. Pegna, M. A. Perez-Torres, M. Persic, J. Peruzzo, J. Pochon, F. Prada, P. G. Prada Moroni, E. Prand ini, N. Puchades, I. Puljak, T. Reichardt, W. Rhode, M. Ribó, J. Rico, M. Rissi, S. Rügamer, A. Saggion, K. Saito, T. Y. Saito, M. Salvati, M. Sánchez-Conde, K. Satalecka, V. Scalzotto, V. Scapin, C. Schultz, T. Schweizer, M. Shayduk, S. N. Shore, A. Sierpowska-Bartosik, A. Sillanpää, J. Sitarek, D. Sobczynska, F. Spanier, S. Spiro, A. Stamerra, B. Steinke, J. Storz, N. Strah, J. C. Struebig, T. Suric, L. O. Takalo, F. Tavecchio, P. Temnikov, T. Terzić, D. Tescaro, M. Teshima, H. Vankov, R. M. Wagner, Q. Weitzel, V. Zabalza, F. Zandanel, R. Zanin, MAGIC Collaboration, M. Villata, C. Raiteri, H. D. Aller, M. F. Aller, W. P. Chen, B. Jordan, E. Koptelova, O. M. Kurtanidze, A. Lähteenmäki, B. McBreen, V. M. Larionov, C. S. Lin, M. G. Nikolashvili, R. Reinthal, E. Angelakis, M. Capalbi, A. Carramiñana, L. Carrasco, P. Cassaro, A. Cesarini, A. Falcone, M. A. Gurwell, T. Hovatta, Yu. A. Kovalev, Y. Y. Kovalev, T. P. Krichbaum, H. A. Krimm, M. L. Lister, J. W. Moody, G. Maccaferri, Y. Mori, I. Nestoras, A. Orlati, C. Pace, C. Pagani, R. Pearson, M. Perri, B. G.

Piner, E. Ros, A. C. Sadun, T. Sakamoto, J. Tammi, and A. Zook.
Fermi Large Area Telescope Observations of Markarian 421: The Missing Piece of its Spectral Energy Distribution.
ApJ, 736(2):131, August 2011.

[5] S. Abdollahi, F. Acero, M. Ackermann, M. Ajello, W. B. Atwood, M. Axelsson, L. Baldini, J. Ballet, G. Barbiellini, D. Bastieri, J. Becerra Gonzalez, R. Bellazzini, A. Berretta, E. Bissaldi, R. D. Bland ford, E. D. Bloom, R. Bonino, E. Bottacini, T. J. Brandt, J. Bregeon, P. Bruel, R. Buehler, T. H. Burnett, S. Buson, R. A. Cameron, R. Caputo, P. A. Caraveo, J. M. Casandjian, D. Castro, E. Cavazzuti, E. Charles, S. Chaty, S. Chen, C. C. Cheung, G. Chiaro, S. Ciprini, J. Cohen-Tanugi, L. R. Cominsky, J. Coronado-Blázquez, D. Costantin, A. Cuoco, S. Cutini, F. D'Ammando, M. DeKlotz, P. de la Torre Luque, F. de Palma, A. Desai, S. W. Digel, N. Di Lalla, M. Di Mauro, L. Di Venere, A. Domínguez, D. Dumora, F. Fana Dirirsa, S. J. Fegan, E. C. Ferrara, A. Franckowiak, Y. Fukazawa, S. Funk, P. Fusco, F. Gargano, D. Gasparrini, N. Giglietto, P. Giommi, F. Giordano, M. Giroletti, T. Glanzman, D. Green, I. A. Grenier, S. Griffin, M. H. Grondin, J. E. Grove, S. Guiriec, A. K. Harding, K. Hayashi, E. Hays, J. W. Hewitt, D. Horan, G. Jóhannesson, T. J. Johnson, T. Kamae, M. Kerr, D. Kocevski, M. Kovac'evic', M. Kuss, D. Landriu, S. Larsson, L. Latronico, M. Lemoine-Goumard, J. Li, I. Liodakis, F. Longo, F. Loparco, B. Lott, M. N. Lovellette, P. Lubrano, G. M. Madejski, S. Maldera, D. Malyshev, A. Manfreda, E. J. Marchesini, L. Marcotulli, G. Martí-Devesa, P. Martin, F. Massaro, M. N. Mazziotta, J. E. McEnery, I. Mereu, M. Meyer, P. F. Michelson, N. Mirabal, T. Mizuno, M. E. Monzani, A. Morselli, I. V. Moskalenko, M. Negro, E. Nuss, R. Ojha, N. Omodei, M. Orienti, E. Orlando, J. F. Ormes, M. Palatiello, V. S. Paliya, D. Paneque, Z. Pei, H. Peña-Herazo, J. S. Perkins, M. Persic, M. Pesce-Rollins, V. Petrosian, L. Petrov, F. Piron, H. Poon, T. A. Porter, G. Principe, S. Rainò, R. Rando, M. Razzano, S. Razzaque, A. Reimer, O. Reimer, Q. Remy, T. Reposeur, R. W. Romani, P. M. Saz Parkinson, F. K. Schinzel, D. Serini, C. Sgrò, E. J. Siskind, D. A. Smith, G. Spandre, P. Spinelli, A. W. Strong, D. J. Suson, H. Tajima, M. N. Takahashi, D. Tak, J. B. Thayer, D. J. Thompson, L. Tibaldo, D. F. Torres, E. Torresi, J. Valverde, B. Van Klaveren, P. van Zyl, K. Wood, M. Yassine, and G. Zaharijas.
Fermi Large Area Telescope Fourth Source Catalog.
ApJSS, 247(1):33, March 2020.

[6] A. U. Abeysekara, S. Archambault, A. Archer, T. Aune, A. Barnacka, W. Benbow, R. Bird, J. Biteau, J. H. Buckley, V. Bugaev, J. V. Cardenzana, M. Cerruti, X. Chen, J. L. Christiansen, L. Ciupik, M. P. Connolly, P. Coppi, W. Cui, H. J. Dickinson, J. Dumm, J. D. Eisch, M. Errando, A. Falcone, Q. Feng, J. P. Finley, H. Fleischhack, A. Flinders, P. Fortin, L. Fortson, A. Furniss, G. H. Gilland ers, S. Griffin, J. Grube, G. Gyuk, M. Hütten, N. Håkansson, D. Hanna, J. Holder, T. B. Humensky, C. A. Johnson, P. Kaaret, P. Kar, N. Kelley-Hoskins, Y. Khassen, D. Kieda, M. Krause, F. Krennrich, S. Kumar, M. J. Lang, G. Maier, S. McArthur, A. McCann, K. Meagher, P. Moriarty, R. Mukherjee, D. Nieto, A. O'Faoláin de Bhróithe, R. A. Ong, A. N. Otte, N. Park, J. S. Perkins, A. Petrashyk, M. Pohl, A. Popkow, E. Pueschel, J. Quinn, K. Ragan, G. Ratliff, P. T. Reynolds, G. T. Richards, E. Roache, J. Rousselle, M. Santander, G. H. Sembroski, K. Shahinyan, A. W. Smith, D. Staszak, I. Telezhinsky, N. W. Todd, J. V. Tucci, J. Tyler, V. V. Vassiliev, S. Vincent, S. P. Wakely, O. M. Weiner, A. Weinstein, A. Wilhelm, D. A. Williams, B. Zitzer, VERITAS, P. S. Smith, SPOL, T. W. S. Holoien, J. L. Prieto, C. S. Kochanek, K. Z. Stanek, B. Shappee, ASAS-SN, T. Hovatta, W. Max-Moerbeck, T. J. Pearson, R. A. Reeves, J. L. Richards, A. C. S. Readhead, OVRO, G. M. Madejski, NuSTAR, S. G. Djorgovski, A. J. Drake, M. J. Graham, A. Mahabal, and CRTS.

Gamma-Rays from the Quasar PKS 1441+25: Story of an Escape.
ApJL, 815(2):L22, December 2015.

[7] V. A. Acciari, E. Aliu, T. Arlen, M. Beilicke, W. Benbow, S. M. Bradbury, J. H. Buckley, V. Bugaev, Y. Butt, K. L. Byrum, O. Celik, A. Cesarini, L. Ciupik, Y. C. K. Chow, P. Cogan, P. Colin, W. Cui, M. K. Daniel, T. Ergin, A. D. Falcone, S. J. Fegan, J. P. Finley, P. Fortin, L. F. Fortson, A. Furniss, G. H. Gilland ers, J. Grube, R. Guenette, G. Gyuk, D. Hanna, E. Hays, J. Holder, D. Horan, C. M. Hui, T. B. Humensky, A. Imran, P. Kaaret, N. Karlsson, M. Kertzman, D. B. Kieda, J. Kildea, A. Konopelko, H. Krawczynski, F. Krennrich, M. J. Lang, S. LeBohec, G. Maier, A. McCann, M. McCutcheon, P. Moriarty, R. Mukherjee, T. Nagai, J. Niemiec, R. A. Ong, D. Pandel, J. S. Perkins, M. Pohl, J. Quinn, K. Ragan, L. C. Reyes, P. T. Reynolds, H. J. Rose, M. Schroedter, G. H. Sembroski, A. W. Smith, D. Steele, S. P. Swordy, J. A. Toner, L. Valcarcel, V. V. Vassiliev, R. Wagner, S. P. Wakely, J. E. Ward, T. C. Weekes, A. Weinstein, R. J. White, D. A. Williams, S. A. Wissel, M. Wood, and B. Zitzer.

VERITAS Observations of the BL Lac Object 1ES 1218+304.
ApJ, 695(2):1370–1375, April 2009.

[8] V. A. Acciari, E. Aliu, M. Beilicke, W. Benbow, D. Boltuch, M. Böttcher, S. M. Bradbury, V. Bugaev, K. Byrum, A. Cesarini, L. Ciupik, P. Cogan, W. Cui, R. Dickherber, C. Duke, A. Falcone, J. P. Finley, G. Finnegan, L. Fortson, A. Furniss, N. Galante, D. Gall, K. Gibbs, R. Guenette, G. H. Gillanders, S. Godambe, J. Grube, D. Hanna, C. M. Hui, T. B. Humensky, A. Imran, P. Kaaret, N. Karlsson, M. Kertzman, D. Kieda, H. Krawczynski, F. Krennrich, M. J. Lang, S. LeBohec, G. Maier, S. McArthur, A. McCann, P. Moriarty, T. Nagai, R. A. Ong, A. N. Otte, D. Pandel, J. S. Perkins, A. Pichel, M. Pohl, J. Quinn, K. Ragan, L. C. Reyes, P. T. Reynolds, E. Roache, H. J. Rose, M. Schroedter, G. H. Sembroski, A. W. Smith, D. Steele, S. P. Swordy, M. Theiling, S. Thibadeau, V. V. Vassiliev, S. Vincent, S. P. Wakely, T. C. Weekes, A. Weinstein, T. Weisgarber, D. A. Williams, and VERITAS Collaboration.

Discovery of Variability in the Very High Energy γ-Ray Emission of 1ES 1218+304 with VERITAS.

ApJL, 709(2):L163–L167, February 2010.

[9] M. Ackermann, M. Ajello, A. Allafort, P. Schady, L. Baldini, J. Ballet, G. Barbiellini, D. Bastieri, R. Bellazzini, R. D. Blandford, E. D. Bloom, A. W. Borgland, E. Bottacini, A. Bouvier, J. Bregeon, M. Brigida, P. Bruel, R. Buehler, S. Buson, G. A. Caliandro, R. A. Cameron, P. A. Caraveo, E. Cavazzuti, C. Cecchi, E. Charles, R. C. G. Chaves, A. Chekhtman, C. C. Cheung, J. Chiang, G. Chiaro, S. Ciprini, R. Claus, J. Cohen-Tanugi, J. Conrad, S. Cutini, F. D'Ammando, F. de Palma, C. D. Dermer, S. W. Digel, E. do Couto e Silva, A. Domínguez, P. S. Drell, A. Drlica-Wagner, C. Favuzzi, S. J. Fegan, W. B. Focke, A. Franckowiak, Y. Fukazawa, S. Funk, P. Fusco, F. Gargano, D. Gasparrini, N. Gehrels, S. Germani, N. Giglietto, F. Giordano, M. Giroletti, T. Glanzman, G. Godfrey, I. A. Grenier, J. E. Grove, S. Guiriec, M. Gustafsson, D. Hadasch, M. Hayashida, E. Hays, M. S. Jackson, T. Jogler, J. Kataoka, J. Knödlseder, M. Kuss, J. Lande, S. Larsson, L. Latronico, F. Longo, F. Loparco, M. N. Lovellette, P. Lubrano, M. N. Mazziotta, J. E. McEnery, J. Mehault, P. F. Michelson, T. Mizuno, C. Monte, M. E. Monzani, A. Morselli, I. V. Moskalenko, S. Murgia, A. Tramacere, E. Nuss, J. Greiner, M. Ohno, T. Ohsugi, N. Omodei, M. Orienti, E. Orland o, J. F. Ormes, D. Paneque, J. S. Perkins, M. Pesce-Rollins, F. Piron, G. Pivato, T. A. Porter, S. Rainò, R. Rando, M. Razzano, S. Razzaque, A. Reimer, O. Reimer, L. C. Reyes, S. Ritz, A. Rau, C. Romoli, M. Roth, M. Sánchez-Conde, D. A. Sanchez, J. D. Scargle, C. Sgrò, E. J. Siskind, G. Spandre, P. Spinelli, Łukasz Stawarz, D. J. Suson,

H. Takahashi, T. Tanaka, J. G. Thayer, D. J. Thompson, L. Tibaldo, M. Tinivella, D. F. Torres, G. Tosti, E. Troja, T. L. Usher, J. Vandenbroucke, V. Vasileiou, G. Vianello, V. Vitale, A. P. Waite, B. L. Winer, K. S. Wood, and M. Wood.
The Imprint of the Extragalactic Background Light in the Gamma-Ray Spectra of Blazars.
Science, 338(6111):1190, November 2012.

[10] M. Ackermann, M. Ajello, L. Baldini, J. Ballet, G. Barbiellini, D. Bastieri, J. Becerra Gonzalez, R. Bellazzini, E. Bissaldi, R. D. Blandford, E. D. Bloom, R. Bonino, E. Bottacini, J. Bregeon, P. Bruel, R. Buehler, S. Buson, R. A. Cameron, M. Caragiulo, P. A. Caraveo, E. Cavazzuti, C. Cecchi, C. C. Cheung, J. Chiang, G. Chiaro, S. Ciprini, J. Conrad, D. Costantin, F. Costanza, S. Cutini, F. D'Ammando, F. de Palma, R. Desiante, S. W. Digel, N. Di Lalla, M. Di Mauro, L. Di Venere, A. Domínguez, P. S. Drell, C. Favuzzi, S. J. Fegan, E. C. Ferrara, J. Finke, W. B. Focke, Y. Fukazawa, S. Funk, P. Fusco, F. Gargano, D. Gasparrini, N. Giglietto, F. Giordano, M. Giroletti, D. Green, I. A. Grenier, L. Guillemot, S. Guiriec, D. H. Hartmann, E. Hays, D. Horan, T. Jogler, G. Jóhannesson, A. S. Johnson, M. Kuss, G. La Mura, S. Larsson, L. Latronico, J. Li, F. Longo, F. Loparco, M. N. Lovellette, P. Lubrano, J. D. Magill, S. Maldera, A. Manfreda, L. Marcotulli, M. N. Mazziotta, P. F. Michelson, N. Mirabal, W. Mitthumsiri, T. Mizuno, M. E. Monzani, A. Morselli, I. V. Moskalenko, M. Negro, E. Nuss, T. Ohsugi, R. Ojha, N. Omodei, M. Orienti, E. Orlando, J. F. Ormes, V. S. Paliya, D. Paneque, J. S. Perkins, M. Persic, M. Pesce-Rollins, F. Piron, T. A. Porter, G. Principe, S. Rainò, R. Rando, B. Rani, M. Razzano, S. Razzaque, A. Reimer, O. Reimer, R. W. Romani, C. Sgrò, D. Simone, E. J. Siskind, F. Spada, G. Spandre, P. Spinelli, C. S. Stalin, L. Stawarz, D. J. Suson, M. Takahashi, K. Tanaka, J. B. Thayer, D. J. Thompson, D. F. Torres, E. Torresi, G. Tosti, E. Troja, G. Vianello, and K. S. Wood.
Gamma-Ray Blazars within the First 2 Billion Years.
ApJL, 837(1):L5, March 2017.

[11] M. Ackermann, R. Anantua, and et al.
Minute-timescale 100 MeV γ-Ray Variability during the Giant Outburst of Quasar 3C 279 Observed by Fermi-LAT in 2015 June.
ApJL, 824:L20, June 2016.

[12] M. L. Ahnen, S. Ansoldi, L. A. Antonelli, P. Antoranz, A. Babic, B. Banerjee, P. Bangale, U. Barres de Almeida, J. A. Barrio, W. Bednarek, E. Bernardini, B. Biasuzzi, A. Biland, O. Blanch,

S. Bonnefoy, G. Bonnoli, F. Borracci, T. Bretz, E. Carmona, A. Carosi, A. Chatterjee, R. Clavero, P. Colin, E. Colombo, J. L. Contreras, J. Cortina, S. Covino, P. Da Vela, F. Dazzi, A. De Angelis, B. De Lotto, E. de Oña Wilhelmi, C. Delgado Mendez, F. Di Pierro, D. Dominis Prester, D. Dorner, M. Doro, S. Einecke, D. Eisenacher Glawion, D. Elsaesser, A. Fernández-Barral, D. Fidalgo, M. V. Fonseca, L. Font, K. Frantzen, C. Fruck, D. Galindo, R. J. García López, M. Garczarczyk, D. Garrido Terrats, M. Gaug, P. Giammaria, N. Godinović, A. González Muñoz, D. Guberman, A. Hahn, Y. Hanabata, M. Hayashida, J. Herrera, J. Hose, D. Hrupec, G. Hughes, W. Idec, K. Kodani, Y. Konno, H. Kubo, J. Kushida, A. La Barbera, D. Lelas, E. Lindfors, S. Lombardi, M. López, R. López-Coto, A. López-Oramas, E. Lorenz, P. Majumdar, M. Makariev, K. Mallot, G. Maneva, M. Manganaro, K. Mannheim, L. Maraschi, B. Marcote, M. Mariotti, M. Martínez, D. Mazin, U. Menzel, J. M. Mirand a, R. Mirzoyan, A. Moralejo, E. Moretti, D. Nakajima, V. Neustroev, A. Niedzwiecki, M. Nievas Rosillo, K. Nilsson, K. Nishijima, K. Noda, R. Orito, A. Overkemping, S. Paiano, J. Palacio, M. Palatiello, D. Paneque, R. Paoletti, J. M. Paredes, X. Paredes-Fortuny, M. Persic, J. Poutanen, P. G. Prada Moroni, E. Prand ini, I. Puljak, W. Rhode, M. Ribó, J. Rico, J. Rodriguez Garcia, T. Saito, K. Satalecka, C. Schultz, T. Schweizer, S. N. Shore, A. Sillanpää, J. Sitarek, I. Snidaric, D. Sobczynska, A. Stamerra, T. Steinbring, M. Strzys, L. Takalo, H. Takami, F. Tavecchio, P. Temnikov, T. Terzić, D. Tescaro, M. Teshima, J. Thaele, D. F. Torres, T. Toyama, A. Treves, V. Verguilov, I. Vovk, J. E. Ward, M. Will, M. H. Wu, R. Zanin, MAGIC Collaboration, M. Ajello, L. Baldini, G. Barbiellini, D. Bastieri, J. Becerra González, R. Bellazzini, E. Bissaldi, R. D. Blandford, R. Bonino, J. Bregeon, P. Bruel, S. Buson, G. A. Caliandro, R. A. Cameron, M. Caragiulo, P. A. Caraveo, E. Cavazzuti, J. Chiang, G. Chiaro, S. Ciprini, F. D'Ammando, F. de Palma, R. Desiante, L. Di Venere, A. Domínguez, P. Fusco, F. Gargano, D. Gasparrini, N. Giglietto, F. Giordano, M. Giroletti, I. A. Grenier, S. Guiriec, E. Hays, J. W. Hewitt, T. Jogler, M. Kuss, S. Larsson, J. Li, L. Li, F. Longo, F. Loparco, M. N. Lovellette, P. Lubrano, S. Maldera, M. Mayer, M. N. Mazziotta, J. E. McEnery, N. Mirabal, T. Mizuno, M. E. Monzani, A. Morselli, I. V. Moskalenko, E. Nuss, R. Ojha, T. Ohsugi, N. Omodei, E. Orland o, J. S. Perkins, M. Pesce-Rollins, F. Piron, G. Pivato, T. A. Porter, S. Raino, R. Rando, M. Razzano, A. Reimer, O. Reimer, C. Sgro, E. J. Siskind, F. Spada, G. Spandre, P. Spinelli, H. Tajima, H. Takahashi, J. B. Thayer, D. J. Thompson, E. Troja, K. S. Wood, Fermi-LAT Collaboration, M. Balokovic, A. Berdyugin,

A. Carraminana, L. Carrasco, V. Chavushyan, V. Fallah Ramazani, M. Feige, S. Haarto, P. Haeusner, T. Hovatta, J. Kania, J. Klamt, A. Lähteenmäki, J. Leon-Tavares, C. Lorey, L. Pacciani, A. Porras, E. Recillas, R. Reinthal, M. Tornikoski, D. Wolfert, and N. Zottmann.
Very High Energy γ-Rays from the Universe's Middle Age: Detection of the z = 0.940 Blazar PKS 1441+25 with MAGIC.
ApJL, 815(2):L23, December 2015.

[13] M. Ajello, R. Angioni, M. Axelsson, J. Ballet, G. Barbiellini, D. Bastieri, J. Becerra Gonzalez, R. Bellazzini, E. Bissaldi, E. D. Bloom, R. Bonino, E. Bottacini, P. Bruel, S. Buson, F. Cafardo, R. A. Cameron, E. Cavazzuti, S. Chen, C. C. Cheung, S. Ciprini, D. Costantin, S. Cutini, F. D'Ammando, P. de la Torre Luque, R. de Menezes, F. de Palma, A. Desai, N. Di Lalla, L. Di Venere, A. Domínguez, F. Fana Dirirsa, E. C. Ferrara, J. Finke, A. Franckowiak, Y. Fukazawa, S. Funk, P. Fusco, F. Gargano, S. Garrappa, D. Gasparrini, N. Giglietto, F. Giordano, M. Giroletti, D. Green, I. A. Grenier, S. Guiriec, S. Harita, E. Hays, D. Horan, R. Itoh, G. Jóhannesson, M. Kovac'evic', F. Krauss, M. Kreter, M. Kuss, S. Larsson, C. Leto, J. Li, I. Liodakis, F. Longo, F. Loparco, B. Lott, M. N. Lovellette, P. Lubrano, G. M. Madejski, S. Maldera, A. Manfreda, G. Martí-Devesa, F. Massaro, M. N. Mazziotta, I. Mereu, M. Meyer, G. Migliori, N. Mirabal, T. Mizuno, M. E. Monzani, A. Morselli, I. V. Moskalenko, M. Negro, R. Nemmen, E. Nuss, L. S. Ojha, R. Ojha, N. Omodei, M. Orienti, E. Orlando, J. F. Ormes, V. S. Paliya, Z. Pei, H. Peña-Herazo, M. Persic, M. Pesce-Rollins, L. Petrov, F. Piron, H. Poon, G. Principe, S. Rainò, R. Rando, B. Rani, M. Razzano, S. Razzaque, A. Reimer, O. Reimer, F. K. Schinzel, D. Serini, C. Sgrò, E. J. Siskind, G. Spandre, P. Spinelli, D. J. Suson, Y. Tachibana, D. J. Thompson, D. F. Torres, E. Torresi, E. Troja, J. Valverde, P. van Zyl, and M. Yassine.
The Fourth Catalog of Active Galactic Nuclei Detected by the Fermi Large Area Telescope.
ApJ, 892(2):105, April 2020.

[14] M. Ajello, G. Ghisellini, V. S. Paliya, D. Kocevski, G. Tagliaferri, G. Madejski, A. Rau, P. Schady, J. Greiner, F. Massaro, M. Baloković, R. Bühler, M. Giomi, L. Marcotulli, F. D'Ammando, D. Stern, S. E. Boggs, F. E. Christensen, W. W. Craig, C. J. Hailey, F. A. Harrison, and W. W. Zhang.
NuSTAR, Swift, and GROND Observations of the Flaring MeV Blazar PMN J0641-0320.

ApJ, 826(1):76, July 2016.

[15] J. Albert, E. Aliu, H. Anderhub, P. Antoranz, A. Armada, M. Asensio, C. Baixeras, J. A. Barrio, M. Bartelt, H. Bartko, D. Bastieri, S. R. Bavikadi, W. Bednarek, K. Berger, C. Bigongiari, A. Biland, E. Bisesi, R. K. Bock, T. Bretz, I. Britvitch, M. Camara, A. Chilingarian, S. Ciprini, J. A. Coarasa, S. Commichau, J. L. Contreras, J. Cortina, V. Curtef, V. Danielyan, F. Dazzi, A. De Angelis, R. de los Reyes, B. De Lotto, E. Domingo-Santamaría, D. Dorner, M. Doro, M. Errand o, M. Fagiolini, D. Ferenc, E. Fernández, R. Firpo, J. Flix, M. V. Fonseca, L. Font, N. Galante, M. Garczarczyk, M. Gaug, M. Giller, F. Goebel, D. Hakobyan, M. Hayashida, T. Hengstebeck, D. Höhne, J. Hose, P. Jacon, O. Kalekin, D. Kranich, A. Laille, T. Lenisa, P. Liebing, E. Lindfors, F. Longo, J. López, M. López, E. Lorenz, F. Lucarelli, P. Majumdar, G. Maneva, K. Mannheim, M. Mariotti, M. Martínez, K. Mase, D. Mazin, M. Meucci, M. Meyer, J. M. Miranda, R. Mirzoyan, S. Mizobuchi, A. Moralejo, K. Nilsson, E. Oña-Wilhelmi, R. Orduña, N. Otte, I. Oya, D. Paneque, R. Paoletti, M. Pasanen, D. Pascoli, F. Pauss, N. Pavel, R. Pegna, M. Persic, L. Peruzzo, A. Piccioli, M. Poller, E. Prandini, W. Rhode, J. Rico, B. Riegel, M. Rissi, A. Robert, S. Rügamer, A. Saggion, A. Sánchez, P. Sartori, V. Scalzotto, R. Schmitt, T. Schweizer, M. Shayduk, K. Shinozaki, S. N. Shore, N. Sidro, A. Sillanpää, D. Sobczyńska, A. Stamerra, L. S. Stark, L. Takalo, P. Temnikov, D. Tescaro, M. Teshima, N. Tonello, A. Torres, D. F. Torres, N. Turini, H. Vankov, A. Vardanyan, V. Vitale, R. M. Wagner, T. Wibig, W. Wittek, and J. Zapatero.
Discovery of Very High Energy Gamma Rays from 1ES 1218+30.4.
ApJL, 642(2):L119–L122, May 2006.

[16] R. Angioni, R. Nesci, J. D. Finke, S. Buson, and S. Ciprini.
The large gamma-ray flare of the flat-spectrum radio quasar PKS 0346-27.
A&A, 627:A140, July 2019.

[17] S. Ansoldi, L. A. Antonelli, C. Arcaro, D. Baack, A. Babić, B. Banerjee, P. Bangale, U. Barres de Almeida, J. A. Barrio, J. Becerra González, W. Bednarek, E. Bernardini, R. C. Berse, A. Berti, J. Besenrieder, W. Bhattacharyya, C. Bigongiari, A. Biland, O. Blanch, G. Bonnoli, R. Carosi, G. Ceribella, A. Chatterjee, S. M. Colak, P. Colin, E. Colombo, J. L. Contreras, J. Cortina, S. Covino, P. Cumani, V. D'Elia, P. Da Vela, F. Dazzi, A. De Angelis, B. De Lotto, M. Delfino, J. Delgado, F. Di Pierro, A. Domínguez, D. Dominis

Prester, D. Dorner, M. Doro, S. Einecke, D. Elsaesser, V. Fallah Ramazani, A. Fattorini, A. Fernández-Barral, G. Ferrara, D. Fidalgo, L. Foffano, M. V. Fonseca, L. Font, C. Fruck, S. Gallozzi, R. J. García López, M. Garczarczyk, M. Gaug, P. Giammaria, N. Godinović, D. Guberman, D. Hadasch, A. Hahn, T. Hassan, M. Hayashida, J. Herrera, J. Hoang, D. Hrupec, S. Inoue, K. Ishio, Y. Iwamura, Y. Konno, H. Kubo, J. Kushida, A. Lamastra, D. Lelas, F. Leone, E. Lindfors, S. Lombardi, F. Longo, M. López, C. Maggio, P. Majumdar, M. Makariev, G. Maneva, M. Manganaro, K. Mannheim, L. Maraschi, M. Mariotti, M. Martínez, S. Masuda, D. Mazin, K. Mielke, M. Minev, J. M. Miranda, R. Mirzoyan, A. Moralejo, V. Moreno, E. Moretti, V. Neustroev, A. Niedzwiecki, M. Nievas Rosillo, C. Nigro, K. Nilsson, D. Ninci, K. Nishijima, K. Noda, L. Nogués, S. Paiano, J. Palacio, D. Paneque, R. Paoletti, J. M. Paredes, G. Pedaletti, P. Peñil, M. Peresano, M. Persic, K. Pfrang, P. G. Prada Moroni, E. Prandini, I. Puljak, J. R. Garcia, W. Rhode, M. Ribó, J. Rico, C. Righi, A. Rugliancich, L. Saha, T. Saito, K. Satalecka, T. Schweizer, J. Sitarek, I. Šnidarić, D. Sobczynska, A. Stamerra, M. Strzys, T. Surić, F. Tavecchio, P. Temnikov, T. Terzić, M. Teshima, N. Torres-Albá, S. Tsujimoto, G. Vanzo, M. Vazquez Acosta, I. Vovk, J. E. Ward, M. Will, D. Zarić, and M. Cerruti.
The Blazar TXS 0506+056 Associated with a High-energy Neutrino: Insights into Extragalactic Jets and Cosmic-Ray Acceleration.
ApJL, 863:L10, August 2018.

[18] A. T. Araudo, V. Bosch-Ramon, and G. E. Romero.
Gamma rays from cloud penetration at the base of AGN jets.
A&A, 522:A97, November 2010.

[19] A. Archer, W. Benbow, R. Bird, R. Brose, M. Buchovecky, V. Bugaev, W. Cui, M. K. Daniel, A. Falcone, Q. Feng, J. P. Finley, A. Flinders, L. Fortson, A. Furniss, G. H. Gillanders, M. Hütten, D. Hanna, O. Hervet, J. Holder, G. Hughes, T. B. Humensky, C. A. Johnson, P. Kaaret, P. Kar, N. Kelley-Hoskins, D. Kieda, M. Krause, F. Krennrich, S. Kumar, M. J. Lang, T. T. Y. Lin, S. McArthur, P. Moriarty, R. Mukherjee, D. Nieto, S. O'Brien, R. A. Ong, A. N. Otte, N. Park, A. Petrashyk, M. Pohl, A. Popkow, E. Pueschel, J. Quinn, K. Ragan, P. T. Reynolds, G. T. Richards, E. Roache, C. Rulten, I. Sadeh, G. H. Sembroski, K. Shahinyan, J. Tyler, S. P. Wakely, O. M. Weiner, A. Weinstein, R. M. Wells, P. Wilcox, A. Wilhelm, D. A. Williams, VERITAS Collaboration, W. F. Brisken, and P. Pontrelli.

HESS J1943+213: An Extreme Blazar Shining through the Galactic Plane.
ApJ, 862(1):41, July 2018.

[20] W. B. Atwood, A. A. Abdo, M. Ackermann, W. Althouse, B. Anderson, M. Axelsson, L. Baldini, J. Ballet, D. L. Band, G. Barbiellini, J. Bartelt, D. Bastieri, B. M. Baughman, K. Bechtol, D. Bédérède, F. Bellardi, R. Bellazzini, B. Berenji, G. F. Bignami, D. Bisello, E. Bissaldi, R. D. Blandford, E. D. Bloom, J. R. Bogart, E. Bonamente, J. Bonnell, A. W. Borgland , A. Bouvier, J. Bregeon, A. Brez, M. Brigida, P. Bruel, T. H. Burnett, G. Busetto, G. A. Caliandro, R. A. Cameron, P. A. Caraveo, S. Carius, P. Carlson, J. M. Casandjian, E. Cavazzuti, M. Ceccanti, C. Cecchi, E. Charles, A. Chekhtman, C. C. Cheung, J. Chiang, R. Chipaux, A. N. Cillis, S. Ciprini, R. Claus, J. Cohen-Tanugi, S. Condamoor, J. Conrad, R. Corbet, L. Corucci, L. Costamante, S. Cutini, D. S. Davis, D. Decotigny, M. DeKlotz, C. D. Dermer, A. de Angelis, S. W. Digel, E. do Couto e Silva, P. S. Drell, R. Dubois, D. Dumora, Y. Edmonds, D. Fabiani, C. Farnier, C. Favuzzi, D. L. Flath, P. Fleury, W. B. Focke, S. Funk, P. Fusco, F. Gargano, D. Gasparrini, N. Gehrels, F. X. Gentit, S. Germani, B. Giebels, N. Giglietto, P. Giommi, F. Giordano, T. Glanzman, G. Godfrey, I. A. Grenier, M. H. Grondin, J. E. Grove, L. Guillemot, S. Guiriec, G. Haller, A. K. Harding, P. A. Hart, E. Hays, S. E. Healey, M. Hirayama, L. Hjalmarsdotter, R. Horn, R. E. Hughes, G. Jóhannesson, G. Johansson, A. S. Johnson, R. P. Johnson, T. J. Johnson, W. N. Johnson, T. Kamae, H. Katagiri, J. Kataoka, A. Kavelaars, N. Kawai, H. Kelly, M. Kerr, W. Klamra, J. Knödlseder, M. L. Kocian, N. Komin, F. Kuehn, M. Kuss, D. Landriu, L. Latronico, B. Lee, S. H. Lee, M. Lemoine-Goumard, A. M. Lionetto, F. Longo, F. Loparco, B. Lott, M. N. Lovellette, P. Lubrano, G. M. Madejski, A. Makeev, B. Marangelli, M. M. Massai, M. N. Mazziotta, J. E. McEnery, N. Menon, C. Meurer, P. F. Michelson, M. Minuti, N. Mirizzi, W. Mitthumsiri, T. Mizuno, A. A. Moiseev, C. Monte, M. E. Monzani, E. Moretti, A. Morselli, I. V. Moskalenko, S. Murgia, T. Nakamori, S. Nishino, P. L. Nolan, J. P. Norris, E. Nuss, M. Ohno, T. Ohsugi, N. Omodei, E. Orlando, J. F. Ormes, A. Paccagnella, D. Paneque, J. H. Panetta, D. Parent, M. Pearce, M. Pepe, A. Perazzo, M. Pesce-Rollins, P. Picozza, L. Pieri, M. Pinchera, F. Piron, T. A. Porter, L. Poupard, S. Rainò, R. Rando, E. Rapposelli, M. Razzano, A. Reimer, O. Reimer, T. Reposeur, L. C. Reyes, S. Ritz, L. S. Rochester, A. Y. Rodriguez, R. W. Romani, M. Roth, J. J. Russell, F. Ryde, S. Sabatini, H. F. W. Sadrozinski, D. Sanchez, A. Sand er, L. Sapozhnikov, P. M. Saz Parkinson,

J. D. Scargle, T. L. Schalk, G. Scolieri, C. Sgrò, G. H. Share, M. Shaw, T. Shimokawabe, C. Shrader, A. Sierpowska-Bartosik, E. J. Siskind, D. A. Smith, P. D. Smith, G. Spandre, P. Spinelli, J. L. Starck, T. E. Stephens, M. S. Strickman, A. W. Strong, D. J. Suson, H. Tajima, H. Takahashi, T. Takahashi, T. Tanaka, A. Tenze, S. Tether, J. B. Thayer, J. G. Thayer, D. J. Thompson, L. Tibaldo, O. Tibolla, D. F. Torres, G. Tosti, A. Tramacere, M. Turri, T. L. Usher, N. Vilchez, V. Vitale, P. Wang, K. Watters, B. L. Winer, K. S. Wood, T. Ylinen, and M. Ziegler.
The Large Area Telescope on the Fermi Gamma-Ray Space Telescope Mission.
ApJ, 697(2):1071–1102, June 2009.

[21] V. Baghmanyan, S. Gasparyan, and N. Sahakyan.
Rapid Gamma-Ray Variability of NGC 1275.
ApJ, 848(2):111, October 2017.

[22] Matthew G. Baring, Markus Böttcher, and Errol J. Summerlin.
Probing acceleration and turbulence at relativistic shocks in blazar jets.
MNRAS, 464(4):4875–4894, Feb 2017.

[23] J. H. Beall and W. Bednarek.
On the Hadronic Beam Model for Gamma-Ray Production in Blazars.
ApJ, 510:188–196, January 1999.

[24] W. Bednarek and P. Banasiński.
Non-thermal Radiation from Collisions of Compact Objects with Intermediate-scale Jets in Active Galaxies.
ApJ, 807:168, July 2015.

[25] W. Bednarek and R. J. Protheroe.
Gamma-rays from interactions of stars with active galactic nucleus jets.
MNRAS, 287:L9–L13, May 1997.

[26] M. Błażejowski, M. Sikora, R. Moderski, and G. M. Madejski.
Comptonization of Infrared Radiation from Hot Dust by Relativistic Jets in Quasars.
ApJ, 545:107–116, December 2000.

[27] M. Błażejowski, M. Sikora, R. Moderski, and G. M. Madejski.
Comptonization of Infrared Radiation from Hot Dust by Relativistic Jets in Quasars.
ApJ, 545(1):107–116, December 2000.

[28] H. Bloemen, K. Bennett, J. J. Blom, W. Collmar, W. Hermsen, G. G. Lichti, D. Morris, V. Schoenfelder, J. G. Stacy, A. W. Strong, and C. Winkler.
New COMPTEL gamma-ray source (GRO J0516-609) near PKS 0506-612/0522-611: first evidence for "MeV Blazars".
A&A, 293:L1–L4, January 1995.

[29] S. D. Bloom and A. P. Marscher.
An Analysis of the Synchrotron Self-Compton Model for the Multi–Wave Band Spectra of Blazars.
ApJ, 461:657, April 1996.

[30] Steven D. Bloom and Alan P. Marscher.
An Analysis of the Synchrotron Self-Compton Model for the Multi–Wave Band Spectra of Blazars.
ApJ, 461:657, April 1996.

[31] G. Bonnoli, F. Tavecchio, G. Ghisellini, and T. Sbarrato.
An emerging population of BL Lacs with extreme properties: towards a class of EBL and cosmic magnetic field probes?
MNRAS, 451(1):611–621, July 2015.

[32] Eugenio Bottacini, Markus Böttcher, Elena Pian, and Werner Collmar.
3C 279 in Outburst in 2015 June: A Broadband SED Study Based on the INTEGRAL Detection.
ApJ, 832(1):17, November 2016.

[33] M. Böttcher, A. Reimer, K. Sweeney, and A. Prakash.
Leptonic and Hadronic Modeling of Fermi-detected Blazars.
ApJ, 768(1):54, May 2013.

[34] A. M. Brown.
Locating the γ-ray emission region of the flat spectrum radio quasar PKS 1510-089.
MNRAS, 431:824–835, May 2013.

[35] David N. Burrows, J. E. Hill, J. A. Nousek, J. A. Kennea, A. Wells, J. P. Osborne, A. F. Abbey, A. Beardmore, K. Mukerjee, A. D. T. Short, G. Chincarini, S. Campana, O. Citterio, A. Moretti, C. Pagani, G. Tagliaferri, P. Giommi, M. Capalbi, F. Tamburelli, L. Angelini, G. Cusumano, H. W. Bräuninger, W. Burkert, and G. D. Hartner.
The Swift X-Ray Telescope.
Space Science Reviews, 120(3-4):165–195, October 2005.

[36] G. Calderone, G. Ghisellini, M. Colpi, and M. Dotti.
Black hole mass estimate for a sample of radio-loud narrow-line Seyfert 1 galaxies.
MNRAS, 431(1):210–239, May 2013.

[37] W. Cash.
Parameter estimation in astronomy through application of the likelihood ratio.
ApJ, 228:939–947, March 1979.

[38] A. Cavaliere and V. D'Elia.
The Blazar Main Sequence.
ApJ, 571(1):226–233, May 2002.

[39] A. Celotti, G. Ghisellini, and A. C. Fabian.
Bulk Comptonization spectra in blazars.
MNRAS, 375(2):417–424, February 2007.

[40] Annalisa Celotti and Gabriele Ghisellini.
The power of blazar jets.
MNRAS, 385(1):283–300, March 2008.

[41] M. Cerruti, A. Zech, C. Boisson, G. Emery, S. Inoue, and J.-P. Lenain.
Leptohadronic single-zone models for the electromagnetic and neutrino emission of TXS 0506+056.
MNRAS, 483:L12–L16, February 2019.

[42] M. Cerruti, A. Zech, C. Boisson, and S. Inoue.
A hadronic origin for ultra-high-frequency-peaked BL Lac objects.
MNRAS, 448(1):910–927, March 2015.

[43] C. C. Cheung.
Fermi LAT detection of a GeV flare from High-redshift Blazar PKS 0537-286.
The Astronomer's Telegram, 10356:1, May 2017.

[44] Marco Chiaberge and Gabriele Ghisellini.
Rapid variability in the synchrotron self-Compton model for blazars.
MNRAS, 306(3):551–560, July 1999.

[45] L. Costamante, G. Bonnoli, F. Tavecchio, G. Ghisellini, G. Tagliaferri, and D. Khangulyan.
The NuSTAR view on hard-TeV BL Lacs.
MNRAS, 477(3):4257–4268, July 2018.

[46] L. Costamante, G. Ghisellini, P. Giommi, G. Tagliaferri, A. Celotti, M. Chiaberge, G. Fossati, L. Maraschi, F. Tavecchio, A. Treves, and A. Wolter.
Extreme synchrotron BL Lac objects. Stretching the blazar sequence.
A&A, 371:512–526, May 2001.

[47] S. Cutini, S. Ciprini, M. Orienti, A. Tramacere, F. D'Ammando, F. Verrecchia, G. Polenta, L. Carrasco, V. D'Elia, P. Giommi, J. González-Nuevo, P. Grandi, D. Harrison, E. Hays, S. Larsson, A. Lähteenmäki, J. León-Tavares, M. López-Caniego, P. Natoli, R. Ojha, B. Partridge, A. Porras, L. Reyes, E. Recillas, and E. Torresi.
Radio-gamma-ray connection and spectral evolution in 4C +49.22 (S4 1150+49): the Fermi, Swift and Planck view.
MNRAS, 445(4):4316–4334, December 2014.

[48] A. Dar and A. Laor.
Hadronic Production of TeV Gamma-Ray Flares from Blazars.
ApJL, 478:L5–L8, March 1997.

[49] Charles D. Dermer and Reinhard Schlickeiser.
On the Location of the Acceleration and Emission Sites in Gamma-Ray Blazars.
ApJSS, 90:945, February 1994.

[50] Charles D. Dermer, Dahai Yan, Li Zhang, Justin D. Finke, and Benoit Lott.
Near-equipartition Jets with Log-parabola Electron Energy Distribution and the Blazar Spectral-index Diagrams.
ApJ, 809(2):174, August 2015.

[51] A. Desai, K. Helgason, M. Ajello, V. Paliya, A. Domínguez, J. Finke, and D. Hartmann.
A GeV-TeV Measurement of the Extragalactic Background Light.
ApJL, 874(1):L7, March 2019.

[52] A. Domínguez, J. R. Primack, D. J. Rosario, F. Prada, R. C. Gilmore, S. M. Faber, D. C. Koo, R. S. Somerville, M. A. Pérez-Torres, P. Pérez-González, J. S. Huang, M. Davis, P. Guhathakurta, P. Barmby, C. J. Conselice, M. Lozano, J. A. Newman, and M. C. Cooper.
Extragalactic background light inferred from AEGIS galaxy-SED-type fractions.
MNRAS, 410(4):2556–2578, February 2011.

[53] L. Oc. Drury.

REVIEW ARTICLE: An introduction to the theory of diffusive shock acceleration of energetic particles in tenuous plasmas.
Reports on Progress in Physics, 46(8):973–1027, Aug 1983.

[54] Michael S. Dutka, Bryce D. Carpenter, Roopesh Ojha, Justin D. Finke, Filippo D'Ammando, Matthias Kadler, Philip G. Edwards, Jamie Stevens, Eleonora Torresi, Paola Grandi, Roberto Nesci, Felicia Krauß, Cornelia Müller, Joern Wilms, and Neil Gehrels.
Multiband Observations of the Quasar PKS 2326-502 during Active and Quiescent Gamma-Ray States in 2010-2012.
ApJ, 835(2):182, February 2017.

[55] Donald C. Ellison, Frank C. Jones, and Stephen P. Reynolds.
First-Order Fermi Particle Acceleration by Relativistic Shocks.
ApJ, 360:702, Sep 1990.

[56] P. A. Evans, A. P. Beardmore, K. L. Page, J. P. Osborne, P. T. O'Brien, R. Willingale, R. L. C. Starling, D. N. Burrows, O. Godet, L. Vetere, J. Racusin, M. R. Goad, K. Wiersema, L. Angelini, M. Capalbi, G. Chincarini, N. Gehrels, J. A. Kennea, R. Margutti, D. C. Morris, C. J. Mountford, C. Pagani, M. Perri, P. Romano, and N. Tanvir.
Methods and results of an automatic analysis of a complete sample of Swift-XRT observations of GRBs.
MNRAS, 397(3):1177–1201, August 2009.

[57] Fermi-LAT Collaboration, S. Abdollahi, M. Ackermann, M. Ajello, W. B. Atwood, L. Baldini, J. Ballet, G. Barbiellini, D. Bastieri, J. Becerra Gonzalez, R. Bellazzini, E. Bissaldi, R. D. Blandford, E. D. Bloom, R. Bonino, E. Bottacini, S. Buson, J. Bregeon, P. Bruel, R. Buehler, R. A. Cameron, R. Caputo, P. A. Caraveo, E. Cavazzuti, E. Charles, S. Chen, C. C. Cheung, G. Chiaro, S. Ciprini, J. Cohen-Tanugi, L. R. Cominsky, J. Conrad, D. Costantin, S. Cutini, F. D'Ammando, F. de Palma, A. Desai, S. W. Digel, N. Di Lalla, M. Di Mauro, L. Di Venere, A. Domínguez, C. Favuzzi, S. J. Fegan, J. Finke, A. Franckowiak, Y. Fukazawa, S. Funk, P. Fusco, G. Gallardo Romero, F. Gargano, D. Gasparrini, N. Giglietto, F. Giordano, M. Giroletti, D. Green, I. A. Grenier, L. Guillemot, S. Guiriec, D. H. Hartmann, E. Hays, K. Helgason, D. Horan, G. Jóhannesson, D. Kocevski, M. Kuss, S. Larsson, L. Latronico, J. Li, F. Longo, F. Loparco, B. Lott, M. N. Lovellette, P. Lubrano, G. M. Madejski, J. D. Magill, S. Maldera, A. Manfreda, L. Marcotulli, M. N. Mazziotta, J. E. McEnery, M. Meyer, P. F. Michelson, T. Mizuno, M. E. Monzani, A. Morselli, I. V. Moskalenko, M. Negro, E. Nuss, R. Ojha,

N. Omodei, M. Orienti, E. Orlando, J. F. Ormes, M. Palatiello, V. S. Paliya, D. Paneque, J. S. Perkins, M. Persic, M. Pesce-Rollins, V. Petrosian, F. Piron, T. A. Porter, J. R. Primack, G. Principe, S. Rainò, R. Rand o, M. Razzano, S. Razzaque, A. Reimer, O. Reimer, P. M. Saz Parkinson, C. Sgrò, E. J. Siskind, G. Spandre, P. Spinelli, D. J. Suson, H. Tajima, M. Takahashi, J. B. Thayer, L. Tibaldo, D. F. Torres, E. Torresi, G. Tosti, A. Tramacere, E. Troja, J. Valverde, G. Vianello, M. Vogel, K. Wood, and G. Zaharijas.
A gamma-ray determination of the Universe's star formation history.
Science, 362(6418):1031–1034, November 2018.

[58] L. Foschini, G. Bonnoli, G. Ghisellini, G. Tagliaferri, F. Tavecchio, and A. Stamerra.
Fermi/LAT detection of extraordinary variability in the gamma-ray emission of the blazar PKS 1510-089.
A&A, 555:A138, July 2013.

[59] L. Foschini, G. Ghisellini, F. Tavecchio, G. Bonnoli, and A. Stamerra.
Search for the shortest variability at gamma rays in flat-spectrum radio quasars.
A&A, 530:A77, June 2011.

[60] Wendy L. Freedman, Barry F. Madore, Brad K. Gibson, Laura Ferrarese, Daniel D. Kelson, Shoko Sakai, Jeremy R. Mould, Jr. Kennicutt, Robert C., Holland C. Ford, John A. Graham, John P. Huchra, Shaun M. G. Hughes, Garth D. Illingworth, Lucas M. Macri, and Peter B. Stetson.
Final Results from the Hubble Space Telescope Key Project to Measure the Hubble Constant.
ApJ, 553(1):47–72, May 2001.

[61] S. Gao, A. Fedynitch, W. Winter, and M. Pohl.
Modelling the coincident observation of a high-energy neutrino and a bright blazar flare.
Nature Astronomy, 3:88–92, January 2019.

[62] S. Gasparyan, N. Sahakyan, V. Baghmanyan, and D. Zargaryan.
On the Multiwavelength Emission from CTA 102.
ApJ, 863(2):114, August 2018.

[63] N. Gehrels, G. Chincarini, P. Giommi, K. O. Mason, J. A. Nousek, A. A. Wells, N. E. White, S. D. Barthelmy, D. N. Burrows, L. R. Cominsky, K. C. Hurley, F. E. Marshall, P. Mészáros, P. W. A. Roming, L. Angelini, L. M. Barbier, T. Belloni, S. Campana, P. A. Caraveo,

M. M. Chester, O. Citterio, T. L. Cline, M. S. Cropper, J. R. Cummings, A. J. Dean, E. D. Feigelson, E. E. Fenimore, D. A. Frail, A. S. Fruchter, G. P. Garmire, K. Gendreau, G. Ghisellini, J. Greiner, J. E. Hill, S. D. Hunsberger, H. A. Krimm, S. R. Kulkarni, P. Kumar, F. Lebrun, N. M. Lloyd-Ronning, C. B. Markwardt, B. J. Mattson, R. F. Mushotzky, J. P. Norris, J. Osborne, B. Paczynski, D. M. Palmer, H. S. Park, A. M. Parsons, J. Paul, M. J. Rees, C. S. Reynolds, J. E. Rhoads, T. P. Sasseen, B. E. Schaefer, A. T. Short, A. P. Smale, I. A. Smith, L. Stella, G. Tagliaferri, T. Takahashi, M. Tashiro, L. K. Townsley, J. Tueller, M. J. L. Turner, M. Vietri, W. Voges, M. J. Ward, R. Willingale, F. M. Zerbi, and W. W. Zhang.
The Swift Gamma-Ray Burst Mission.
ApJ, 611(2):1005–1020, August 2004.

[64] G. Ghisellini, R. Della Ceca, M. Volonteri, G. Ghirland a, F. Tavecchio, L. Foschini, G. Tagliaferri, F. Haardt, G. Pareschi, and J. Grindlay.
Chasing the heaviest black holes of jetted active galactic nuclei.
MNRAS, 405(1):387–400, June 2010.

[65] G. Ghisellini, L. Foschini, M. Volonteri, G. Ghirland a, F. Haardt, D. Burlon, and F. Tavecchio.
The blazar S5 0014+813: a real or apparent monster?
MNRAS, 399(1):L24–L28, October 2009.

[66] G. Ghisellini, L. Maraschi, and A. Treves.
Inhomogeneous synchrotron-self-Compton models and the problem of relativistic beaming of BL Lac objects.
A&A, 146:204–212, May 1985.

[67] G. Ghisellini, L. Maraschi, and A. Treves.
Inhomogeneous synchrotron-self-compton models and the problem of relativistic beaming of BL Lac objects.
A&A, 146:204–212, May 1985.

[68] G. Ghisellini, G. Tagliaferri, L. Foschini, G. Ghirland a, F. Tavecchio, R. Della Ceca, F. Haardt, M. Volonteri, and N. Gehrels.
High-redshift Fermi blazars.
MNRAS, 411(2):901–914, February 2011.

[69] G. Ghisellini and F. Tavecchio.
Canonical high-power blazars.
MNRAS, 397:985–1002, August 2009.

[70] G. Ghisellini and F. Tavecchio.

Canonical high-power blazars.
MNRAS, 397(2):985–1002, August 2009.

[71] G. Ghisellini and F. Tavecchio.
Fermi/LAT broad emission line blazars.
MNRAS, 448(2):1060–1077, April 2015.

[72] G. Ghisellini, F. Tavecchio, L. Foschini, G. Ghirland a, L. Maraschi, and A. Celotti.
General physical properties of bright Fermi blazars.
MNRAS, 402(1):497–518, February 2010.

[73] G. Ghisellini, F. Tavecchio, and G. Ghirlanda.
Jet and accretion power in the most powerful Fermi blazars.
MNRAS, 399(4):2041–2054, November 2009.

[74] G. Ghisellini, F. Tavecchio, L. Maraschi, A. Celotti, and T. Sbarrato.
The power of relativistic jets is larger than the luminosity of their accretion disks.
Nature, 515(7527):376–378, November 2014.

[75] Gabriele Ghisellini.
Extreme blazars.
Astroparticle Physics, 11(1-2):11–18, June 1999.

[76] P. Giommi, G. Arrigo, U. Barres De Almeida, M. De Angelis, J. Del Rio Vera, S. Di Ciaccio, S. Di Pippo, S. Iacovoni, and A. M. T. Pollock.
The Open Universe Initiative.
arXiv e-prints, page arXiv:1805.08505, May 2018.

[77] P. Giommi and P. Padovani.
BL Lac reunification.
MNRAS, 268:L51–L54, May 1994.

[78] P. Giommi, P. Padovani, and E. Perlman.
Detection of exceptional X-ray spectral variability in the TeV BL Lac 1ES 2344+514.
MNRAS, 317(4):743–749, October 2000.

[79] P. Giommi, P. Padovani, G. Polenta, S. Turriziani, V. D'Elia, and S. Piranomonte.
A simplified view of blazars: clearing the fog around long-standing selection effects.
MNRAS, 420(4):2899–2911, March 2012.

[80] Paolo Giommi.
Multi-frequency, multi-messenger astrophysics with Swift. The case of blazars.
Journal of High Energy Astrophysics, 7:173–179, September 2015.

[81] Fiona A. Harrison, William W. Craig, Finn E. Christensen, Charles J. Hailey, William W. Zhang, Steven E. Boggs, Daniel Stern, W. Rick Cook, Karl Forster, Paolo Giommi, Brian W. Grefenstette, Yunjin Kim, Takao Kitaguchi, Jason E. Koglin, Kristin K. Madsen, Peter H. Mao, Hiromasa Miyasaka, Kaya Mori, Matteo Perri, Michael J. Pivovaroff, Simonetta Puccetti, Vikram R. Rana, Niels J. Westergaard, Jason Willis, Andreas Zoglauer, Hongjun An, Matteo Bachetti, Nicolas M. Barrière, Eric C. Bellm, Varun Bhalerao, Nicolai F. Brejnholt, Felix Fuerst, Carl C. Liebe, Craig B. Markwardt, Melania Nynka, Julia K. Vogel, Dominic J. Walton, Daniel R. Wik, David M. Alexander, Lynn R. Cominsky, Ann E. Hornschemeier, Allan Hornstrup, Victoria M. Kaspi, Greg M. Madejski, Giorgio Matt, Silvano Molendi, David M. Smith, John A. Tomsick, Marco Ajello, David R. Ballantyne, Mislav Baloković, Didier Barret, Franz E. Bauer, Roger D. Blandford, W. Niel Brandt, Laura W. Brenneman, James Chiang, Deepto Chakrabarty, Jerome Chenevez, Andrea Comastri, Francois Dufour, Martin Elvis, Andrew C. Fabian, Duncan Farrah, Chris L. Fryer, Eric V. Gotthelf, Jonathan E. Grindlay, David J. Helfand, Roman Krivonos, David L. Meier, Jon M. Miller, Lorenzo Natalucci, Patrick Ogle, Eran O. Ofek, Andrew Ptak, Stephen P. Reynolds, Jane R. Rigby, Gianpiero Tagliaferri, Stephen E. Thorsett, Ezequiel Treister, and C. Megan Urry.
The Nuclear Spectroscopic Telescope Array (NuSTAR) High-energy X-Ray Mission.
ApJ, 770(2):103, June 2013.

[82] M. Hayashida, K. Nalewajko, and et al.
Rapid Variability of Blazar 3C 279 during Flaring States in 2013-2014 with Joint Fermi-LAT, NuSTAR, Swift, and Ground-Based Multi-wavelength Observations.
ApJ, 807:79, July 2015.

[83] M. Hayashida, K. Nalewajko, G. M. Madejski, M. Sikora, R. Itoh, M. Ajello, R. D. Blandford, S. Buson, J. Chiang, Y. Fukazawa, A. K. Furniss, C. M. Urry, I. Hasan, F. A. Harrison, D. M. Alexand er, M. Baloković, D. Barret, S. E. Boggs, F. E. Christensen, W. W. Craig, K. Forster, P. Giommi, B. Grefenstette, C. Hailey, A. Hornstrup, T. Kitaguchi, J. E. Koglin, K. K. Madsen, P. H. Mao, H. Miyasaka,

K. Mori, M. Perri, M. J. Pivovaroff, S. Puccetti, V. Rana, D. Stern, G. Tagliaferri, N. J. Westergaard, W. W. Zhang, A. Zoglauer, M. A. Gurwell, M. Uemura, H. Akitaya, K. S. Kawabata, K. Kawaguchi, Y. Kanda, Y. Moritani, K. Takaki, T. Ui, M. Yoshida, A. Agarwal, and A. C. Gupta.

Rapid Variability of Blazar 3C 279 during Flaring States in 2013-2014 with Joint Fermi-LAT, NuSTAR, Swift, and Ground-Based Multi-wavelength Observations.

ApJ, 807(1):79, July 2015.

[84] IceCube Collaboration, M. G. Aartsen, M. Ackermann, J. Adams, J. A. Aguilar, M. Ahlers, M. Ahrens, I. Al Samarai, D. Altmann, K. Andeen, T. Anderson, I. Ansseau, G. Anton, C. Argüelles, J. Auffenberg, S. Axani, H. Bagherpour, X. Bai, J. P. Barron, S. W. Barwick, V. Baum, R. Bay, J. J. Beatty, J. Becker Tjus, K. H. Becker, S. Ben-Zvi, D. Berley, E. Bernardini, D. Z. Besson, G. Binder, D. Bindig, E. Blaufuss, S. Blot, C. Bohm, M. Börner, F. Bos, S. Böser, O. Botner, E. Bourbeau, J. Bourbeau, F. Bradascio, J. Braun, M. Brenzke, H. P. Bretz, S. Bron, J. Brostean-Kaiser, A. Burgman, R. S. Busse, T. Carver, E. Cheung, D. Chirkin, A. Christov, K. Clark, L. Classen, S. Coenders, G. H. Collin, J. M. Conrad, P. Coppin, P. Correa, D. F. Cowen, R. Cross, P. Dave, M. Day, J. P. A. M. de André, C. De Clercq, J. J. DeLaunay, H. Dembinski, S. De Ridder, P. Desiati, K. D. de Vries, G. de Wasseige, M. de With, T. DeYoung, J. C. Díaz-Vélez, V. di Lorenzo, H. Dujmovic, J. P. Dumm, M. Dunkman, E. Dvorak, B. Eberhardt, T. Ehrhardt, B. Eichmann, P. Eller, P. A. Evenson, S. Fahey, A. R. Fazely, J. Felde, K. Filimonov, C. Finley, S. Flis, A. Franckowiak, E. Friedman, A. Fritz, T. K. Gaisser, J. Gallagher, L. Gerhardt, K. Ghorbani, T. Glauch, T. Glüsenkamp, A. Goldschmidt, J. G. Gonzalez, D. Grant, Z. Griffith, C. Haack, A. Hallgren, F. Halzen, K. Hanson, D. Hebecker, D. Heereman, K. Helbing, R. Hellauer, S. Hickford, J. Hignight, G. C. Hill, K. D. Hoffman, R. Hoffmann, T. Hoinka, B. Hokanson-Fasig, K. Hoshina, F. Huang, M. Huber, K. Hultqvist, M. Hünnefeld, R. Hussain, S. In, N. Iovine, A. Ishihara, E. Jacobi, G. S. Japaridze, M. Jeong, K. Jero, B. J. P. Jones, P. Kalaczynski, W. Kang, A. Kappes, D. Kappesser, T. Karg, A. Karle, U. Katz, M. Kauer, A. Keivani, J. L. Kelley, A. Kheirandish, J. Kim, M. Kim, T. Kintscher, J. Kiryluk, T. Kittler, S. R. Klein, R. Koirala, H. Kolanoski, L. Köpke, C. Kopper, S. Kopper, J. P. Koschinsky, D. J. Koskinen, M. Kowalski, K. Krings, M. Kroll, G. Krückl, S. Kunwar, N. Kurahashi, T. Kuwabara, A. Kyriacou, M. Labare, J. L. Lanfranchi, M. J. Larson, F. Lauber, K. Leonard,

M. Lesiak-Bzdak, M. Leuermann, Q. R. Liu, C. J. Lozano Mariscal, L. Lu, J. Lünemann, W. Luszczak, J. Madsen, G. Maggi, K. B. M. Mahn, S. Mancina, R. Maruyama, K. Mase, R. Maunu, K. Meagher, M. Medici, M. Meier, T. Menne, G. Merino, T. Meures, S. Miarecki, J. Micallef, G. Momenté, T. Montaruli, R. W. Moore, S, R. Morse, M. Moulai, R. Nahnhauer, P. Nakarmi, U. Naumann, G. Neer, H. Niederhausen, S. C. Nowicki, D. R. Nygren, A. Obertacke Pollmann, A. Olivas, A. O'Murchadha, E. O'Sullivan, T. Palczewski, H. Pandya, D. V. Pankova, P. Peiffer, J. A. Pepper, C. Pérez de los Heros, D. Pieloth, E. Pinat, M. Plum, P. B. Price, G. T. Przybylski, C. Raab, L. Rädel, M. Rameez, L. Rauch, K. Rawlins, I. C. Rea, R. Reimann, B. Relethford, M. Relich, E. Resconi, W. Rhode, M. Richman, S. Robertson, M. Rongen, C. Rott, T. Ruhe, D. Ryckbosch, D. Rysewyk, I. Safa, T. Sälzer, S. E. Sanchez Herrera, A. Sandrock, J. Sandroos, M. Santander, S. Sarkar, S. Sarkar, K. Satalecka, P. Schlunder, T. Schmidt, A. Schneider, S. Schoenen, S. Schöneberg, L. Schumacher, S. Sclafani, D. Seckel, S. Seunarine, J. Soedingrekso, D. Soldin, M. Song, G. M. Spiczak, C. Spiering, J. Stachurska, M. Stamatikos, T. Stanev, A. Stasik, R. Stein, J. Stettner, A. Steuer, T. Stezelberger, R. G. Stokstad, A. Stößl, N. L. Strotjohann, T. Stuttard, G. W. Sullivan, M. Sutherland, I. Taboada, J. Tatar, F. Tenholt, S. Ter-Antonyan, A. Terliuk, S. Tilav, P. A. Toale, M. N. Tobin, C. Toennis, S. Toscano, D. Tosi, M. Tselengidou, C. F. Tung, A. Turcati, C. F. Turley, B. Ty, E. Unger, M. Usner, J. Vandenbroucke, W. Van Driessche, D. van Eijk, N. van Eijndhoven, S. Vanheule, J. van Santen, E. Vogel, M. Vraeghe, C. Walck, A. Wallace, M. Wallraff, F. D. Wandler, N. Wandkowsky, A. Waza, C. Weaver, M. J. Weiss, C. Wendt, J. Werthebach, S. Westerhoff, B. J. Whelan, N. Whitehorn, K. Wiebe, C. H. Wiebusch, L. Wille, D. R. Williams, L. Wills, M. Wolf, J. Wood, T. R. Wood, K. Woschnagg, D. L. Xu, X. W. Xu, Y. Xu, J. P. Yanez, G. Yodh, S. Yoshida, T. Yuan, Fermi-LAT Collaboration, S. Abdollahi, M. Ajello, R. Angioni, L. Baldini, J. Ballet, G. Barbiellini, D. Bastieri, K. Bechtol, R. Bellazzini, B. Berenji, E. Bissaldi, R. D. Blandford, R. Bonino, E. Bottacini, J. Bregeon, P. Bruel, R. Buehler, T. H. Burnett, E. Burns, S. Buson, R. A. Cameron, R. Caputo, P. A. Caraveo, E. Cavazzuti, E. Charles, S. Chen, C. C. Cheung, J. Chiang, G. Chiaro, S. Ciprini, J. Cohen-Tanugi, J. Conrad, D. Costantin, S. Cutini, F. D'Ammando, F. de Palma, S. W. Digel, N. Di Lalla, M. Di Mauro, L. Di Venere, A. Domínguez, C. Favuzzi, A. Franckowiak, Y. Fukazawa, S. Funk, P. Fusco, F. Gargano, D. Gasparrini, N. Giglietto, M. Giomi, P. Giommi, F. Giordano, M. Giroletti, T. Glanzman, D. Green, I. A. Grenier, M. H. Grondin, S. Guiriec, A. K. Harding,

M. Hayashida, E. Hays, J. W. Hewitt, D. Horan, G. Jóhannesson, M. Kadler, S. Kensei, D. Kocevski, F. Krauss, M. Kreter, M. Kuss, G. La Mura, S. Larsson, L. Latronico, M. Lemoine-Goumard, J. Li, F. Longo, F. Loparco, M. N. Lovellette, P. Lubrano, J. D. Magill, S. Maldera, D. Malyshev, A. Manfreda, M. N. Mazziotta, J. E. McEnery, M. Meyer, P. F. Michelson, T. Mizuno, M. E. Monzani, A. Morselli, I. V. Moskalenko, M. Negro, E. Nuss, R. Ojha, N. Omodei, M. Orienti, E. Orlando, M. Palatiello, V. S. Paliya, J. S. Perkins, M. Persic, M. Pesce-Rollins, F. Piron, T. A. Porter, G. Principe, S. Rainò, R. Rando, B. Rani, M. Razzano, S. Razzaque, A. Reimer, O. Reimer, N. Renault-Tinacci, S. Ritz, L. S. Rochester, P. M. Saz Parkinson, C. Sgrò, E. J. Siskind, G. Spandre, P. Spinelli, D. J. Suson, H. Tajima, M. Takahashi, Y. Tanaka, J. B. Thayer, D. J. Thompson, L. Tibaldo, D. F. Torres, E. Torresi, G. Tosti, E. Troja, J. Valverde, G. Vianello, M. Vogel, K. Wood, M. Wood, G. Zaharijas, MAGIC Collaboration, M. L. Ahnen, S. Ansoldi, L. A. Antonelli, C. Arcaro, D. Baack, A. Babić, B. Banerjee, P. Bangale, U. Barres de Almeida, J. A. Barrio, J. Becerra González, W. Bednarek, E. Bernardini, A. Berti, W. Bhattacharyya, A. Biland, O. Blanch, G. Bonnoli, A. Carosi, R. Carosi, G. Ceribella, A. Chatterjee, S. M. Colak, P. Colin, E. Colombo, J. L. Contreras, J. Cortina, S. Covino, P. Cumani, P. Da Vela, F. Dazzi, A. De Angelis, B. De Lotto, M. Delfino, J. Delgado, F. Di Pierro, A. Domínguez, D. Dominis Prester, D. Dorner, M. Doro, S. Einecke, D. Elsaesser, V. Fallah Ramazani, A. Fernández-Barral, D. Fidalgo, L. Foffano, K. Pfrang, M. V. Fonseca, L. Font, A. Franceschini, C. Fruck, D. Galindo, S. Gallozzi, R. J. García López, M. Garczarczyk, M. Gaug, P. Giammaria, N. Godinović, D. Gora, D. Guberman, D. Hadasch, A. Hahn, T. Hassan, M. Hayashida, J. Herrera, J. Hose, D. Hrupec, S. Inoue, K. Ishio, Y. Konno, H. Kubo, J. Kushida, D. Lelas, E. Lindfors, S. Lombardi, F. Longo, M. López, C. Maggio, P. Majumdar, M. Makariev, G. Maneva, M. Manganaro, K. Mannheim, L. Maraschi, M. Mariotti, M. Martínez, S. Masuda, D. Mazin, M. Minev, J. M. M, R. Mirzoyan, A. Moralejo, V. Moreno, E. Moretti, T. Nagayoshi, V. Neustroev, A. Niedzwiecki, M. Nievas Rosillo, C. Nigro, K. Nilsson, D. Ninci, K. Nishijima, K. Noda, L. Nogués, S. Paiano, J. Palacio, D. Paneque, R. Paoletti, J. M. Paredes, G. Pedaletti, M. Peresano, M. Persic, P. G. Prada Moroni, E. Prandini, I. Puljak, J. Rodriguez Garcia, I. Reichardt, W. Rhode, M. Ribó, J. Rico, C. Righi, A. Rugliancich, T. Saito, K. Satalecka, T. Schweizer, J. Sitarek, I. Šnidaric , D. Sobczynska, A. Stamerra, M. Strzys, T. Surić, M. Takahashi, F. Tavecchio, P. Temnikov, T. Terzić, M. Teshima, N. Torres-Albà,

A. Treves, S. Tsujimoto, G. Vanzo, M. Vazquez Acosta, I. Vovk, J. E. Ward, M. Will, S, D. Zaric , AGILE Team, F. Lucarelli, M. Tavani, G. Piano, I. Donnarumma, C. Pittori, F. Verrecchia, G. Barbiellini, A. Bulgarelli, P. Caraveo, P. W. Cattaneo, S. Colafrancesco, E. Costa, G. Di Cocco, A. Ferrari, F. Gianotti, A. Giuliani, P. Lipari, S. Mereghetti, A. Morselli, L. Pacciani, F. Paoletti, N. Parmiggiani, A. Pellizzoni, P. Picozza, M. Pilia, A. Rappoldi, A. Trois, S. Vercellone, V. Vittorini, ASAS-SN Team, A. Franckowiak K. Z. Stanek, C. S. Kochanek, J. F. Beacom, T. A. Thompson, T. W. S. Holoien, S. Dong, J. L. Prieto, B. J. Shappee, S. Holmbo, HAWC Collaboration, A. U. Abeysekara, A. Albert, R. Alfaro, C. Alvarez, R. Arceo, J. C. Arteaga-Velázquez, D. Avila Rojas, H. A. Ayala Solares, A. Becerril, E. Belmont-Moreno, A. Bernal, K. S. Caballero-Mora, T. Capistrán, A. Carramiñana, S. Casanova, M. Castillo, U. Cotti, J. Cotzomi, S. Coutiño de León, C. De León, E. De la Fuente, R. Diaz Hernandez, S. Dichiara, B. L. Dingus, M. A. DuVernois, J. C. Díaz-Vélez, R. W. Ellsworth, K. Engel, D. W. Fiorino, H. Fleischhack, N. Fraija, J. A. García-González, F. Garfias, A. González Muñoz, M. M. González, J. A. Goodman, Z. Hampel-Arias, J. P. Harding, S. Hernand ez, B. Hona, F. Hueyotl-Zahuantitla, C. M. Hui, P. Hüntemeyer, A. Iriarte, A. Jardin-Blicq, V. Joshi, S. Kaufmann, G. J. Kunde, A. Lara, R. J. Lauer, W. H. Lee, D. Lennarz, H. León Vargas, J. T. Linnemann, A. L. Longinotti, G. Luis-Raya, R. Luna-García, K. Malone, S. S. Marinelli, O. Martinez, I. Martinez-Castellanos, J. Martínez-Castro, H. Martínez-Huerta, J. A. Matthews, P. Miranda-Romagnoli, E. Moreno, M. Mostafá, A. Nayerhoda, L. Nellen, M. Newbold, M. U. Nisa, R. Noriega-Papaqui, R. Pelayo, J. Pretz, E. G. Pérez-Pérez, Z. Ren, C. D. Rho, C. Rivière, D. Rosa-González, M. Rosenberg, E. Ruiz-Velasco, E. Ruiz-Velasco, F. Salesa Greus, A. Sandoval, M. Schneider, H. Schoorlemmer, G. Sinnis, A. J. Smith, R. W. Springer, P. Surajbali, O. Tibolla, K. Tollefson, I. Torres, L. Villaseñor, T. Weisgarber, F. Werner, T. Yapici, Y. Gaurang, A. Zepeda, H. Zhou, J. D. Álvarez, H. E. S. S. Collaboration, H. Abdalla, E. O. Angüner, C. Armand, M. Backes, Y. Becherini, D. Berge, M. Böttcher, C. Boisson, J. Bolmont, S. Bonnefoy, P. Bordas, F. Brun, M. Büchele, T. Bulik, S. Caroff, A. Carosi, S. Casanova, M. Cerruti, N. Chakraborty, S. Chandra, A. Chen, S. Colafrancesco, I. D. Davids, C. Deil, J. Devin, A. Djannati-Ataï, K. Egberts, G. Emery, S. Eschbach, A. Fiasson, G. Fontaine, S. Funk, M. Füßling, Y. A. Gallant, F. Gaté, G. Giavitto, D. Glawion, J. F. Glicenstein, D. Gottschall, M. H. Grondin, M. Haupt, G. Henri, J. A. Hinton, C. Hoischen, T. L. Holch, D. Huber, M. Jamrozy, D. Jankowsky, F. Jankowsky, L. Jou-

vin, I. Jung-Richardt, D. Kerszberg, B. Khélifi, J. King, S. Klepser, W. Kluz niak, Nu. Komin, M. Kraus, J. Lefaucheur, A. Lemière, M. Lemoine-Goumard, J. P. Lenain, E. Leser, T. Lohse, R. López-Coto, M. Lorentz, I. Lypova, V. Marandon, G. Guillem Martí-Devesa, G. Maurin, A. M. W. Mitchell, R. Moderski, M. Mohamed, L. Mohrmann, E. Moulin, T. Murach, M. de Naurois, F. Niederwanger, J. Niemiec, L. Oakes, P. O'Brien, S. Ohm, M. Ostrowski, I. Oya, M. Panter, R. D. Parsons, C. Perennes, Q. Piel, S. Pita, V. Poireau, A. Priyana Noel, H. Prokoph, G. Pühlhofer, A. Quirrenbach, S. Raab, R. Rauth, M. Renaud, F. Rieger, L. Rinchiuso, C. Romoli, G. Rowell, B. Rudak, D. A. Sasaki, M. Sanchez, R. Schlickeiser, F. Schüssler, A. Schulz, U. Schwanke, M. Seglar-Arroyo, N. Shafi, R. Simoni, H. Sol, C. Stegmann, C. Steppa, T. Tavernier, A. M. Taylor, D. Tiziani, C. Trichard, M. Tsirou, C. van Eldik, C. van Rensburg, B. van Soelen, J. Veh, P. Vincent, F. Voisin, S. J. Wagner, R. M. Wagner, A. Wierzcholska, R. Zanin, A. A. Zdziarski, A. Zech, A. Ziegler, J. Zorn, N. Żywucka, INTEGRAL Team, V. Savchenko, C. Ferrigno, A. Bazzano, R. Diehl, E. Kuulkers, P. Laurent, S. Mereghetti, L. Natalucci, F. Panessa, J. Rodi, P. Ubertini, Kiso Kanata, Subaru Observing Teams, T. Morokuma, K. Ohta, Y. T. Tanaka, H. Mori, M. Yamanaka, K. S. Kawabata, Y. Utsumi, T. Nakaoka, M. Kawabata, H. Nagashima, M. Yoshida, Y. Matsuoka, R. Itoh, Kapteyn Team, W. Keel, Liverpool Telescope Team, C. Copperwheat, I. Steele, Swift/NuSTAR Team, S. B. Cenko, D. F. Cowen, J. J. DeLaunay, P. A. Evans, D. B. Fox, A. Keivani, J. A. Kennea, F. E. Marshall, J. P. Osborne, M. Santander, A. Tohuvavohu, C. F. Turley, VERITAS Collaboration, A. U. Abeysekara, A. Archer, W. Benbow, R. Bird, A. Brill, R. Brose, M. Buchovecky, J. H. Buckley, V. Bugaev, J. L. Christiansen, M. P. Connolly, W. Cui, M. K. Daniel, M. Errando, A. Falcone, Q. Feng, J. P. Finley, L. Fortson, A. Furniss, O. Gueta, M. Hütten, O. Hervet, G. Hughes, T. B. Humensky, C. A. Johnson, P. Kaaret, P. Kar, N. Kelley-Hoskins, M. Kertzman, D. Kieda, M. Krause, F. Krennrich, S. Kumar, M. J. Lang, T. T. Y. Lin, G. Maier, S. McArthur, P. Moriarty, R. Mukherjee, D. Nieto, S. O'Brien, R. A. Ong, A. N. Otte, N. Park, A. Petrashyk, M. Pohl, A. Popkow, S. E. Pueschel, J. Quinn, K. Ragan, P. T. Reynolds, G. T. Richards, E. Roache, C. Rulten, I. Sadeh, M. Santander, S. S. Scott, G. H. Sembroski, K. Shahinyan, I. Sushch, S. Trépanier, J. Tyler, V. V. Vassiliev, S. P. Wakely, A. Weinstein, R. M. Wells, P. Wilcox, A. Wilhelm, D. A. Williams, B. Zitzer, VLA/B Team, A. J. Tetarenko, A. E. Kimball, J. C. A. Miller-Jones, and G. R. Sivakoff.

Multimessenger observations of a flaring blazar coincident with high-

energy neutrino IceCube-170922A.
Science, 361(6398):eaat1378, July 2018.

[85] IceCube Collaboration, M. G. Aartsen, M. Ackermann, J. Adams, J. A. Aguilar, M. Ahlers, M. Ahrens, I. Al Samarai, D. Altmann, K. Andeen, T. Anderson, I. Ansseau, G. Anton, C. Argüelles, B. Arsioli, J. Auffenberg, S. Axani, H. Bagherpour, X. Bai, J. P. Barron, S. W. Barwick, V. Baum, R. Bay, J. J. Beatty, J. Becker Tjus, K. H. Becker, S. BenZvi, D. Berley, E. Bernardini, D. Z. Besson, G. Binder, D. Bindig, E. Blaufuss, S. Blot, C. Bohm, M. Börner, F. Bos, S. Böser, O. Botner, E. Bourbeau, J. Bourbeau, F. Bradascio, J. Braun, M. Brenzke, H. P. Bretz, S. Bron, J. Brostean-Kaiser, A. Burgman, R. S. Busse, T. Carver, E. Cheung, D. Chirkin, A. Christov, K. Clark, L. Classen, S. Coenders, G. H. Collin, J. M. Conrad, P. Coppin, P. Correa, D. F. Cowen, R. Cross, P. Dave, M. Day, J. P. A. M. de André, C. De Clercq, J. J. DeLaunay, H. Dembinski, S. DeRidder, P. Desiati, K. D. de Vries, G. de Wasseige, M. de With, T. DeYoung, J. C. Díaz-Vélez, V. di Lorenzo, H. Dujmovic, J. P. Dumm, M. Dunkman, E. Dvorak, B. Eberhardt, T. Ehrhardt, B. Eichmann, P. Eller, P. A. Evenson, S. Fahey, A. R. Fazely, J. Felde, K. Filimonov, C. Finley, S. Flis, A. Franckowiak, E. Friedman, A. Fritz, T. K. Gaisser, J. Gallagher, L. Gerhardt, K. Ghorbani, P. Giommi, T. Glauch, T. Glüsenkamp, A. Goldschmidt, J. G. Gonzalez, D. Grant, Z. Griffith, C. Haack, A. Hallgren, F. Halzen, K. Hanson, D. Hebecker, D. Heereman, K. Helbing, R. Hellauer, S. Hickford, J. Hignight, G. C. Hill, K. D. Hoffman, R. Hoffmann, T. Hoinka, B. Hokanson-Fasig, K. Hoshina, F. Huang, M. Huber, K. Hultqvist, M. Hünnefeld, R. Hussain, S. In, N. Iovine, A. Ishihara, E. Jacobi, G. S. Japaridze, M. Jeong, K. Jero, B. J. P. Jones, P. Kalaczynski, W. Kang, A. Kappes, D. Kappesser, T. Karg, A. Karle, U. Katz, M. Kauer, A. Keivani, J. L. Kelley, A. Kheirandish, J. Kim, M. Kim, T. Kintscher, J. Kiryluk, T. Kittler, S. R. Klein, R. Koirala, H. Kolanoski, L. Köpke, C. Kopper, S. Kopper, J. P. Koschinsky, D. J. Koskinen, M. Kowalski, B. Krammer, K. Krings, M. Kroll, G. Krückl, S. Kunwar, N. Kurahashi, T. Kuwabara, A. Kyriacou, M. Labare, J. L. Lanfranchi, M. J. Larson, F. Lauber, K. Leonard, M. Lesiak-Bzdak, M. Leuermann, Q. R. Liu, C. J. Lozano Mariscal, L. Lu, J. Lünemann, W. Luszczak, J. Madsen, G. Maggi, K. B. M. Mahn, S. Mancina, R. Maruyama, K. Mase, R. Maunu, K. Meagher, M. Medici, M. Meier, T. Menne, G. Merino, T. Meures, S. Miarecki, J. Micallef, G. Momenté, T. Montaruli, R. W. Moore, R. Morse, M. Moulai, R. Nahnhauer, P. Nakarmi, U. Naumann, G. Neer, H. Niederhausen, S. C. Nowicki, D. R. Nygren,

A. Obertacke Pollmann, A. Olivas, A. O'Murchadha, E. O'Sullivan, P. Padovani, T. Palczewski, H. Pand ya, D. V. Pankova, P. Peiffer, J. A. Pepper, C. Pérez de los Heros, D. Pieloth, E. Pinat, M. Plum, P. B. Price, G. T. Przybylski, C. Raab, L. Rädel, M. Rameez, K. Rawlins, I. C. Rea, R. Reimann, B. Relethford, M. Relich, E. Resconi, W. Rhode, M. Richman, S. Robertson, M. Rongen, C. Rott, T. Ruhe, D. Ryckbosch, D. Rysewyk, I. Safa, N. Sahakyan, T. Sälzer, S. E. Sanchez Herrera, A. Sandrock, J. Sandroos, M. Santander, S. Sarkar, S. Sarkar, K. Satalecka, P. Schlunder, T. Schmidt, A. Schneider, S. Schoenen, S. Schöneberg, L. Schumacher, S. Sclafani, D. Seckel, S. Seunarine, J. Soedingrekso, D. Soldin, M. Song, G. M. Spiczak, C. Spiering, J. Stachurska, M. Stamatikos, T. Stanev, A. Stasik, J. Stettner, A. Steuer, T. Stezelberger, R. G. Stokstad, A. Stößl, N. L. Strotjohann, T. Stuttard, G. W. Sullivan, M. Sutherland, I. Taboada, J. Tatar, F. Tenholt, S. Ter-Antonyan, A. Terliuk, S. Tilav, P. A. Toale, M. N. Tobin, C. Toennis, S. Toscano, D. Tosi, M. Tselengidou, C. F. Tung, A. Turcati, C. F. Turley, B. Ty, E. Unger, M. Usner, J. Vandenbroucke, W. Van Driessche, D. van Eijk, N. van Eijndhoven, S. Vanheule, J. van Santen, E. Vogel, M. Vraeghe, C. Walck, A. Wallace, M. Wallraff, F. D. Wandler, N. Wand kowsky, A. Waza, C. Weaver, M. J. Weiss, C. Wendt, J. Werthebach, S. Westerhoff, B. J. Whelan, N. Whitehorn, K. Wiebe, C. H. Wiebusch, L. Wille, D. R. Williams, L. Wills, M. Wolf, J. Wood, T. R. Wood, K. Woschnagg, D. L. Xu, X. W. Xu, Y. Xu, J. P. Yanez, G. Yodh, S. Yoshida, and T. Yuan.
Neutrino emission from the direction of the blazar TXS 0506+056 prior to the IceCube-170922A alert.
Science, 361(6398):147–151, July 2018.

[86] Susumu Inoue and Fumio Takahara.
Electron Acceleration and Gamma-Ray Emission from Blazars.
ApJ, 463:555, June 1996.

[87] N. S. Kardashev.
Nonstationarity of Spectra of Young Sources of Nonthermal Radio Emission.
, 6:317, December 1962.

[88] A. Kaur, A. Rau, M. Ajello, A. Domínguez, V. S. Paliya, J. Greiner, D. H. Hartmann, and P. Schady.
New High-z BL Lacs Using the Photometric Method with Swift and SARA.
ApJ, 859(2):80, June 2018.

[89] A. Kaur, A. Rau, M. Ajello, J. Greiner, D. H. Hartmann, V. S. Paliya, A. Domínguez, J. Bolmer, and P. Schady.
New High-z Fermi BL Lacs with the Photometric Dropout Technique.
ApJ, 834(1):41, January 2017.

[90] A. Keivani, K. Murase, M. Petropoulou, D. B. Fox, S. B. Cenko, S. Chaty, A. Coleiro, J. J. DeLaunay, S. Dimitrakoudis, P. A. Evans, J. A. Kennea, F. E. Marshall, A. Mastichiadis, J. P. Osborne, M. Santander, A. Tohuvavohu, and C. F. Turley.
A Multimessenger Picture of the Flaring Blazar TXS 0506+056: Implications for High-energy Neutrino Emission and Cosmic-Ray Acceleration.
ApJ, 864:84, September 2018.

[91] J. G. Kirk and A. F. Heavens.
Particle acceleration at oblique shock fronts.
MNRAS, 239:995–1011, Aug 1989.

[92] A. Korochkin, A. Neronov, and D. Semikoz.
Search for spectral features in extragalactic background light with gamma-ray telescopes.
A&A, 633:A74, January 2020.

[93] Shang Li, Zi-Qing Xia, Yun-Feng Liang, Neng-Hui Liao, and Yi-Zhong Fan.
Fast γ-Ray Variability in Blazars beyond Redshift 3.
ApJ, 853(2):159, February 2018.

[94] N.-H. Liao, Y.-L. Xin, Y.-F. Liang, X.-L. Guo, S. Li, H.-N. He, Q. Yuan, and Y.-Z. Fan.
Active galactic nuclei with GeV activities and the PeV neutrino source candidate TXS 0506+056.
ArXiv e-prints, July 2018.

[95] I. Liodakis and V. Pavlidou.
Population statistics of beamed sources - II. Evaluation of Doppler factor estimates.
MNRAS, 454(2):1767–1777, December 2015.

[96] B. Lott, L. Escande, S. Larsson, and J. Ballet.
An adaptive-binning method for generating constant-uncertainty/constant-significance light curves with Fermi-LAT data.
A&A, 544:A6, August 2012.

[97] B. Lott, L. Escande, S. Larsson, and J. Ballet.
An adaptive-binning method for generating constant-uncertainty/constant-significance light curves with Fermi-LAT data.
A&A, 544:A6, August 2012.

[98] MAGIC Collaboration, V. A. Acciari, S. Ansoldi, L. A. Antonelli, A. Arbet Engels, C. Arcaro, D. Baack, A. Babić, B. Banerjee, P. Bangale, U. Barres de Almeida, J. A. Barrio, W. Bednarek, E. Bernardini, A. Berti, J. Besenrieder, W. Bhattacharyya, C. Bigongiari, A. Biland, O. Blanch, G. Bonnoli, R. Carosi, G. Ceribella, S. Cikota, S. M. Colak, P. Colin, E. Colombo, J. L. Contreras, J. Cortina, S. Covino, V. D'Elia, P. da Vela, F. Dazzi, A. de Angelis, B. de Lotto, M. Delfino, J. Delgado, F. di Pierro, E. Do Souto Espiñera, A. Domínguez, D. Dominis Prester, D. Dorner, M. Doro, S. Einecke, D. Elsaesser, V. Fallah Ramazani, A. Fattorini, A. Fernández-Barral, G. Ferrara, D. Fidalgo, L. Foffano, M. V. Fonseca, L. Font, C. Fruck, D. Galindo, S. Gallozzi, R. J. García López, M. Garczarczyk, M. Gaug, P. Giammaria, N. Godinović, D. Guberman, D. Hadasch, A. Hahn, T. Hassan, J. Herrera, J. Hoang, D. Hrupec, S. Inoue, K. Ishio, Y. Iwamura, H. Kubo, J. Kushida, D. Kuveždić, A. Lamastra, D. Lelas, F. Leone, E. Lindfors, S. Lombardi, F. Longo, M. López, A. López-Oramas, C. Maggio, P. Majumdar, M. Makariev, G. Maneva, M. Manganaro, K. Mannheim, L. Maraschi, M. Mariotti, M. Martínez, S. Masuda, D. Mazin, M. Minev, J. M. Miranda, R. Mirzoyan, E. Molina, A. Moralejo, V. Moreno, E. Moretti, P. Munar-Adrover, V. Neustroev, A. Niedzwiecki, M. Nievas Rosillo, C. Nigro, K. Nilsson, D. Ninci, K. Nishijima, K. Noda, L. Nogués, S. Paiano, J. Palacio, D. Paneque, R. Paoletti, J. M. Paredes, G. Pedaletti, P. Peñil, M. Peresano, M. Persic, P. G. Prada Moroni, E. Prand ini, I. Puljak, J. R. Garcia, W. Rhode, M. Ribó, J. Rico, C. Righi, A. Rugliancich, L. Saha, T. Saito, K. Satalecka, T. Schweizer, J. Sitarek, I. Šnidarić, D. Sobczynska, A. Somero, A. Stamerra, M. Strzys, T. Surić, F. Tavecchio, P. Temnikov, T. Terzić, M. Teshima, N. Torres-Albà, S. Tsujimoto, J. van Scherpenberg, G. Vanzo, M. Vazquez Acosta, I. Vovk, J. E. Ward, M. Will, D. Zarić, Fermi-Lat Collaboration, J. Becerra González, C. M. Raiteri, A. Sandrinelli, T. Hovatta, S. Kiehlmann, W. Max-Moerbeck, M. Tornikoski, A. Lähteenmäki, J. Tammi, V. Ramakrishnan, C. Thum, I. Agudo, S. N. Molina, J. L. Gómez, A. Fuentes, C. Casadio, E. Traianou, I. Myserlis, and J. Y. Kim.
Detection of persistent VHE gamma-ray emission from PKS 1510-089 by the MAGIC telescopes during low states between 2012 and 2017.

A&A, 619:A159, November 2018.

[99] MAGIC Collaboration, V. A. Acciari, S. Ansoldi, L. A. Antonelli, A. Arbet Engels, D. Baack, A. Babić, B. Banerjee, U. Barres de Almeida, J. A. Barrio, J. Becerra González, W. Bednarek, L. Bellizzi, E. Bernardini, A. Berti, J. Besenrieder, W. Bhattacharyya, C. Bigongiari, A. Biland , O. Blanch, G. Bonnoli, Z. Bosnjak, G. Busetto, R. Carosi, G. Ceribella, Y. Chai, S. Cikota, S. M. Colak, U. Colin, E. Colombo, J. L. Contreras, J. Cortina, S. Covino, V. D'Elia, P. Da Vela, F. Dazzi, A. De Angelis, B. De Lotto, M. Delfino, J. Delgado, F. Di Pierro, E. Do Souto Espiñeira, D. Dominis Prester, A. Donini, D. Dorner, M. Doro, D. Elsaesser, V. Fallah Ramazani, A. Fattorini, A. Fernández-Barral, G. Ferrara, D. Fidalgo, L. Foffano, M. V. Fonseca, L. Font, C. Fruck, S. Fukami, S. Gallozzi, R. J. García López, M. Garczarczyk, S. Gasparyan, M. Gaug, N. Godinović, D. Green, D. Guberman, D. Hadasch, A. Hahn, J. Herrera, J. Hoang, D. Hrupec, T. Inada, S. Inoue, K. Ishio, Y. Iwamura, L. Jouvin, H. Kubo, J. Kushida, A. Lamastra, D. Lelas, F. Leone, E. Lindfors, S. Lombardi, F. Longo, M. López, R. López-Coto, A. López-Oramas, B. Machado de Oliveira Fraga, C. Maggio, P. Majumdar, M. Makariev, M. Mallamaci, G. Maneva, M. Manganaro, K. Mannheim, L. Maraschi, M. Mariotti, M. Martínez, S. Masuda, D. Mazin, S. Mićanović, D. Miceli, M. Minev, J. M. Miranda, R. Mirzoyan, E. Molina, A. Moralejo, D. Morcuende, V. Moreno, E. Moretti, P. Munar-Adrover, V. Neustroev, A. Niedzwiecki, C. Nigro, K. Nilsson, D. Ninci, K. Nishijima, K. Noda, L. Nogués, M. Nöthe, S. Nozaki, S. Paiano, J. Palacio, M. Palatiello, D. Paneque, R. Paoletti, J. M. Paredes, P. Peñil, M. Peresano, M. Persic, P. G. Prada Moroni, E. Prand ini, I. Puljak, W. Rhode, M. Ribó, J. Rico, C. Righi, A. Rugliancich, L. Saha, N. Sahakyan, T. Saito, S. Sakurai, K. Satalecka, T. Schweizer, J. Sitarek, I. Šnidarić, D. Sobczynska, A. Somero, A. Stamerra, D. Strom, M. Strzys, T. Surić, M. Takahashi, F. Tavecchio, P. Temnikov, T. Terzić, M. Teshima, N. Torres-Albà, S. Tsujimoto, J. van Scherpenberg, G. Vanzo, M. Vazquez Acosta, I. Vovk, M. Will, D. Zarić, Fermi-LAT Collaboration, :, and M. Hayashida.
Broadband characterisation of the very intense TeV flares of the blazar 1ES 1959+650 in 2016.
arXiv e-prints, page arXiv:2002.00129, January 2020.

[100] K. Mannheim.
The proton blazar.

A&A, 269:67–76, March 1993.

[101] K. Mannheim.
High-energy neutrinos from extragalactic jets.
Astroparticle Physics, 3:295–302, May 1995.

[102] K. Mannheim and P. L. Biermann.
Photomeson production in active galactic nuclei.
A&A, 221:211–220, September 1989.

[103] L. Maraschi, G. Ghisellini, and A. Celotti.
A Jet Model for the Gamma-Ray–emitting Blazar 3C 279.
ApJL, 397:L5, September 1992.

[104] L. Maraschi, G. Ghisellini, and A. Celotti.
A jet model for the gamma-ray emitting blazar 3C 279.
ApJL, 397:L5–L9, September 1992.

[105] Laura Maraschi and Fabrizio Tavecchio.
The Jet-Disk Connection and Blazar Unification.
ApJ, 593(2):667–675, August 2003.

[106] L. Marcotulli, V. S. Paliya, M. Ajello, A. Kaur, D. H. Hartmann, D. Gasparrini, J. Greiner, A. Rau, P. Schady, M. Baloković, D. Stern, and G. Madejski.
High-redshift Blazars through NuSTAR Eyes.
ApJ, 839(2):96, April 2017.

[107] A. P. Marscher and W. K. Gear.
Models for high-frequency radio outbursts in extragalactic sources, with application to the early 1983 millimeter-to-infrared flare of 3C 273.
ApJ, 298:114–127, November 1985.

[108] E. Massaro, A. Tramacere, M. Perri, P. Giommi, and G. Tosti.
Log-parabolic spectra and particle acceleration in blazars. III. SSC emission in the TeV band from Mkn501.
A&A, 448(3):861–871, March 2006.

[109] J. R. Mattox, D. L. Bertsch, J. Chiang, B. L. Dingus, S. W. Digel, J. A. Esposito, J. M. Fierro, R. C. Hartman, S. D. Hunter, G. Kanbach, D. A. Kniffen, Y. C. Lin, D. J. Macomb, H. A. Mayer-Hasselwander, P. F. Michelson, C. von Montigny, R. Mukherjee, P. L. Nolan, P. V. Ramanamurthy, E. Schneid, P. Sreekumar, D. J. Thompson, and T. D. Willis.

The Likelihood Analysis of EGRET Data.
ApJ, 461:396, April 1996.

[110] Alberto Moretti, Sergio Campana, T. Mineo, Patrizia Romano, A. F. Abbey, L. Angelini, A. Beardmore, W. Burkert, D. N. Burrows, M. Capalbi, G. Chincarini, O. Citterio, G. Cusumano, M. J. Freyberg, P. Giommi, M. R. Goad, O. Godet, G. D. Hartner, J. E. Hill, J. Kennea, V. La Parola, V. Mangano, D. Morris, J. A. Nousek, J. Osborne, K. Page, C. Pagani, M. Perri, G. Tagliaferri, F. Tamburelli, and A. Wells.
In-flight calibration of the Swift XRT Point Spread Function.
In Oswald H. W. Siegmund, editor, , volume 5898 of *Society of Photo-Optical Instrumentation Engineers (SPIE) Conference Series*, pages 360–368, August 2005.

[111] A. Mücke and R. J. Protheroe.
A proton synchrotron blazar model for flaring in Markarian 501.
Astroparticle Physics, 15:121–136, March 2001.

[112] A. Mücke and R. J. Protheroe.
A proton synchrotron blazar model for flaring in Markarian 501.
Astroparticle Physics, 15(1):121–136, March 2001.

[113] A. Mücke, R. J. Protheroe, R. Engel, J. P. Rachen, and T. Stanev.
BL Lac objects in the synchrotron proton blazar model.
Astroparticle Physics, 18:593–613, March 2003.

[114] K. Murase, F. Oikonomou, and M. Petropoulou.
Blazar Flares as an Origin of High-energy Cosmic Neutrinos?
ApJ, 865:124, October 2018.

[115] K. Nalewajko.
The brightest gamma-ray flares of blazars.
MNRAS, 430:1324–1333, April 2013.

[116] Maia Nenkova, Matthew M. Sirocky, Robert Nikutta, Željko Ivezić, and Moshe Elitzur.
AGN Dusty Tori. II. Observational Implications of Clumpiness.
ApJ, 685(1):160–180, September 2008.

[117] L. Pacciani, F. Tavecchio, I. Donnarumma, A. Stamerra, L. Carrasco, E. Recillas, A. Porras, and M. Uemura.
Exploring the Blazar Zone in High-energy Flares of FSRQs.
ApJ, 790(1):45, August 2014.

[118] P. Padovani, D. M. Alexander, R. J. Assef, B. De Marco, P. Giommi, R. C. Hickox, G. T. Richards, V. Smolčić, E. Hatziminaoglou, V. Mainieri, and M. Salvato.
Active galactic nuclei: what's in a name?
A&AR, 25(1):2, August 2017.

[119] P. Padovani, P. Giommi, E. Resconi, T. Glauch, B. Arsioli, N. Sahakyan, and M. Huber.
Dissecting the region around IceCube-170922A: the blazar TXS 0506+056 as the first cosmic neutrino source.
MNRAS, 480(1):192–203, October 2018.

[120] P. Padovani, E. Resconi, P. Giommi, B. Arsioli, and Y. L. Chang.
Extreme blazars as counterparts of IceCube astrophysical neutrinos.
MNRAS, 457(4):3582–3592, April 2016.

[121] Paolo Padovani and Paolo Giommi.
The Connection between X-Ray– and Radio-selected BL Lacertae Objects.
ApJ, 444:567, May 1995.

[122] A. Paggi, A. Cavaliere, V. Vittorini, F. D'Ammando, and M. Tavani.
Flaring Patterns in Blazars.
ApJ, 736(2):128, August 2011.

[123] Vaidehi S. Paliya.
The High-redshift Blazar S5 0836+71: A Broadband Study.
ApJ, 804(1):74, May 2015.

[124] Vaidehi S. Paliya, M. Ajello, R. Ojha, R. Angioni, C. C. Cheung, K. Tanada, T. Pursimo, P. Galindo, I. R. Losada, L. Siltala, A. A. Djupvik, L. Marcotulli, and D. Hartmann.
Detection of a Gamma-Ray Flare from the High-redshift Blazar DA 193.
ApJ, 871(2):211, February 2019.

[125] Vaidehi S. Paliya, C. C. Teddy Cheung, Daniel Kocevski, and Roberto Angioni.
Fermi-LAT detection of high gamma-ray activity from the z=3.6 quasar NVSS J163547+362930.
The Astronomer's Telegram, 11847:1, July 2018.

[126] Vaidehi S. Paliya, L. Marcotulli, M. Ajello, M. Joshi, S. Sahayanathan, A. R. Rao, and D. Hartmann.
General Physical Properties of CGRaBS Blazars.
ApJ, 851(1):33, December 2017.

[127] Vaidehi S. Paliya, M. L. Parker, A. C. Fabian, and C. S. Stalin.
Broadband Observations of High Redshift Blazars.
ApJ, 825(1):74, July 2016.

[128] Elena Pian, Giuseppe Vacanti, Gianpiero Tagliaferri, Gabriele Ghisellini, Laura Maraschi, Aldo Treves, C. Megan Urry, Fabrizio Fiore, Paolo Giommi, Eliana Palazzi, Lucio Chiappetti, and Rita M. Sambruna.
BeppoSAX Observations of Unprecedented Synchrotron Activity in the BL Lacertae Object Markarian 501.
ApJL, 492(1):L17–L20, January 1998.

[129] T. S. Poole, A. A. Breeveld, M. J. Page, W. Landsman, S. T. Holland, P. Roming, N. P. M. Kuin, P. J. Brown, C. Gronwall, S. Hunsberger, S. Koch, K. O. Mason, P. Schady, D. vanden Berk, A. J. Blustin, P. Boyd, P. Broos, M. Carter, M. M. Chester, A. Cucchiara, B. Hancock, H. Huckle, S. Immler, M. Ivanushkina, T. Kennedy, F. Marshall, A. Morgan, S. B. Pandey, M. de Pasquale, P. J. Smith, and M. Still.
Photometric calibration of the Swift ultraviolet/optical telescope.
MNRAS, 383:627–645, January 2008.

[130] B. Rani, T. P. Krichbaum, L. Fuhrmann, M. Böttcher, B. Lott, H. D. Aller, M. F. Aller, E. Angelakis, U. Bach, D. Bastieri, A. D. Falcone, Y. Fukazawa, K. E. Gabanyi, A. C. Gupta, M. Gurwell, R. Itoh, K. S. Kawabata, M. Krips, A. A. Lähteenmäki, X. Liu, N. Marchili, W. Max-Moerbeck, I. Nestoras, E. Nieppola, G. Quintana-Lacaci, A. C. S. Readhead, J. L. Richards, M. Sasada, A. Sievers, K. Sokolovsky, M. Stroh, J. Tammi, M. Tornikoski, M. Uemura, H. Ungerechts, T. Urano, and J. A. Zensus.
Radio to gamma-ray variability study of blazar S5 0716+714.
A&A, 552:A11, April 2013.

[131] B. Rani, B. Lott, T. P. Krichbaum, L. Fuhrmann, and J. A. Zensus.
Constraining the location of rapid gamma-ray flares in the flat spectrum radio quasar 3C 273.
A&A, 557:A71, September 2013.

[132] B. Rani, B. Lott, T. P. Krichbaum, L. Fuhrmann, and J. A. Zensus.
Constraining the location of rapid gamma-ray flares in the flat spectrum radio quasar 3C 273.
A&A, 557:A71, Sep 2013.

[133] E. Resconi, S. Coenders, P. Padovani, P. Giommi, and L. Caccianiga.

Connecting blazars with ultrahigh-energy cosmic rays and astrophysical neutrinos.
MNRAS, 468(1):597–606, June 2017.

[134] Stephen P. Reynolds.
Synchrotron-Loss Spectral Breaks in Pulsar-Wind Nebulae and Extragalactic Jets.
ApJ, 703(1):662–670, September 2009.

[135] Frank M. Rieger, Valentí Bosch-Ramon, and Peter Duffy.
Fermi acceleration in astrophysical jets.
Ap&SS, 309(1-4):119–125, June 2007.

[136] C. Righi, F. Tavecchio, and S. Inoue.
Neutrino emission from BL Lac objects: the role of radiatively inefficient accretion flows.
MNRAS, 483(1):L127–L131, February 2019.

[137] C. Righi, F. Tavecchio, and L. Pacciani.
A multiwavelength view of BL Lac neutrino candidates.
MNRAS, 484(2):2067–2077, April 2019.

[138] Peter W. A. Roming, Thomas E. Kennedy, Keith O. Mason, John A. Nousek, Lindy Ahr, Richard E. Bingham, Patrick S. Broos, Mary J. Carter, Barry K. Hancock, Howard E. Huckle, S. D. Hunsberger, Hajime Kawakami, Ronnie Killough, T. Scott Koch, Michael K. McLelland, Kelly Smith, Philip J. Smith, Juan Carlos Soto, Patricia T. Boyd, Alice A. Breeveld, Stephen T. Holland, Mariya Ivanushkina, Michael S. Pryzby, Martin D. Still, and Joseph Stock.
The Swift Ultra-Violet/Optical Telescope.
Space Science Reviews, 120(3-4):95–142, October 2005.

[139] M. Rüger, F. Spanier, and K. Mannheim.
Spectral modelling of 1 ES 1218+30.4.
MNRAS, 401(2):973–976, January 2010.

[140] George B. Rybicki and Alan P. Lightman.
Radiative Processes in Astrophysics.
1986.

[141] N. Sahakyan.
Lepto-hadronic γ-Ray and Neutrino Emission from the Jet of TXS 0506+056.
ApJ, 866:109, October 2018.

[142] N. Sahakyan.
Origin of the multiwavelength emission of PKS 0502+049.
A&A, 622:A144, Feb 2019.

[143] N. Sahakyan.
Investigation of the γ-ray spectrum of CTA 102 during the exceptional flaring state in 2016-2017.
A&A, 635:A25, March 2020.

[144] N. Sahakyan, V. Baghmanyan, and D. Zargaryan.
Fermi-LAT observation of nonblazar AGNs.
A&A, 614:A6, June 2018.

[145] N. Sahakyan and S. Gasparyan.
High energy gamma-ray emission from PKS 1441+25.
MNRAS, 470(3):2861–2869, September 2017.

[146] S. Saito, Ł. Stawarz, and et al.
Very Rapid High-amplitude Gamma-Ray Variability in Luminous Blazar PKS 1510-089 Studied with Fermi-LAT.
ApJL, 766:L11, March 2013.

[147] T. Sbarrato, G. Ghisellini, L. Maraschi, and M. Colpi.
The relation between broad lines and γ-ray luminosities in Fermi blazars.
MNRAS, 421(2):1764–1778, April 2012.

[148] N. I. Shakura and R. A. Sunyaev.
Reprint of 1973A&A....24..337S. Black holes in binary systems. Observational appearance.
A&A, 500:33–51, June 1973.

[149] Michael S. Shaw, Roger W. Romani, Garret Cotter, Stephen E. Healey, Peter F. Michelson, Anthony C. S. Readhead, Joseph L. Richards, Walter Max-Moerbeck, Oliver G. King, and William J. Potter.
Spectroscopy of Broad-line Blazars from 1LAC.
ApJ, 748(1):49, March 2012.

[150] Yue Shen, Gordon T. Richards, Michael A. Strauss, Patrick B. Hall, Donald P. Schneider, Stephanie Snedden, Dmitry Bizyaev, Howard Brewington, Viktor Malanushenko, Elena Malanushenko, Dan Oravetz, Kaike Pan, and Audrey Simmons.
A Catalog of Quasar Properties from Sloan Digital Sky Survey Data Release 7.
ApJSS, 194(2):45, June 2011.

[151] M. Sikora, M. C. Begelman, and M. J. Rees.
Comptonization of diffuse ambient radiation by a relativistic jet: The source of gamma rays from blazars?
ApJ, 421:153–162, January 1994.

[152] M. Sikora, M. Błażejowski, R. Moderski, and G. M. Madejski.
On the Nature of MeV Blazars.
ApJ, 577(1):78–84, September 2002.

[153] Marek Sikora, Łukasz Stawarz, Rafał Moderski, Krzysztof Nalewajko, and Greg M. Madejski.
Constraining Emission Models of Luminous Blazar Sources.
ApJ, 704(1):38–50, October 2009.

[154] K. K. Singh, B. Bisschoff, B. van Soelen, A. Tolamatti, J. P. Marais, and P. J. Meintjes.
Long-term multiwavelength view of the blazar 1ES 1218+304.
MNRAS, 489(4):5076–5086, November 2019.

[155] F. W. Stecker, M. A. Malkan, and S. T. Scully.
Intergalactic Photon Spectra from the Far-IR to the UV Lyman Limit for 0 < z < 6 and the Optical Depth of the Universe to High-Energy Gamma Rays.
ApJ, 648(2):774–783, September 2006.

[156] Errol J. Summerlin and Matthew G. Baring.
Diffusive Acceleration of Particles at Oblique, Relativistic, Magnetohydrodynamic Shocks.
ApJ, 745(1):63, Jan 2012.

[157] F. Tavecchio, G. Ghisellini, G. Bonnoli, and L. Foschini.
Extreme TeV blazars and the intergalactic magnetic field.
MNRAS, 414(4):3566–3576, July 2011.

[158] Fabrizio Tavecchio, Laura Maraschi, Rita M. Sambruna, and C. Megan Urry.
The X-Ray Jet of PKS 0637-752: Inverse Compton Radiation from the Cosmic Microwave Background?
ApJL, 544(1):L23–L26, November 2000.

[159] A. M. Taylor, I. Vovk, and A. Neronov.
Extragalactic magnetic fields constraints from simultaneous GeV-TeV observations of blazars.
A&A, 529:A144, May 2011.

[160] A. Tramacere, P. Giommi, M. Perri, F. Verrecchia, and G. Tosti.
Swift observations of the very intense flaring activity of Mrk 421 during 2006. I. Phenomenological picture of electron acceleration and predictions for MeV/GeV emission.
A&A, 501(3):879–898, July 2009.

[161] A. Tramacere, E. Massaro, and A. M. Taylor.
Stochastic Acceleration and the Evolution of Spectral Distributions in Synchro-Self-Compton Sources: A Self-consistent Modeling of Blazars' Flares.
ApJ, 739(2):66, October 2011.

[162] C. M. Urry and P. Padovani.
Unified Schemes for Radio-Loud Active Galactic Nuclei.
, 107:803, September 1995.

[163] C. Megan Urry and Paolo Padovani.
Unified Schemes for Radio-Loud Active Galactic Nuclei.
, 107:803, September 1995.

[164] M. P. Véron-Cetty and P. Véron.
A catalogue of quasars and active nuclei: 11th edition.
A&A, 412:399–403, December 2003.

[165] Marta Volonteri.
Formation of supermassive black holes.
A&AR, 18(3):279–315, July 2010.

[166] K. Wang, R.-Y. Liu, Z. Li, X.-Y. Wang, and Z.-G. Dai.
Jet-cloud/star interaction as an interpretation of neutrino outburst from the blazar TXS 0506+056.
ArXiv e-prints, September 2018.

[167] M. Weidinger and F. Spanier.
Modelling the variability of 1ES1218+30.4.
A&A, 515:A18, June 2010.

[168] A. S. Wilson, M. J. Ward, D. J. Axon, M. Elvis, and E. J. A. Meurs.
On the identification of the high-latitude X-ray source 2A 1219+305.
MNRAS, 187:109–115, April 1979.

[169] Edward L. Wright, Peter R. M. Eisenhardt, Amy K. Mainzer, Michael E. Ressler, Roc M. Cutri, Thomas Jarrett, J. Davy Kirkpatrick, Deborah Padgett, Robert S. McMillan, Michael Skrutskie, S. A. Stanford, Martin Cohen, Russell G. Walker, John C. Mather, David Leisawitz, III

Gautier, Thomas N., Ian McLean, Dominic Benford, Carol J. Lonsdale, Andrew Blain, Bryan Mendez, William R. Irace, Valerie Duval, Fengchuan Liu, Don Royer, Ingolf Heinrichsen, Joan Howard, Mark Shannon, Martha Kendall, Amy L. Walsh, Mark Larsen, Joel G. Cardon, Scott Schick, Mark Schwalm, Mohamed Abid, Beth Fabinsky, Larry Naes, and Chao-Wei Tsai.
The Wide-field Infrared Survey Explorer (WISE): Mission Description and Initial On-orbit Performance.
AJ, 140(6):1868–1881, December 2010.

[170] Dahai Yan, Li Zhang, Qiang Yuan, Zhonghui Fan, and Houdun Zeng.
Emitting Electrons Spectra and Acceleration Processes in the Jet of Mrk 421: From the Low State to the Giant Flare State.
ApJ, 765(2):122, March 2013.

[171] Donald G. York, J. Adelman, Jr. Anderson, John E., Scott F. Anderson, James Annis, Neta A. Bahcall, J. A. Bakken, Robert Barkhouser, Steven Bastian, Eileen Berman, William N. Boroski, Steve Bracker, Charlie Briegel, John W. Briggs, J. Brinkmann, Robert Brunner, Scott Burles, Larry Carey, Michael A. Carr, Francisco J. Castander, Bing Chen, Patrick L. Colestock, A. J. Connolly, J. H. Crocker, István Csabai, Paul C. Czarapata, John Eric Davis, Mamoru Doi, Tom Dombeck, Daniel Eisenstein, Nancy Ellman, Brian R. Elms, Michael L. Evans, Xiaohui Fan, Glenn R. Federwitz, Larry Fiscelli, Scott Friedman, Joshua A. Frieman, Masataka Fukugita, Bruce Gillespie, James E. Gunn, Vijay K. Gurbani, Ernst de Haas, Merle Haldeman, Frederick H. Harris, J. Hayes, Timothy M. Heckman, G. S. Hennessy, Robert B. Hindsley, Scott Holm, Donald J. Holmgren, Chi-hao Huang, Charles Hull, Don Husby, Shin-Ichi Ichikawa, Takashi Ichikawa, Željko Ivezić, Stephen Kent, Rita S. J. Kim, E. Kinney, Mark Klaene, A. N. Kleinman, S. Kleinman, G. R. Knapp, John Korienek, Richard G. Kron, Peter Z. Kunszt, D. Q. Lamb, B. Lee, R. French Leger, Siriluk Limmongkol, Carl Lindenmeyer, Daniel C. Long, Craig Loomis, Jon Loveday, Rich Lucinio, Robert H. Lupton, Bryan MacKinnon, Edward J. Mannery, P. M. Mantsch, Bruce Margon, Peregrine McGehee, Timothy A. McKay, Avery Meiksin, Aronne Merelli, David G. Monet, Jeffrey A. Munn, Vijay K. Narayanan, Thomas Nash, Eric Neilsen, Rich Neswold, Heidi Jo Newberg, R. C. Nichol, Tom Nicinski, Mario Nonino, Norio Okada, Sadanori Okamura, Jeremiah P. Ostriker, Russell Owen, A. George Pauls, John Peoples, R. L. Peterson, Donald Petravick, Jeffrey R. Pier, Adrian Pope, Ruth Pordes, Angela Prosapio, Ron

Rechenmacher, Thomas R. Quinn, Gordon T. Richards, Michael W. Richmond, Claudio H. Rivetta, Constance M. Rockosi, Kurt Ruthmansdorfer, Dale Sand ford, David J. Schlegel, Donald P. Schneider, Maki Sekiguchi, Gary Sergey, Kazuhiro Shimasaku, Walter A. Siegmund, Stephen Smee, J. Allyn Smith, S. Snedden, R. Stone, Chris Stoughton, Michael A. Strauss, Christopher Stubbs, Mark SubbaRao, Alexander S. Szalay, Istvan Szapudi, Gyula P. Szokoly, Anirudda R. Thakar, Christy Tremonti, Douglas L. Tucker, Alan Uomoto, Dan Vanden Berk, Michael S. Vogeley, Patrick Waddell, Shu-i. Wang, Masaru Watanabe, David H. Weinberg, Brian Yanny, Naoki Yasuda, and SDSS Collaboration.
The Sloan Digital Sky Survey: Technical Summary.
AJ, 120(3):1579–1587, September 2000.

[172] D. Zargaryan, S. Gasparyan, V. Baghmanyan, and N. Sahakyan.
Comparing 3C 120 jet emission at small and large scales.
A&A, 608:A37, December 2017.

[173] Jin Zhang, Xiao-Na Sun, En-Wei Liang, Rui-Jing Lu, Ye Lu, and Shuang-Nan Zhang.
Relativistic Jet Properties of GeV-TeV Blazars and Possible Implications for the Jet Formation, Composition, and Cavity Kinematics.
ApJ, 788(2):104, June 2014.

[174] Y. G. Zheng, G. B. Long, C. Y. Yang, and J. M. Bai.
Formation of the Electronic Spectrum in Relativistic Jets of Gamma-Ray Blazars.
, 130(990):083001, August 2018.